OBSERVABLE ASPECTS OF BLACK HOLES

A THESIS SUBMITTED TO
THE GRADUATE SCHOOL OF NATURAL AND APPLIED SCIENCES
OF
MIDDLE EAST TECHNICAL UNIVERSITY

BY

AYDIN TAVLAYAN

IN PARTIAL FULFILLMENT OF THE REQUIREMENTS
FOR
THE DEGREE OF DOCTOR OF PHILOSOPHY
IN
PHYSICS

JANUARY 2026

Approval of the thesis:

OBSERVABLE ASPECTS OF BLACK HOLES

submitted by **AYDIN TAVLAYAN** in partial fulfillment of the requirements for the degree of **Doctor of Philosophy in Physics Department, Middle East Technical University** by,

Prof. Dr. Naci Emre Altun
Dean, Graduate School of **Natural and Applied Sciences** _____

Prof. Dr. Seçkin Kürkcüoğlu
Head of Department, **Physics** _____

Prof. Dr. Bayram Tekin
Supervisor, **Physics, METU** _____

Examining Committee Members:

Prof. Dr. Seçkin Kürkcüoğlu
Physics, METU _____

Prof. Dr. Bayram Tekin
Physics, METU _____

Prof. Dr. Tahsin Çağrı Şişman
Astronautical Engineering, UTAA _____

Prof. Dr. Çetin Şentürk
Aeronautical Engineering, UTAA _____

Assoc. Prof. Dr. Yaghoub Heydarzade
Mathematics, Bilkent University _____

Date:22.01.2026

I hereby declare that all information in this document has been obtained and presented in accordance with academic rules and ethical conduct. I also declare that, as required by these rules and conduct, I have fully cited and referenced all material and results that are not original to this work.

Name, Surname: Aydın Tavlayan

Signature :

ABSTRACT

OBSERVABLE ASPECTS OF BLACK HOLES

Tavlayan, Aydın
Ph.D., Department of Physics
Supervisor: Prof. Dr. Bayram Tekin

January 2026, 142 pages

In this thesis, some of the crucial observable aspects of black holes are investigated. The existence of the light rings around black holes in five dimensional spacetime is considered by using topological invariants. It is shown that the method is robust and can be also applied to higher dimensions. Some specific cases indicating the possible existence of the naked singularities are analyzed with the help of both null and time-like geodesics around it. The shadow and the accretion disc around this hypothetical naked singularity are examined. In addition to geodesic investigation, the black hole thermodynamics is also considered. A recently developed method of assigning entropy to some fixed volume in Einstein's gravity is generalized to the higher powers of curvature in three dimensions. Then, by using background Killing charges, the thermodynamic charges and their corresponding conjugates are redefined and checked whether they obey the laws of black hole thermodynamics and the geometrical relations of the corresponding spacetime. Finally, the instability of a particle around a black hole is investigated by considering the exponentially unstable motion it performs when perturbed and the corresponding Lyapunov exponents of this motion. A possible connection is proposed between the instability and the black hole thermodynamics. The importance of non-equatorial contributions to the shadow image is

discussed.

Keywords: Black Holes, Light Rings, Singularity, Black Hole Thermodynamics, Instability.

ÖZ

KARA DELİKLERİN GÖZLEMLENEBİLİR YÖNLERİ

Tavlayan, Aydın
Doktora, Fizik Bölümü
Tez Yöneticisi: Prof. Dr. Bayram Tekin

Ocak 2026 , 142 sayfa

Bu tezde, kara deliklerin en önemli gözlemlenebilir yönlerinden bazıları incelenmiştir. Beş boyutlu uzay-zamanda kara deliklerin etrafındaki ışık halkalarının varlığı, topolojik değişmezler kullanılarak ele alınmıştır. Yöntemin sağlam olduğu ve daha yüksek boyutlara da uygulanabileceği gösterilmiştir. Çıplak tekilliklerin olası varlığını gösteren bazı özel durumlar, etrafındaki hem ışıksal hem de zamansal jeodezikler yardımıyla analiz edilmiştir. Bu varsayımsal çıplak tekilliğin etrafındaki gölge ve yığılma diski incelenmiştir. Jeodezik incelemeye ek olarak, kara delik termodinamiği de ele alınmıştır. Einstein yerçekiminde belirli bir hacme entropi atama yöntemi, üç boyutta eğriliğin daha yüksek kuvvetlerine genelleştirilmiştir. Daha sonra, arka plan Killing yükleri kullanılarak, termodinamik yükler ve bunlara karşılık gelen eşlenikler yeniden tanımlanmış ve kara delik termodinamiği yasalarına ve ilgili uzay-zamanın geometrik ilişkilerine uyup uymadıkları kontrol edilmiştir. Son olarak, bir kara deliğin etrafındaki bir parçacığın kararsızlığı, uyarıldığında gerçekleştirdiği üstel olarak kararsız hareket ve bu harekete karşılık gelen Lyapunov üsleri dikkate alınarak incelenmiştir. Kararsızlık ile kara deliğin termodinamiği arasında olası bir bağlantı önerilmiştir. Gölge görüntüsüne ekvator dışı katkıların önemi tartışılmıştır.

Anahtar Kelimeler: Kara Delik, Işık Halkaları, Tekillik, Kara Delik Termodinamiği, İnstabilite.

To my family

ACKNOWLEDGMENTS

My fascination with black holes has shaped my academic path since the day I first read an article about them, and this thesis is a result of that long-standing curiosity.

I would like to express my sincere gratitude to my supervisor, Prof. Dr. Bayram Tekin, for his guidance and support throughout this thesis. His encouragement, patience, and clarity of thought have been invaluable at every stage of this work, and I am especially grateful for the time and care he devoted to mentoring me.

I am also grateful to Prof. Dr. Tahsin Çağrı Şişman for his valuable advice and insightful comments. I would like to thank Prof. Dr. Seçkin Kürkcüoğlu and Prof. Dr. Tahmasib Aliyev for their excellent courses during my education and for their encouragement in my academic and professional development.

I also thank my friends for their help and support during this demanding process.

I acknowledge TÜBİTAK for the financial support during my graduate education through 2211-A scholarship program.

Finally, I am deeply grateful to my family; without their unwavering encouragement and endless support, none of this would have been possible.

TABLE OF CONTENTS

LIST OF TABLES

TABLES

LIST OF FIGURES

FIGURES

LIST OF ABBREVIATIONS

ABRREVIATONS

KS Entropy	Kolmogorov-Sinai Entropy
dS	de Sitter
AdS	Anti-de Sitter
GH	Gibbons-Hawking
EGB	Einstein-Gauss-Bonnet
NMG	New massive gravity
BINMG	Born-Infeld new massive gravity

CHAPTER 1

INTRODUCTION

1.1 Motivation

This thesis is based on the following papers, of which the underlying theme is the study of observable properties of black holes:

- A. Tavlayan and B. Tekin, "Instability and information production around Kerr black holes: effects on entropy and the shadow," Eur. Phys. J. C **85** (2025) no.11, 1259.
- A. Tavlayan and B. Tekin, "Refined thermodynamics of black holes with proper conserved charges," Phys. Rev. D **110** (2024) no.8, 084049.
- A. Tavlayan and B. Tekin, "Partition function of a volume of space in a higher curvature theory," Phys. Rev. D **108** (2023) no.4, L041902.
- A. Tavlayan and B. Tekin, "Instability of a Kerr-type naked singularity due to light and matter accretion and its shadow," Class. Quant. Grav. **41** (2024) no.6, 065004.
- A. Tavlayan and B. Tekin, "Light rings around five dimensional stationary black holes and naked singularities," Phys. Rev. D **107** (2023) no.2, 024016.

Here, we shall summarize what was explored in these works. The rest of this thesis will be an expansion of these ideas and is based on the above works.

The existence of light rings in a spacetime is closely related to the existence of black hole horizons and observables such as the ringdown and the shadow. Black holes,

compared to nonvacuum ultracompact objects, have rather unique environments. To this aim, recently [1] topological arguments, independent of the underlying gravity theory, were developed to prove the existence of unstable light rings outside the Killing horizon of *four* dimensional asymptotically flat, stationary, axisymmetric, nonextremal black holes. Here, we extend these arguments to five-dimensional stationary black holes. Generically in five dimensions, there are two possible conserved angular momenta, hence the four-dimensional discussion does not extend verbatim to five dimensions; nevertheless, we prove that there is a light ring for each rotation sense for a stationary black hole. We give the static and the Myers-Perry rotating black holes as examples. We also show that when the horizon of the black hole disappears and the singularity becomes naked, only one of the light rings survives; a similar phenomenon also occurs in four dimensions, which might allow testing the cosmic censorship hypothesis.

We study null and timelike constant radii geodesics in the environment of an overspinning putative Kerr-type naked singularity. We are particularly interested in two topics: first, the differences of the shadows of the naked rotating singularity and the Kerr black hole; and second, the spinning down effect of the particles falling from the accretion disk. Around the naked singularity, the non-equatorial prograde orbits in the Kerr black hole remain intact up to a critical rotation parameter ($\alpha = \sqrt{6\sqrt{3}-9}$) and cease to exist above this value [2]. This has an important consequence in the shadow of the naked singularity if the shadow is registered by an observer on the polar plane or close to it as the shadow cannot be distinguished from that of a Kerr black hole viewed from the same angle considering only the light emanating from the unstable photon orbits. We show that the timelike retrograde orbits in the equatorial plane immediately (after about an 8% increase in mass for the case of initial $\alpha = 1.5$) reduce the spin parameter of the naked singularity from larger values to $\alpha = 1$ at which an event horizon appears. This happens because the retrograde orbits have a larger capture cross-section than the prograde ones. So if a naked singularity happens to have an accretion disk, it will not remain naked for long, an event horizon forms.

Recently in [3], Jacobson and Visser calculated the quantum partition function of a fixed, finite volume of a region with the topology of a ball in the saddle point approximation within the context of Einstein's gravity with or without a cosmological

constant. The result can be interpreted as the dimension of Hilbert space of the theory. Here, we extend their computation to a theory defined in principle with infinitely many powers of curvature in three dimensions. We confirm their result: The partition function of a spatial region in the leading saddle point approximation is given as the exponential of the Bekenstein-Hawking or the Wald entropy of the boundary of the finite spatial region both in the case of zero and finite cosmological constant. In the latter case, the effective Newton's constant appears in the entropy formula. The calculations lend support to the holographic nature of gravity for finite regions of space with a boundary.

Field equations of a classical, geometric, theory of gravity, augmented with some semiclassical considerations strongly suggest that the gravitational field representing a stationary black hole can be simply described with a few thermodynamical coordinates and their conjugates that obey the four laws of thermodynamics plus the Smarr formula and the reverse isoperimetric inequality that bounds the maximum entropy for a given effective volume of space. The thermodynamics of black holes is a promising window to the quantum nature of black holes; hence, it is important to understand all the details of these laws. The identification and the meaning of these thermodynamic coordinates depend on the gravity theory under consideration. For example, the existence of dimensionful coupling constants, such as the cosmological constant, changes the scaling properties of the theory, its solutions, and the laws of thermodynamics. Here we show, using the background Killing charge method, which applies to the black hole solutions of any gravity theory that has a maximally symmetric vacuum, to define the mass and angular momentum, instead of using the Komar mass and the angular momentum, how the thermodynamics of black holes such as the D dimensional Kerr-AdS black holes in cosmological Einstein's theory and the spherically symmetric black holes in the Einstein-Gauss-Bonnet theory changes. We give the effective volume of black holes even without a cosmological constant.

Massless or massive particles in unstable orbits around a Kerr black hole exhibit exponentially unstable motion when perturbed. They either plunge into the black hole or escape to infinity after making some oscillations around the equatorial plane. This exponentially unstable motion causes information production. In the case of the photons that escape to infinity, it was recently suggested that this information can be

used to resolve the subring structure of the shadow image and obtain more precise data about the black hole mass and spin [4]. Here, we extend this method to obtain more precise results by including the *non-equatorial* contributions to the Lyapunov exponents. For massive particles plunging into the Kerr black hole, we show that the associated Kolmogorov-Sinai entropy derived from the Lyapunov exponents can be interpreted in the context of black hole thermodynamics and obeys Bekenstein's bound on the entropy of a physical system. Thus, the perturbed unstable orbits, either ending inside the black hole or at the observer's screen, have physical consequences.

1.2 Light Rings Around Five-Dimensional Stationary Black Holes and Naked Singularities

Once considered as highly exotic objects that may not even exist, black holes have entered into the realm of direct observations in various ways: as sources of gravitational waves produced by their merger with each other [5, 6] (or with other compact objects such as neutron stars [7]); or via the image of their environment [8]. In both types of these observations, it is clear that the observables associated with the black holes are quite subtle: for the merger of binary black holes, the gravitational wave that hits the detector has a specific amplitude and frequency *variation* over the time of observation which match the combined analytical and numerical predictions of general relativity (in the inspiral, merger and ringdown phases of the event). These allow one to determine the properties of the individual black holes (such as their masses) that take part in the merger; and the luminosity distance at which the event took place. For the image of the supermassive black holes taken by the Event Horizon Telescope, one relies on the light rings, which are special bound null unstable geodesics around the black hole: basically, a photon can orbit around a black hole at a constant radius along the equatorial plane like a planet rotating around a central body. But there could in principle be ultracompact objects without horizons, made of some form of matter, that can mimic black holes. The question is to understand the differences in the environments of horizonless ultracompact objects and black holes.

A black hole in a vacuum, without a nontrivial environment, is hard to detect: to be clear, it certainly has a very unique gravitational skeleton (*i.e.* all its multipole

moments are related to each other as it has no additional hair beside its mass, angular momentum, and electric charge) which can be compared to a neutron star with all different multipole moments. But, the observables we can practically measure about a black hole are not the gravitational multipole moments. Hence one must resort to the environment of a black hole which seems to have rather unique properties (just like the mentioned unique properties of the vacuum black hole itself), such as the light rings; and these are related to the observables such as the ringdown and the shadow of the black hole. From this vantage point, the result of [1] becomes quite remarkable: under certain assumptions of symmetry and regularity, the existence of an unstable light ring (for each rotation sense) is related to the existence of null Killing horizons. On the other hand, ultracompact objects without horizons have a different environment as far as the light ring structure is concerned [9]. Hence, one can detect a black hole by observing its environment, and in particular, its light ring structure and the substructure. For generic photon orbits (not just the light rings) around the Kerr black hole [10], see [11] and [12] for the discussions and the references therein.

In the current work, we extend the topological arguments of [1] (which essentially boils down to defining a vector field that vanishes only at the location of the light ring) to generic five-dimensional stationary black holes. To understand the light ring structure around these black holes, it is clear that the effective potential for light must be chosen carefully, since there are two conserved angular momenta in five dimensions, and the impact parameters of light enter the effective potential functions. To properly set the stage, in Chapter 2 Section 2.1, we begin with the static five-dimensional spacetime and use the Schwarzschild-Tangherlini black hole as an example. In Section 2.2, we introduce the topological techniques and apply them to the static black hole. In Section 2.3, a generic stationary black hole is studied: first we discuss the degenerate angular momenta case and then move on to the distinct angular momenta case. As an example, we also study the Myers-Perry rotating solution. Section 2.4 is devoted to a brief study of the case when the event horizon disappears and one is left with a rotating, massive naked singularity. We show that in this case, in four and five dimensions, there is a single light ring.

1.3 Instability of a Kerr-Type Naked Singularity due to Light and Matter Accretion and Its Shadow

Nature has a very efficient way of constraining some physical quantities; it just uses square roots. For example, the speed of any object is restricted to less than the speed of light as the factor $\sqrt{1-v^2/c^2}$ appears in relativistic physics. Similarly, in black hole physics, the rotation of a black hole is restricted because the factor $\sqrt{1-\alpha^2}$, with α being the dimensionless rotation parameter given in SI units in terms of the spin J and mass m as $\alpha = cJ/(Gm^2)$, appears in the location of the event horizon. If $\alpha > 1$, there is no event horizon, and the black hole becomes a rotating, massive naked singularity that remains a solution to the vacuum Einstein equations.

As the stars or star systems typically have $\alpha > 1$ before a black hole is produced, it is clear that the angular momentum of the collapsing matter must be depleted to the values $\alpha < 1$ to form a black hole, otherwise a naked singularity is formed. Although one can envisage ways to deplete angular momentum, we still do not know exactly how Nature solves this problem. [For example, for our solar system $\alpha \approx 35$, most of the contribution comes from Jupiter's angular momentum, which is located far away from the central mass, the Sun.] Some observed black holes are rotating close to the extreme value $\alpha = 1$. With the singularity theorem of Penrose [13], a singularity is guaranteed to occur in a gravitational collapse under reasonable assumptions on the energy-momentum tensor of matter. However an event horizon is not guaranteed to form, we only have an expectation dubbed "the cosmic censorship hypothesis" [14] which states that collapsing matter does not form a naked singularity but it does not state that naked singularities do not exist on their own. Due to this state of affairs, one is necessarily curious about the observable differences in the causal environment of a naked singularity and the Kerr black hole. For example, can a naked singularity mimic the Kerr black hole [10] as far as its shadow [8] is concerned? Can accretion of matter to a naked singularity spin down its rotation in such a way that an event horizon forms? In this work, we study various null and timelike orbits around a naked singularity and make comparisons with the Kerr black hole; we also give a detailed account of the accretion of matter carrying angular momentum and mass to a naked singularity, assuming a thin equatorial accretion disk about it.

The layout of this work is as follows: In Chapter 3 Section 3.1 we study the null spherical geodesics around the naked singularity. In Section 3.2, we plot the shadows of various naked singularities. In Section 3.3, we concentrate on the null orbits at the critical inclination angle. In Section 3.4, we extend the discussion to timelike geodesics. In Section 3.5, we give a detailed study of the accretion for both the Kerr black hole and the Kerr-type singularity for thin disks and show the spinning-down effect for the naked singularity due to the matter falling from the unstable interior part of the disk.

1.4 Partition Function of a Volume of Space in a Higher Curvature Theory

Over the last five decades, we have come to understand that the gravitational field has typically a finite (nonzero) entropy; but which kinds of gravitational fields have entropy and how this entropy is defined is a subtle problem. However, the fact that the entropy has both macroscopic and microscopic definitions, and its microscopic description is most probably tied to the quantum version of the theory, makes it an invaluable tool in understanding some properties of low-energy quantum gravity. In the original incarnation [15, 16], the entropy of the gravitational field was assigned to *black hole horizons*. For example, the Bekenstein-Hawking entropy of a Schwarzschild black hole is

$$S_{BH} = \frac{k_B c^3}{4G\hbar} A_H, \tag{1.1}$$

where A_H is the area of the event horizon. Gibbons and Hawking [17] extended this result to the case of *de Sitter horizons*

$$S_{GH} = \frac{k_B c^3}{4G\hbar} A_{dS} = \frac{3\pi k_B c^3}{G\hbar\Lambda}, \tag{1.2}$$

where A_{dS} is the area of the cosmological horizon located at $r_H = \sqrt{3/\Lambda}$ in the usual coordinates. Note also that Λ is defined as $\Lambda = R/4$ with R being the constant scalar curvature of the de Sitter spacetime. In the same work, Gibbons and Hawking argue that the gravitational field of a stationary star has zero entropy. The physical meaning of the de Sitter entropy is not so clear; for example, in [18] seven possible interpretations were given. Here we will follow the interpretation advocated in [19, 20] which states that the de Sitter entropy is equal to the logarithm of the dimension of

the Hilbert space. One can understand the viability of this interpretation as follows: The trace of the unit operator ($\mathrm{Tr}\,\mathbb{1}$) which, for a finite-dimensional Hilbert space, is equal to the dimension of the Hilbert space. For de Sitter space, which does not have a boundary, the total Hamiltonian vanishes identically, and one has ($\dim\mathcal{H} = \mathrm{Tr}\,\mathbb{1} = \mathrm{Tr}e^{-\beta\hat{H}}$). The right-hand side at the same time is the partition function, which can be evaluated in the Euclidean path integral formulation. The new and exciting development in this subject is the work of Jacobson and Visser [3] where the entropy of a spatial region of space with a fixed proper volume and a boundary was defined in Einstein's theory with or without a cosmological constant. See [21] for more details. They show that in the saddle point approximation, the quantum gravity path integral under the fixed volume condition is dominated by the so-called constrained instantons [22, 23] of which the Euclidean action is minus the Bekenstein-Hawking entropy calculated for the area bounding the spatial volume. As long as Einstein's gravity is correct as an effective field theory, this computation is robust with only one caveat: There is a mild singularity in the Ricci tensor and the energy-momentum tensor in the boundary which does not make the action divergent. This divergence is expected to be cured when higher powers of curvature are added. This point motivated us to carry out an analogous computation in a higher curvature theory, which has rather nice properties and extends Einstein's gravity to infinitely many curvatures. The mild singularity observed in [3] is not cured, but the results of the computations lend strong support to [3].

The layout of this work is as follows: In Chapter 4, Section 4.1, we study the action of the Born-Infeld new massive gravity (BINMG) theory with the addition of the fixed volume constraint, and consider the corresponding partition function and field equations. In Section 4.2 and Section 4.3, we show how an entropy can be assigned to the fixed volumes to $\lambda_0 = 0$ and $\lambda_0 \neq 0$ solutions, respectively.

1.5 Refined Thermodynamics of Black Holes with Proper Conserved Charges

Quantum mechanics was born as a continuation of thermodynamics; an arduous process best exemplified by the long search of understanding the details, such as the exact spectrum of the black-body radiation. Fully understanding the fundamental

physics of the microscopic degrees of freedom that emit and absorb electromagnetic waves from a heated object required almost a century of work between the 1860s to 1960s, when quantum electrodynamics was established as a consistent theory of light and charged particles. Since the 1970s we are, in some sense, in a similar, albeit a much harder path: we are trying to understand the thermodynamics of a black-body that also self-gravitates, the case which necessarily forces us to understand the thermodynamics of the gravitational field. If the history rhymes, one hopes that after formulating consistent macroscopic thermodynamics for the gravitational field, one will also understand the statistical origins of these laws and eventually arrive at the quantum nature of gravity which presumably would involve identifying the microscopic degrees of freedom responsible for generating gravity. At the moment, we are far from this goal. Yet, so far, much has been accomplished in this vein: for example, we now understand that a quantum mechanical temperature that is proportional to $\hbar$ times the surface gravity can be assigned to a quasistationary black hole [16]; and one can associate an entropy with an arbitrary portion of a gravitational field both in Einstein's gravity [3] and in higher curvature theories [24], in the same way that the entropy was assigned to black holes [15] or de Sitter spacetimes [17]. In Einstein's gravity, besides the four laws of black hole mechanics, three of which are relations between the infinitesimal thermodynamical coordinates and their conjugates, one also has the Smarr relation [25] that arises as a result of dimensional analysis and connects the finite versions of these coordinates, which is akin to the Gibbs-Duhem relation in classical thermodynamics. Even though we only have theoretical arguments, the fact that some gravitational fields, such as those describing stationary black holes, obey the laws of thermodynamics is rather remarkable and by no means obvious because some of these solutions are pure geometry with no matter fields.

Einstein's gravity is expected to receive higher curvature corrections at small scales, most relevant to singularities of black holes and cosmological singularities. Understanding the refined thermodynamics of the gravitational field in these better-UV-behaved theories is crucial for quantum gravity. For example, the Smarr relation often fails when one considers these extended theories of gravity just like the laws of black hole thermodynamics unless one accommodates the corresponding corrections associated with the coupling constants that appear in each added term in the

action in a proper way [26, 27]. The crux of the matter here is the following: thermodynamical coordinates approximate the gravitational field in some sense, and must be defined properly not just as geometric objects computed from the metric or the geometry alone, but computed in a given theory. For example, the mass and angular momenta can be defined as Komar charges in a purely geometric way [28] or, as conserved charges in a given theory [29, 30, 31] corresponding to asymptotic or background symmetries. Here we follow the latter method: given a generic gravity theory defined by the covariant field equations $\mathcal{E}_{\mu\nu} = \kappa\mathcal{T}_{\mu\nu}$, one first searches for a vacuum solution (i.e., the background) $(\bar{g}_{\mu\nu})$ which is maximally symmetric with Killing vectors $\bar{\xi}^{\mu}$. Then for any other solution $g_{\mu\nu}$, be it a vacuum or nonvacuum solution, that asymptotically locally approaches the background solution, one can construct the *partially* conserved current $j^{\mu} := \sqrt{|\bar{g}|}\mathcal{E}_{L}^{\mu\nu}\bar{\xi}_{\nu}$. Integration of the zeroth component over the spatial volume yields the corresponding Killing charge $Q[\bar{\xi}] := \int_{\bar{\Sigma}} d^{(D-1)}x\sqrt{|\bar{g}|}\mathcal{E}_{L}^{0\nu}\bar{\xi}_{\nu}$. Furthermore, this integral can be reduced to a surface integral over $\partial\bar{\Sigma}$: For cosmological Einstein gravity, one arrives at the formula (5.12). The versatility of the model is clear: unlike the Komar charge definition that has a different numerical factor (i.e., Komar anomaly) for the mass and angular momentum, there is a single formula for all conserved charges; and the charge expression can easily be found for any geometric theory of gravity. One important caveat is the following: the background spacetime is assumed to have zero conserved charges in this method. Using these expressions, we establish the following: First in Chapter 5 Section 5.1, we show that the laws of black hole thermodynamics and the Smarr relation are satisfied for the cosmological Einstein gravity [32, 33, 34, 35]. Then, we show that these quantities respect the geometry such as the reverse isoperimetric inequality [36]. Finally in Section 5.2, we concentrate on the Einstein-Gauss-Bonnet (EGB) theory which has a dimensionful coupling constant and show that, by adding proper terms associated with it, new definitions of mass and angular momenta satisfy thermodynamics laws and the Smarr relation. The procedure outlined here can be extended to any gravity theory that admits a maximally symmetric spacetime as a solution as long as the black hole solutions are known.

1.6 Instability and Information Production Around Kerr Black Holes: Effects on Entropy and the Shadow

The Event Horizon Telescope (EHT) collaboration published the images of the environments of two supermassive black holes, the one at the center of the M87 galaxy [8] and our own Sagittarius A* [37]. What makes these images possible at all is the existence of unstable null orbits around the black hole: light revolves around the black hole like a planet in certain orbits, but either plunges into the hole or escapes to infinity when slightly perturbed. So, a black hole with an environment is prone to observation. As noted in [4], the images captured by the EHT Collaboration resolve the diameters of these black holes (40μas for M87 and 51.8μas for Sgt A*) but not the *subring structure* that is produced by photons, which complete, say $n/2$ complete orbits before they escape to the telescope. It was shown in [4] that the first few subrings (produced by the $n = 1$, $n = 2$, and $n = 3$ orbits) leave strong and universal signatures carrying information about the black hole parameters. These subrings are expected to be resolved by space-based sparse interferometric detectors. Here, one of our goals is to show that the addition of non-equatorial contributions from the accretion disc yields more precise information, especially for lower subring considerations. The contributions of the non-equatorial orbits were not considered in [4].

In addition to the orbits of light, we also study the orbits of massive particles that are slightly perturbed and end up inside the black hole, and interpret the information content of these orbits and their relation to entropy. Possible connections between information theory and black hole thermodynamics were first proposed almost half a century ago [15]. The subject started with the question of what happens if a spin-$1/2$ particle, of which every parameter is known except its spin, falls into the black hole. Unknown parameters introduce entropy according to information theory, and one should account for all possible states. In this particular question, the spin is unknown, and because there are only two possibilities, the associated entropy contains an $\ln 2$ term in units of the Boltzmann constant. We follow the same path here. We consider a particle with well-known position, mass, and energy orbiting in the vicinity of a Kerr black hole with given mass and rotation parameter. Then, we consider what happens if the particle in an unstable orbit is slightly perturbed and causing

it to plunge into the black hole. In this case, we demonstrate that it will exhibit exponentially unstable motion, producing an enormous amount of information. We should note that all causal geodesics are Liouville-integrable around a Kerr black hole owing to the existence of four conserved quantities, including Carter's constant, energy, z component of angular momentum, and the value of $g(p,p)$, where g is the metric and p is the four-momentum. Nevertheless, integrability does not require stability, and we are studying unstable orbits here. This increase in information can be associated with an increase in entropy, the Kolmogorov-Sinai entropy [38]. It is crucial to state that this entropy is a mathematical concept based on the Lyapunov exponents of the exponentially unstable motion. Nevertheless, here we suggest that it can be interpreted as a physical entropy, and, as a check, we show that it respects the theory's bounds. This interpretation means that there is a significant increase in the total entropy of the particle-black hole system when the particle undergoes exponentially unstable motion and passes the event horizon. The bound we consider is the Bekenstein bound [39], which puts dimensional constraints on the physical system that is orbiting the black hole with a known energy and entropy, to protect the generalized second law of black hole thermodynamics when it plunges into the black hole [40]. We assign the same amount of entropy that is produced by the exponentially unstable motion of the particle to a spherical volume by the method suggested in [3] in Einstein's theory and extended to higher derivative gravity in Chapter 4 [24]. We show that the entropy associated with this method satisfies the Bekenstein bound for a material system. This may be a new connection between information theory and black hole thermodynamics, and the concepts of this theory could be employed to explore statistical black hole thermodynamics, which may be a crucial step in finding a quantum gravity theory.

Let us note that the exponentially unstable motion around a black hole has been studied in the literature before: see [41, 42, 43, 44] and more recently [45], whose conventions as well as the conventions of [4] and [46] have been followed here. The layout of the work is as follows: In Chapter 6 Section 6.1, we discuss the basics of Lyapunov exponents and geodesic motion of the unstable orbits around the Kerr black hole. In Section 6.2, we consider the case of massive orbits for which we calculate the associated Lyapunov exponents, the Kolmogorov-Sinai entropy, and its relation to

the Bekenstein bound. In Section 6.3, we investigate the massless orbits that escape to infinity and demonstrate the connection between Lyapunov exponents and the sub-ring structure of the shadow image. The current work appears to discuss two separate topics: entropy and shadow. However, from our vantage point, the unifying theme is the study of the physical and, perhaps, observable consequences of the unstable orbits of massless and massive particles around a Kerr black hole.

CHAPTER 2

LIGHT RINGS AROUND FIVE DIMENSIONAL STATIONARY BLACK HOLES AND NAKED SINGULARITIES

2.1 Five Dimensional Static Spacetimes

In the coordinates $(t, r, \theta, \phi_1, \phi_2)$ [35], with the ranges,

$$t \in (-\infty, \infty), \;\; r \in [r_H, \infty), \;\; \theta \in \left[0, \frac{\pi}{2}\right], \;\; \phi_1 \in [0, 2\pi], \;\; \phi_2 \in [0, 2\pi], \tag{2.1}$$

the metric of the $4+1$ dimensional static black hole spacetime can be written as

$$ds^2 \;\; = \;\; \xi^2 dt^2 + g_{rr}\left(r, \theta\right) dr^2 + g_{\theta\theta}\left(r, \theta\right) d\theta^2 + \eta_1^2 d\phi_1^2 + \eta_2^2 d\phi_2^2, \tag{2.2}$$

where the timelike Killing vector field reads as $\xi := \frac{\partial}{\partial t}$ with the norm $\xi^2 = g_{tt}\left(r, \theta\right)$, and the rotation Killing vectors read as $\eta_1 := \frac{\partial}{\partial \phi_1}$ and $\eta_2 := \frac{\partial}{\partial \phi_2}$ with the obvious norms $\eta_1^2 = g_{\phi_1\phi_1}\left(r, \theta\right)$ and $\eta_2^2 = g_{\phi_2\phi_2}\left(r, \theta\right)$. So (t, ϕ_1, ϕ_2) are Killing coordinates, and (r, θ) are essential coordinates. We assume that there is a Killing horizon $r_H > 0$ at which $\xi^2(r_H) = 0$ and for all $r > r_H$, we have $\xi^2(r) < 0$. We also assume asymptotic flatness and causality $\xi^2(r \to \infty) \to -1$ and $\eta_{1,2}$ are spacelike.

In this background, we are interested in the existence of bound null geodesics, and in particular light rings. One way to do is to study the null Hamiltonian condition for a photon, which states that

$$H = \frac{1}{2} g^{\mu\nu} p_\mu p_\nu = 0, \tag{2.3}$$

where $p^\mu = \frac{dx^\mu}{d\lambda}$ represents the momentum of the photon where λ is an affine parameter. The Killing symmetries, dictate the following conserved quantities

$$\begin{aligned} p_t &= \langle \xi, p \rangle =: -E, \\ p_{\phi_1} &= \langle \eta_1, p \rangle =: \Phi_1, \\ p_{\phi_2} &= \langle \eta_2, p \rangle =: \Phi_2, \end{aligned} \tag{2.4}$$

where the inner product here is defined as $\langle \xi, p \rangle = \xi^\mu p_\mu$ and E, Φ_1, and Φ_2 represent the energy and angular momenta of the photon at spatial infinity, respectively.

We can split the Hamiltonian into a kinetic and a potential part as

$$\begin{aligned} K &= g^{rr} p_r^2 + g^{\theta\theta} p_\theta^2, \\ V &= g^{tt} E^2 + g^{\phi_1\phi_1} \Phi_1^2 + g^{\phi_2\phi_2} \Phi_2^2. \end{aligned} \tag{2.5}$$

If we restrict to the light ring, we have

$$p_r = p_\theta = \dot{p}_\mu = 0, \tag{2.6}$$

which implies that $K = 0$ and therefore $V = 0$. This is the *first* light ring condition. The second light ring condition follows from the Hamilton's equations which state that

$$\dot{p}_\mu \;=\; -\partial_\mu \left(\frac{1}{2} g^{\alpha\beta} p_\alpha p_\beta \right) = -\frac{1}{2} \left(\partial_\mu g^{rr} p_r^2 + \partial_\mu g^{\theta\theta} p_\theta^2 + \partial_\mu V \right). \tag{2.7}$$

The equation (2.7) together with (2.6) implies that $\partial_\mu V = 0$ which is the *second* light ring condition.

The crux of the above argument is this: one can study the light rings by just looking at the potential term only. But the drawback of this potential is that it directly depends on the parameters of the photon, E, Φ_1, and Φ_2. We would like to separate the properties of the photon from the properties of the background spacetime. In order to get rid of this dependence, it is useful to write the potential in the following form: first let us define

$$D := -\xi^2 \eta_1^2 \eta_2^2, \tag{2.8}$$

and multiply it with the potential

$$-V \times D = \eta_1^2 \eta_2^2 E^2 + \xi^2 \eta_2^2 \Phi_1^2 + \xi^2 \eta_1^2 \Phi_2^2. \tag{2.9}$$

At this stage, to better understand the problem, let us take the angular momenta to be equal (a simplification which we shall remove in the spinning black hole case). Then $\Phi_1 = \Phi_2 := \Phi$. Furthermore, due to the equivalence principle, there is no gravitational rainbow (photons with different energies can circle the same geodesic),

therefore we can eliminate the energy of the photon by using the inverse impact parameter as usual[1]

$$\sigma := \frac{E}{\Phi}, \tag{2.10}$$

with the help of which, the effective potential factors as

$$V = \frac{\Phi^2}{\xi^2}\left(\sigma - \sigma_-\right)\left(\sigma - \sigma_+\right) \tag{2.11}$$

where the effective potential functions are independent of the properties of the light and are determined by the geometry alone:

$$\sigma_\pm = \pm\sqrt{-\xi^2\left(\frac{1}{\eta_1^2} + \frac{1}{\eta_2^2}\right)}. \tag{2.12}$$

Now, the first light ring condition ($V = 0$) states that σ is either equal to σ_- or σ_+, and this only determines the impact parameter in terms of the geometry. But, the second light ring condition, that is the flatness of the potential in *all* directions $\partial_\mu V = 0$, carries a great deal more information which we shall explore now.

In order to understand the 'gradient flows' associated with the second light ring condition, it is best to define a two dimensional vector field as [9]

$$v_r := \frac{\partial_r \sigma_\pm}{\sqrt{g_{rr}}}, \quad v_\theta := \frac{\partial_\theta \sigma_\pm}{\sqrt{g_{\theta\theta}}}, \tag{2.13}$$

which was normalized as above to yield $\partial^\mu \sigma_\pm \partial_\mu \sigma_\pm = v_r^2 + v_\theta^2 =: v^2$ Hence the second light ring condition dictates that $\vec{v} = 0$. Furthermore, defining the angle Ω as $v_r = v\cos\Omega$ and $v_\theta = v\sin\Omega$, one can see that the integral $\oint_C d\Omega$ over a closed curve C in the (r, θ) space should yield $2\pi w$ with w being the winding number taking values in integers. Hence as shown in [1], w is a well-defined topological number that one can assign to light rings:

$$w = \frac{1}{2\pi}\oint_C d\Omega(r, \theta), \tag{2.14}$$

where C can be deformed to any other contour as long as a light ring is not crossed. The sign of w is just a convention: for a counterclockwise C, negative winding corresponds to a standard light ring.

[1] Here, we assume that the photon is sufficiently energetic so that its wavelength is small compared to the variations in the gravitational field, hence the ray optics approximation works.

At this stage, let us consider the simplest case: the five dimensional Schwarzschild-Tangherlini black hole with the metric functions given as

$$\begin{aligned} &g_{tt} = -\left(1 - \frac{\mu}{r^2}\right), \quad g_{rr} = \left(1 - \frac{\mu}{r^2}\right)^{-1} \\ &g_{\theta\theta} = r^2, \quad g_{\phi_1\phi_1} = r^2 \sin^2\theta, \quad g_{\phi_2\phi_2} = r^2 \cos^2\theta, \\ &D = \left(r^2 - \mu\right) r^2 \sin^2\theta \cos^2\theta, \end{aligned} \tag{2.15}$$

where μ is related to the mass of the black hole via

$$\mu = \frac{8GM}{3\pi}. \tag{2.16}$$

Hence, the effective potential functions become

$$\sigma_{\pm} = \frac{\pm 1}{r^2 \sin\theta \cos\theta} \sqrt{r^2 - \mu}. \tag{2.17}$$

The vector field components can be calculated as

$$v_r = \pm \frac{1}{r^4 \sin\theta \cos\theta} \left(2\mu - r^2\right), \tag{2.18}$$

and

$$v_\theta = \mp \frac{4\sqrt{r^2 - \mu}}{r^3} \left(\frac{\cos 2\theta}{\sin^2 2\theta}\right). \tag{2.19}$$

As stated above, the light ring corresponds to the particular point in the vector field which has the property

$$v_r^2 + v_\theta^2 = 0 \rightarrow v = 0. \tag{2.20}$$

Therefore, we can conclude that the light ring is located at $r = \sqrt{2\mu}$ and $\theta = \frac{\pi}{4}$. In other words, we have a standard light ring outside the horizon for a five dimensional static black hole. Now, we can confirm this by using the topological charge and the winding number concepts.

2.2 Contour Analysis and the Winding Number for the static black hole in 5 dimensions

Let us assume, we have a contour outside the horizon which can be described as in Fig. (2.1) with the following line segments

I_1: $r = R, \;\; \delta \leq \theta \leq \frac{\pi}{2} - \delta,$

I_2: $\theta = \frac{\pi}{2} - \delta, \quad r_0 \leq r \leq R,$

I_3: $r = r_0, \quad \delta \leq \theta \leq \frac{\pi}{2} - \delta,$

I_4: $\theta = \delta, \quad r_0 \leq r \leq R.$

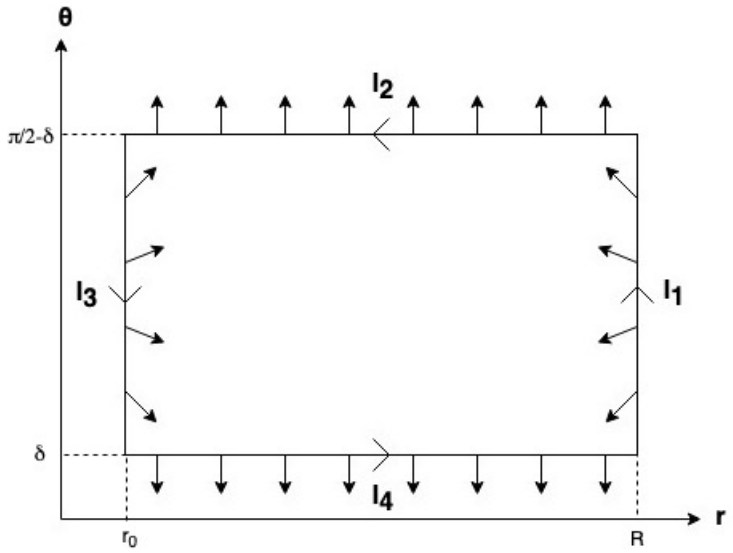

Figure 2.1: The representation of the results found in the contour analysis. The vector field, $\vec{v}$, obtained by using the effective potential of the positive rotation sense can be seen along the contour. The full negative winding is apparent.

Now, we would like to investigate how the vector field $\vec{v}$ changes along this contour. But we must cover all the exterior region to the black hole, which means that at the end, our contour should be extended to all the (r, θ) plane outside the horizon. Hence, we must take the limits $\delta \to 0$, $r_0 \to r_H$ and $R \to \infty$. The order of the limits is important [1]. Let us study each line segment separately.

2.2.1 Line segment I_4

From (2.18) and (2.19), one observes that as $\delta \to 0$ and therefore $\theta \to 0$ along the line segment I_4: the components of the vector field become

$$v_r \propto \pm \frac{1}{\sin\theta} \tag{2.21}$$

and

$$v_\theta \propto \mp \frac{1}{\sin^2 2\theta}. \tag{2.22}$$

Hence, v_θ is the dominant component of the vector field and we have

$$\Omega = \arcsin\left(\frac{v_\theta}{v}\right)\Big|_0 \to \mp\pi/2 \text{ for } \theta \to 0 \tag{2.23}$$

along I_4.

2.2.2 Line segment I_2

Similarly, as $\delta \to 0$ and therefore $\theta \to \frac{\pi}{2}$ along the line segment I_2

$$v_r \propto \pm \frac{1}{\cos\theta} \tag{2.24}$$

and

$$v_\theta \propto \mp \frac{1}{\sin^2 2\theta}. \tag{2.25}$$

Hence, v_θ is the dominant component of the vector field and

$$\Omega = \arcsin\left(\frac{v_\theta}{v}\right)\Big|_{\frac{\pi}{2}} \to \pm\pi/2 \text{ for } \theta \to \frac{\pi}{2} \tag{2.26}$$

along I_2.

2.2.3 Line segment I_3

The event horizon for the five dimensional static black hole in the given coordinates is located at $r_H = \sqrt{\mu}$. While approaching the horizon, the r component of the vector field (2.18) does not change sign along I_3. The term in the parenthesis is always positive while approaching the event horizon and $r^4 \sin\theta\cos\theta = \frac{r^4}{2}\sin 2\theta$ is always positive for $\theta \in \left[0, \frac{\pi}{2}\right]$. Therefore, for

$$\sigma = \sigma_+, \quad v_r \to + \tag{2.27}$$

and for

$$\sigma = \sigma_-, \qquad v_r \to -. \tag{2.28}$$

Yet, the θ component of the vector field changes (2.19) sign along I_3, because it has $\cos 2\theta$, which is negative for $\theta \in \left[\frac{\pi}{4}, \frac{\pi}{2}\right]$ and is positive for $\theta \in \left[0, \frac{\pi}{4}\right]$. This constitutes the half of the winding as can be seen in Fig. (2.1).

2.2.4 Line segment I_1

The same argument as with the line segment I_3 can be used here. The v_r does not change sign along I_1 and points opposite to I_3. The v_θ component of the vector field changes sign because for a counterclockwise rotation, it starts at a negative direction and ends in the positive direction for the positive rotation sense and this constitutes the other half of the winding as can be seen in Fig. (2.1).

To summarize, in order to evaluate (2.14), we decomposed the contour into four lines, and investigated each lines separately. In other words, we wrote the winding number as (where the proper limits are to be understood)

$$\omega := \omega_{I_1} + \omega_{I_2} + \omega_{I_3} + \omega_{I_4}, \tag{2.29}$$

where

$$\omega_{I_i} \;\; := \tfrac{1}{2\pi} \;\; \int_{I_i} d\Omega(r,\theta), \;\; i \in (1,2,3,4). \tag{2.30}$$

We showed that there is no contribution to the winding number along the lines I_2 and I_4, in other words, $\omega_{I_2} = 0$ and $\omega_{I_4} = 0$. We also showed that there are two negative half windings along the lines I_1 and I_3, and hence $\omega_{I_1} = -\frac{1}{2}$ and $\omega_{I_3} = -\frac{1}{2}$. In conclusion, we obtained $\omega = -1$, which implies that we had a standard light ring inside the contour.

The general behavior of the vector field around the light ring is plotted in Fig. (2.2) and Fig. (2.3).

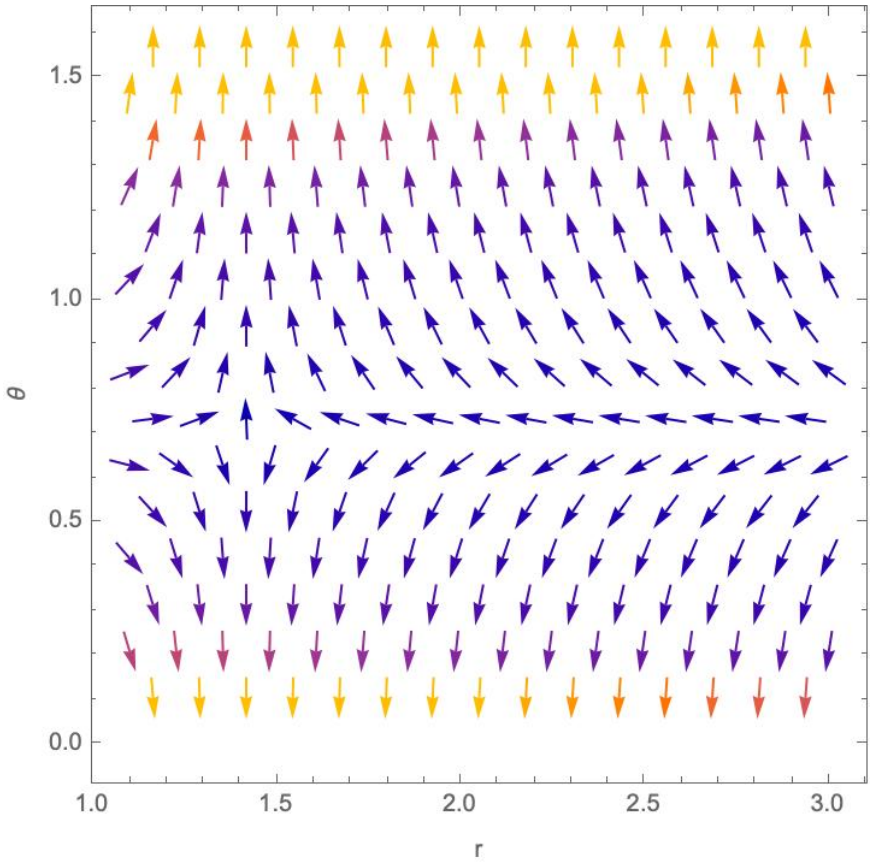

Figure 2.2: $\vec{v} = \left(\frac{1}{r^4 \sin\theta\cos\theta}\left(2-r^2\right), -\frac{4\sqrt{r^2-1}}{r^3}\left(\frac{\cos 2\theta}{\sin^2 2\theta}\right)\right)$ obtained by using the effective potential function associated with the positive rotation sense is plotted in the neighborhood of the standard light ring ($r = \sqrt{2}$, $\theta = \pi/4$) for the static spacetime with two equal angular momenta.

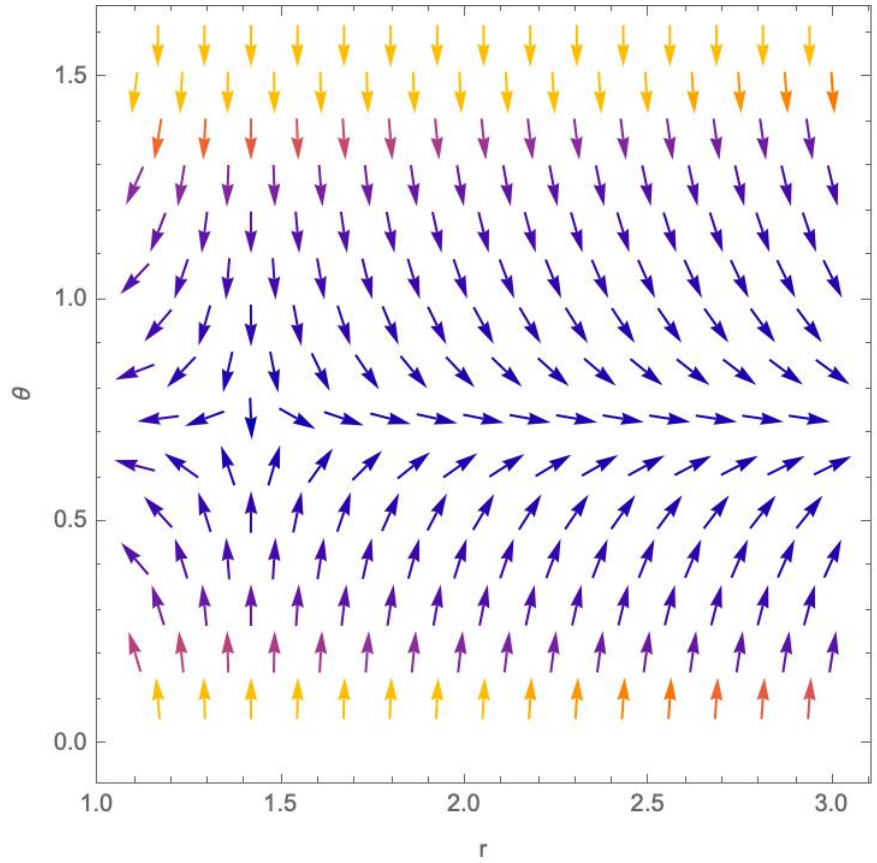

Figure 2.3: $\vec{v} = \left(\frac{-1}{r^4 \sin\theta \cos\theta} \left(2 - r^2\right), \frac{4\sqrt{r^2-1}}{r^3} \left(\frac{\cos 2\theta}{\sin^2 2\theta} \right) \right)$ obtained by using the effective potential function associated with the negative rotation sense is plotted in the neighborhood of the standard light ring ($r = \sqrt{2}$, $\theta = \pi/4$) for the static spacetime with two equal angular momenta.

2.3 Spinning Black Holes in 5 dimensions

Let us now consider three Killing vectors to be nonorthogonal to each other, such that in the coordinates $(t, r, \theta, \phi_1, \phi_2)$ the metric of the five dimensional stationary black hole reads as

$$\begin{aligned} ds^2 &= \xi^2 dt^2 + g_{rr}(r,\theta)\, dr^2 + g_{\theta\theta}(r,\theta)\, d\theta^2 \\ &\quad + \eta_1^2 d\phi_1^2 + \eta_2^2 d\phi_2^2 + 2(\xi,\eta_2) dt d\phi_2 \\ &\quad + 2(\eta_1,\eta_2) d\phi_1 d\phi_2 + 2(\xi,\eta_1) dt d\phi_1, \end{aligned} \tag{2.31}$$

where $(\eta_1, \eta_2) = g_{\phi_1\phi_2}(r,\theta)$ etc. As in the static case, the Hamiltonian can be split into the kinetic and potential parts. The kinetic part is the same as the static case,

$$K = g^{rr} p_r^2 + g^{\theta\theta} p_\theta^2, \tag{2.32}$$

but the potential now has cross terms and reads as

$$V = g^{tt} E^2 + g^{\phi_1\phi_1}\Phi_1^2 + g^{\phi_2\phi_2}\Phi_2^2 - 2g^{t\phi_1} E\Phi_1 - 2g^{t\phi_2} E\Phi_2 + 2g^{\phi_1\phi_2}\Phi_1\Phi_2, \tag{2.33}$$

which can be recast as

$$\begin{aligned} V &= -\frac{1}{D}\left[E^2\left(\eta_1^2\eta_2^2 - (\eta_1,\eta_2)^2\right) + 2\Phi_1\Phi_2\left((\xi,\eta_1)(\xi,\eta_2) - \xi^2(\eta_1,\eta_2)\right)\right. \\ &\quad + \Phi_1^2\left(\xi^2\eta_2^2 - (\xi,\eta_2)^2\right) + 2E\Phi_1\left((\xi,\eta_1)\eta_2^2 - (\xi,\eta_2)(\eta_1,\eta_2)\right) \\ &\quad \left. + \Phi_2^2\left(\xi^2\eta_1^2 - (\xi,\eta_1)^2\right) + 2E\Phi_2\left((\xi,\eta_2)\eta_1^2 - (\xi,\eta_1)(\eta_1,\eta_2)\right)\right], \end{aligned} \tag{2.34}$$

where

$$D := \eta_1^2(\xi,\eta_2)^2 + \eta_2^2(\xi,\eta_1)^2 + \xi^2(\eta_1,\eta_2)^2 - \xi^2\eta_1^2\eta_2^2 - 2(\xi,\eta_1)(\xi,\eta_2)(\eta_1,\eta_2). \tag{2.35}$$

Once again, due the equivalence principle, energy of the light will not play a role by itself, and we can pull it out as a factor in the effective potential. At this stage the discussion bifurcates: if the angular momenta of the light are equal to each other, the problem is easier to handle, if not, one needs to work a little harder. Let us study these two cases separately.

2.3.1 Case I: Equal angular momenta

Let $\Phi_1 = \Phi_2 = \Phi$ and define, as in the static case, the inverse impact parameter

$$\sigma := \frac{E}{\Phi} \tag{2.36}$$

then (2.34) reduces to

$$\begin{aligned} V &= -\frac{\Phi^2}{D}\left[\sigma^2\left(g_{\phi_1\phi_1}g_{\phi_2\phi_2}-g_{\phi_1\phi_2}^2\right)+2\sigma\left(g_{t\phi_1}\left(g_{\phi_2\phi_2}-g_{\phi_1\phi_2}\right)\right.\right. \\ &\quad \left.\left.+g_{t\phi_2}\left(g_{\phi_1\phi_1}-g_{\phi_1\phi_2}\right)\right)+\left(g_{tt}\left(g_{\phi_1\phi_1}+g_{\phi_2\phi_2}-2g_{\phi_1\phi_2}\right)-\left(g_{t\phi_1}-g_{t\phi_2}\right)^2\right)\right] \end{aligned} \tag{2.37}$$

where, we have introduced the metric components explicitly. The effective potential factors as

$$V=-\frac{\Phi^2}{D}\left(\sigma-\sigma_+\right)\left(\sigma-\sigma_-\right) \tag{2.38}$$

with

$$\sigma_\pm := \frac{A_\pm}{B} \tag{2.39}$$

where

$$\begin{aligned} A_\pm := \quad & -g_{\phi_2\phi_2}g_{t\phi_1}-g_{\phi_1\phi_1}g_{t\phi_2}+g_{t\phi_1}g_{\phi_1\phi_2}+g_{t\phi_2}g_{\phi_1\phi_2} \\ & \pm\sqrt{D\left(g_{\phi_1\phi_1}+g_{\phi_2\phi_2}-2g_{\phi_1\phi_2}\right)} \end{aligned} \tag{2.40}$$

and

$$B := g_{\phi_1\phi_1}g_{\phi_2\phi_2}-g_{\phi_1\phi_2}^2. \tag{2.41}$$

In order to find the light ring outside the event horizon, we are going to follow a similar approach with the static case and investigate the gradient flows along a contour and take limits to cover all the space outside the Killing horizon.

2.3.1.1 Axis limits

A: $\theta \to 0$

In order to understand the behavior of the metric components while approaching the axis, it is beneficial to introduce a local coordinate [1]

$$\rho^2 := g_{\phi_1\phi_1} \tag{2.42}$$

and $\rho \to 0$ as $\theta \to 0$. The other metric components can be expanded in terms of ρ as

$\rho \to 0$. Keeping the dominant terms, we have

$$\begin{aligned} g_{tt} &\approx g_{tt}^{(0)} + O(\rho), \\ g_{t\phi_1} &\approx \rho^n + O\left(\rho^{n+1}\right), \\ g_{t\phi_2} &\approx g_{t\phi_2}^{(0)} + O(\rho), \\ g_{\phi_1\phi_2} &\approx \rho^m + O\left(\rho^{m+1}\right), \\ g_{\phi_2\phi_2} &\approx g_{\phi_2\phi_2}^{(0)} + O(\rho). \end{aligned} \tag{2.43}$$

At this point, it is important to emphasize the fact that $n \geq 2$ and $m \geq 2$. This can easily be shown by extending the regularity ideas developed in [1] and require a nonvanishing scalar curvature . [We give the details of this in the Appendix-A: Calculation of the Ricci Scalar.] By using these expansions, one has

$$D \approx \rho^2 \left(\left(g_{t\phi_2}^{(0)}\right)^2 + g_{\phi_2\phi_2}^{(0)} \frac{\rho^{2n}}{\rho^2} + g_{tt}^{(0)} \frac{\rho^{2m}}{\rho^2} - g_{tt}^{(0)} g_{\phi_2\phi_2}^{(0)} - 2 g_{t\phi_2}^{(0)} \frac{\rho^{n+m}}{\rho^2} \right). \tag{2.44}$$

Because of the fact that $g_{\phi_1\phi_1}$ cannot go to zero faster than $g_{t\phi_1}$ and $g_{\phi_1\phi_2}$, one has

$$D \approx \rho^2 \left(\left(g_{t\phi_2}^{(0)}\right)^2 - g_{tt}^{(0)} g_{\phi_2\phi_2}^{(0)} \right), \tag{2.45}$$

while

$$A \approx \rho^2 \left(-g_{t\phi_2}^{(0)} \pm \left[\left(\left(g_{t\phi_2}^{(0)}\right)^2 - g_{tt}^{(0)} g_{\phi_2\phi_2}^{(0)} \right) \left(1 + \frac{g_{\phi_2\phi_2}^{(0)}}{\rho^2} \right) \right]^{\frac{1}{2}} \right), \tag{2.46}$$

and

$$B \approx \quad \rho^2 g_{\phi_2\phi_2}^{(0)} - \rho^{2m} \approx \rho^2 \left(g_{\phi_2\phi_2}^{(0)} \right). \tag{2.47}$$

As a consequence,

$$\begin{aligned} \sigma_\pm &\approx -\frac{g_{t\phi_2}^{(0)}}{g_{\phi_2\phi_2}^{(0)}} \pm \frac{\left[\left(\left(g_{t\phi_2}^{(0)}\right)^2 - g_{tt}^{(0)} g_{\phi_2\phi_2}^{(0)} \right) \left(1 + \frac{g_{\phi_2\phi_2}^{(0)}}{\rho^2} \right) \right]^{\frac{1}{2}}}{g_{\phi_2\phi_2}^{(0)}} \\ &\approx -\frac{g_{t\phi_2}^{(0)}}{g_{\phi_2\phi_2}^{(0)}} \pm \frac{1}{\rho} \frac{\left[\left(\left(g_{t\phi_2}^{(0)}\right)^2 - g_{tt}^{(0)} g_{\phi_2\phi_2}^{(0)} \right) \left(\rho^2 + g_{\phi_2\phi_2}^{(0)} \right) \right]^{\frac{1}{2}}}{g_{\phi_2\phi_2}^{(0)}} \\ &\approx \text{constant} \pm \frac{1}{\rho} \times \text{constant}. \end{aligned} \tag{2.48}$$

The forms of $\sigma_\pm$ imply that $v_r \propto \frac{1}{\rho}$ and $v_\theta \propto \frac{1}{\rho^2}$. Therefore, v_θ is dominant as $\rho \to 0$. As a conclusion,

$$\Omega = \arcsin\left(\frac{v_\theta}{v}\right)\Big|_0 \to \mp\pi/2 \text{ for } \theta \to 0. \tag{2.49}$$

B: $\theta \to \frac{\pi}{2}$

A similar approach in the $\theta \to 0$ limit, after defining the local coordinate as

$$\rho^2 := g_{\phi_2\phi_2}. \tag{2.50}$$

yields

$$\sigma_\pm \approx \text{constant} \pm \frac{1}{\rho} \times \text{constant}. \tag{2.51}$$

In conclusion

$$\Omega = \arcsin\left(\frac{v_\theta}{v}\right)\Big|_{\frac{\pi}{2}} \to \pm\pi/2 \text{ for } \theta \to \frac{\pi}{2}. \tag{2.52}$$

2.3.1.2 Horizon limit

In order to investigate the behavior of the metric components while approaching the horizon, it is useful to introduce the lapse function, defined as

$$N := \left(-g^{tt}\right)^{\left(-\frac{1}{2}\right)} = \left[-\frac{g_{t\phi_2}^2 g_{\phi_1\phi_1} - 2g_{t\phi_1}g_{t\phi_2}g_{\phi_1\phi_2} + g_{t\phi_1}^2 g_{\phi_2\phi_2}}{g_{\phi_1\phi_2}^2 - g_{\phi_1\phi_1}g_{\phi_2\phi_2}} - g_{tt}\right]^{\frac{1}{2}}. \tag{2.53}$$

Recalling that

$$D = g_{\phi_1\phi_1}g_{t\phi_2}^2 + g_{\phi_2\phi_2}g_{t\phi_1}^2 + g_{tt}g_{\phi_1\phi_2}^2 - g_{tt}g_{\phi_1\phi_1}g_{\phi_2\phi_2} - 2g_{t\phi_1}g_{t\phi_2}g_{\phi_1\phi_2}, \tag{2.54}$$

one can write the lapse function as

$$N^2 \;=\; -\frac{D}{g_{\phi_1\phi_2}^2 - g_{\phi_1\phi_1}g_{\phi_2\phi_2}}. \tag{2.55}$$

The Killing vector field (with constant $\Omega_{1,2}$)

$$\chi := \partial_t + \Omega_1\partial_{\phi_1} + \Omega_2\partial_{\phi_2} \tag{2.56}$$

is null on the horizon,

$$\left(\chi_\mu\chi^\mu\right)|_H = 0, \tag{2.57}$$

given that these constants are chosen as

$$\Omega_1 := \left(\frac{g_{t\phi_2}g_{\phi_1\phi_2} - g_{t\phi_1}g_{\phi_2\phi_2}}{g_{\phi_1\phi_1}g_{\phi_2\phi_2} - g_{\phi_1\phi_2}^2}\right)_H \tag{2.58}$$

and

$$\Omega_2 := \left(\frac{g_{t\phi_1}g_{\phi_1\phi_2} - g_{t\phi_2}g_{\phi_1\phi_1}}{g_{\phi_1\phi_1}g_{\phi_2\phi_2} - g_{\phi_1\phi_2}^2}\right)_H. \tag{2.59}$$

By defining two functions that extend $\Omega_{1,2}$ beyond the horizon

$$\omega_1 := \frac{g_{t\phi_2} g_{\phi_1\phi_2} - g_{t\phi_1} g_{\phi_2\phi_2}}{g_{\phi_1\phi_1} g_{\phi_2\phi_2} - g_{\phi_1\phi_2}^2}, \tag{2.60}$$

and

$$\omega_2 := \frac{g_{t\phi_1} g_{\phi_1\phi_2} - g_{t\phi_2} g_{\phi_1\phi_1}}{g_{\phi_1\phi_1} g_{\phi_2\phi_2} - g_{\phi_1\phi_2}^2}, \tag{2.61}$$

we can write the effective potential functions as

$$\sigma_\pm \;=\; \omega_1 + \omega_2 \pm N \sqrt{\frac{g_{\phi_1\phi_1} + g_{\phi_2\phi_2} - 2g_{\phi_1\phi_2}}{g_{\phi_1\phi_1} g_{\phi_2\phi_2} - g_{\phi_1\phi_2}^2}}. \tag{2.62}$$

Note that this can be expressed as a function of the Killing vectors ξ, η_1, η_2, but the above form is easier to work with.

Now, we introduce two coordinates, n, z, where n represents the normal distance to the horizon which vanishes at the horizon, and the z direction is perpendicular to n. One can write the other components as a function of these two coordinates. Without loss of generality, we can safely assume, outside the horizon, $g_{nn} = 1$. By generalizing the approximation ideas introduced in [47], we obtain

$$\begin{aligned}
g_{\phi_1\phi_1}(n,z) &= [g_H]_{\phi_1\phi_1}(z) + O\left(n^2\right), \\
g_{\phi_2\phi_2}(n,z) &= [g_H]_{\phi_2\phi_2}(z) + O\left(n^2\right), \\
g_{\phi_1\phi_2}(n,z) &= [g_H]_{\phi_1\phi_2}(z) + O\left(n^2\right), \\
N(n,z) &= \kappa_H n + O\left(n^3\right), \\
\omega_1(n,z) &= \Omega_1 + O\left(n^3\right), \\
\omega_2(n,z) &= \Omega_2 + O\left(n^3\right),
\end{aligned} \tag{2.63}$$

where κ_H is the surface gravity which is a nonzero constant on the horizon. Therefore, near the horizon, the effective potential functions become

$$\begin{aligned}
\sigma_\pm &\approx \Omega_1 + \Omega_2 \pm \kappa_H n \sqrt{\frac{[g_H]_{\phi_1\phi_1} + [g_H]_{\phi_2\phi_2} - 2[g_H]_{\phi_1\phi_2}}{[g_H]_{\phi_1\phi_1}[g_H]_{\phi_2\phi_2} - [g_H]_{\phi_1\phi_2}^2}} \\
&\approx \text{constant} \pm \kappa_H n \times \text{constant}.
\end{aligned} \tag{2.64}$$

Since,

$$\frac{1}{\sqrt{g_{nn}}}\frac{\partial}{\partial_n} = \frac{1}{\sqrt{g_{rr}}}\frac{\partial}{\partial_r} \tag{2.65}$$

near the horizon, and $g_{nn} = 1$, we have

$$\begin{aligned} v_{r,\pm} &= \frac{1}{\sqrt{g_{rr}}}\frac{\partial}{\partial_r}\sigma_\pm = \frac{\partial}{\partial_n}\sigma_\pm \\ &\approx \pm\kappa_H\sqrt{\frac{[g_H]_{\phi_1\phi_1} + [g_H]_{\phi_2\phi_2} - 2\,[g_H]_{\phi_1\phi_2}}{[g_H]_{\phi_1\phi_1}\,[g_H]_{\phi_2\phi_2} - [g_H]^2_{\phi_1\phi_2}}}. \end{aligned} \tag{2.66}$$

The important observation is that there is no sign change in the horizon limit. Therefore we can say that for positive effective potential, v_r is always positive, and for negative effective potential, v_r is always negative. Nevertheless, the angular component (v_θ) changes sign during the contour, because for a positive rotation sense, it starts in the positive direction and ends in the negative direction. This contributes a negative half winding, as expected.

2.3.1.3 Asymptotic limit

In the asymptotic limit, we have a flat spacetime in spherical coordinates

$$\begin{aligned} &g_{tt} \approx -1, \qquad g_{t\phi_1} = 0, \qquad g_{t\phi_2} = 0, \\ &g_{rr} \approx 1, \qquad g_{\theta\theta} \approx r^2, \qquad g_{\phi_1\phi_2} = 0, \\ &g_{\phi_1\phi_1} \approx r^2\sin^2\theta, \qquad g_{\phi_2\phi_2} \approx r^2\cos^2\theta. \end{aligned} \tag{2.67}$$

This yields

$$v_{r,\pm} = \frac{1}{\sqrt{g_{rr}}}\frac{\partial}{\partial_r}\sigma_\pm = \frac{\partial}{\partial_r}\sigma_\pm \tag{2.68}$$

where

$$\sigma_\pm = \pm\sqrt{-g_{tt}\left(\frac{1}{g_{\phi_1\phi_1}} + \frac{1}{g_{\phi_2\phi_2}}\right)} = \pm\frac{1}{r\sin\theta\cos\theta}. \tag{2.69}$$

Therefore,

$$v_{r,\pm} = \mp\frac{1}{r^2\sin\theta\cos\theta}. \tag{2.70}$$

Since to $\theta \in \left[0, \frac{\pi}{2}\right]$, $\sin\theta\cos\theta > 0$, one has

$$\text{sign}\left(v_{r,\pm}\right)|_\infty = \mp 1. \tag{2.71}$$

This is sufficient. The angular component changes sign and it contributes a negative half winding. The discussion in the paragraph including (2.30) applies here verbatim

and one gets a total winding number -1 which refers to a standard light ring.

2.3.2 Case II: Distinct angular momenta

At this point, we would like to investigate the solutions with distinct angular momenta of light $\Phi_1 \neq \Phi_2$. The effective potential can be written as

$$\begin{aligned} V &= -\frac{1}{D}\left(g_{\phi_1\phi_1}g_{\phi_2\phi_2}-g_{\phi_1\phi_2}^2\right)\times\Bigg[E^2+E\left(2\Phi_1\left(\frac{g_{t\phi_1}g_{\phi_2\phi_2}-g_{t\phi_2}g_{\phi_1\phi_2}}{g_{\phi_1\phi_1}g_{\phi_2\phi_2}-g_{\phi_1\phi_2}^2}\right)\right. \\ &\left.+2\Phi_2\left(\frac{g_{t\phi_2}g_{\phi_1\phi_1}-g_{t\phi_1}g_{\phi_1\phi_2}}{g_{\phi_1\phi_1}g_{\phi_2\phi_2}-g_{\phi_1\phi_2}^2}\right)\right)+\left(\Phi_1^2\left(\frac{g_{tt}g_{\phi_2\phi_2}-g_{t\phi_2}^2}{g_{\phi_1\phi_1}g_{\phi_2\phi_2}-g_{\phi_1\phi_2}^2}\right)\right. \\ &\left.+\Phi_2^2\left(\frac{g_{tt}g_{\phi_1\phi_1}-g_{t\phi_1}^2}{g_{\phi_1\phi_1}g_{\phi_2\phi_2}-g_{\phi_1\phi_2}^2}\right)+2\Phi_1\Phi_2\left(\frac{g_{t\phi_1}g_{t\phi_2}-g_{tt}g_{\phi_1\phi_2}}{g_{\phi_1\phi_1}g_{\phi_2\phi_2}-g_{\phi_1\phi_2}^2}\right)\right)\Bigg]. \end{aligned} \tag{2.72}$$

Here, instead of the inverse impact parameters $\sigma_{1,2}$, it pays to use the impact parameters $b_{1,2}$, hence pulling out the E^2, the effective potential factors as

$$V=-\frac{E^2}{D}\left(g_{\phi_1\phi_1}g_{\phi_2\phi_2}-g_{\phi_1\phi_2}^2\right)\left(1-b_+\right)\left(1-b_-\right), \tag{2.73}$$

where

$$b_\pm := -b_1\left(\frac{g_{t\phi_1}g_{\phi_2\phi_2}-g_{t\phi_2}g_{\phi_1\phi_2}}{g_{\phi_1\phi_1}g_{\phi_2\phi_2}-g_{\phi_1\phi_2}^2}\right)-b_2\left(\frac{g_{t\phi_2}g_{\phi_1\phi_1}-g_{t\phi_1}g_{\phi_1\phi_2}}{g_{\phi_1\phi_1}g_{\phi_2\phi_2}-g_{\phi_1\phi_2}^2}\right)\pm\frac{1}{2}\sqrt{\Delta} \tag{2.74}$$

and

$$\Delta = \frac{4D}{\left(g_{\phi_1\phi_1}g_{\phi_2\phi_2}-g_{\phi_1\phi_2}^2\right)^2}\left(g_{\phi_2\phi_2}b_1^2+g_{\phi_1\phi_1}b_2^2-2g_{\phi_1\phi_2}b_1b_2\right). \tag{2.75}$$

From now on, the vector field will be defined as

$$v_r := \frac{\partial_r b_\pm}{\sqrt{g_{rr}}}, \qquad v_\theta := \frac{\partial_\theta b_\pm}{\sqrt{g_{\theta\theta}}}. \tag{2.76}$$

2.3.2.1 Axis limit-I

One can show that as $\theta \to 0$, one has

$$\begin{aligned} D &\approx \rho^2\left(\left(g_{t\phi_2}^{(0)}\right)^2+g_{\phi_2\phi_2}^{(0)}\left(\frac{\rho^{2n}}{\rho^2}\right)+g_{tt}^{(0)}\left(\frac{\rho^{2m}}{\rho^2}\right)-g_{tt}^{(0)}g_{\phi_2\phi_2}^{(0)}-2g_{t\phi_2}^{(0)}\left(\frac{\rho^{n+m}}{\rho^2}\right)\right) \\ &\approx \rho^2\left(\left(g_{t\phi_2}^{(0)}\right)^2-g_{tt}^{(0)}g_{\phi_2\phi_2}^{(0)}\right). \end{aligned} \tag{2.77}$$

Therefore,

$$b_\pm \approx \frac{1}{\rho^2 g^{(0)}_{\phi_2\phi_2} - \rho^{2m}} \Big[-b_1 \left(\rho^n g^{(0)}_{\phi_2\phi_2} - g^{(0)}_{t\phi_2} \rho^m \right) - b_2 \left(\rho^2 g^{(0)}_{t\phi_2} - \rho^n \rho^m \right) \pm \rho \sqrt{\left(g^{(0)}_{t\phi_2} \right)^2 - g^{(0)}_{tt} g^{(0)}_{\phi_2\phi_2}} \sqrt{g^{(0)}_{\phi_2\phi_2} b_1^2 + \rho^2 b_2^2 - 2\rho^m b_1 b_2} \Big] . \quad (2.78)$$

Keeping the leading and the next to leading terms, one has

$$b_\pm \approx \frac{1}{g^{(0)}_{\phi_2\phi_2}} \left[-b_2 g^{(0)}_{t\phi_2} \pm \frac{1}{\rho} |b_1| \sqrt{g^{(0)}_{\phi_2\phi_2}} \sqrt{\left(g^{(0)}_{t\phi_2} \right)^2 - g^{(0)}_{tt} g^{(0)}_{\phi_2\phi_2}} \right] , \quad (2.79)$$

which compactly reads:

$$b_\pm \approx \text{constant} \pm \frac{1}{\rho} \times \text{constant}. \quad (2.80)$$

Therefore, $v_r \propto \frac{1}{\rho}$ and $v_\theta \propto \frac{1}{\rho^2}$. Thus, we obtained the same result as in the equal angular momenta case.

2.3.2.2 Axis limit -II

This time, as $\theta \to \frac{\pi}{2}$,

$$b_\pm \approx \frac{1}{\rho^2 g^{(0)}_{\phi_1\phi_1} - \rho^{2m}} \Big[-b_1 \left(\rho^2 g^{(0)}_{t\phi_1} - \rho^n \rho^m \right) - b_2 \left(\rho^n g^{(0)}_{\phi_1\phi_1} - g^{(0)}_{t\phi_1} \rho^m \right) \pm \rho \sqrt{\left(g^{(0)}_{t\phi_1} \right)^2 - g^{(0)}_{tt} g^{(0)}_{\phi_1\phi_1}} \sqrt{g^{(0)}_{\phi_1\phi_1} b_2^2 + \rho^2 b_1^2 - 2\rho^m b_1 b_2} \Big] , \quad (2.81)$$

which again has the dominant terms given as

$$b_\pm \approx \frac{1}{g^{(0)}_{\phi_1\phi_1}} \left[-b_1 g^{(0)}_{t\phi_1} \pm \frac{1}{\rho} |b_2| \sqrt{g^{(0)}_{\phi_1\phi_1}} \sqrt{\left(g^{(0)}_{t\phi_1} \right)^2 - g^{(0)}_{tt} g^{(0)}_{\phi_1\phi_1}} \right] . \quad (2.82)$$

In other words, we obtained a result in the form of

$$b_\pm \approx \text{constant} \pm \frac{1}{\rho} \times \text{constant}. \quad (2.83)$$

Therefore, $v_r \propto \frac{1}{\rho}$ and $v_\theta \propto \frac{1}{\rho^2}$. We obtained the same result as in the equal angular momenta case.

2.3.2.3 Horizon limit

We can write the effective potential functions as

$$b_\pm = \omega_1 b_1 + \omega_2 b_2 \pm \frac{\sqrt{D}}{g_{\phi_1\phi_1} g_{\phi_2\phi_2} - g^2_{\phi_1\phi_2}} \sqrt{g_{\phi_2\phi_2} b_1^2 + g_{\phi_1\phi_1} b_2^2 - 2 g_{\phi_1\phi_2} b_1 b_2}. \quad (2.84)$$

With the help of the lapse function, one has

$$b_\pm = \omega_1 b_1 + \omega_2 b_2 \pm N \sqrt{\frac{g_{\phi_2\phi_2} b_1^2 + g_{\phi_1\phi_1} b_2^2 - 2 g_{\phi_1\phi_2} b_1 b_2}{g_{\phi_1\phi_1} g_{\phi_2\phi_2} - g^2_{\phi_1\phi_2}}}, \quad (2.85)$$

which in the near the horizon limit, yields

$$\begin{aligned} b_\pm &\approx \Omega_1 b_1 + \Omega_2 b_2 \pm \kappa_H n \sqrt{\frac{g_{H,\phi_2\phi_2} b_1^2 + g_{H,\phi_1\phi_1} b_2^2 - 2 g_{H,\phi_1\phi_2} b_1 b_2}{g_{H,\phi_1\phi_1} g_{H,\phi_2\phi_2} - g^2_{H,\phi_1\phi_2}}} \quad (2.86) \\ &\approx \text{constant} \pm \kappa_H n \times \text{constant}. \end{aligned}$$

Since, we have

$$v_{r,\pm} = \partial_n b_\pm \quad (2.87)$$

the discussion around (2.66) for the equal momenta case applies here; and this gives a negative half winding.

2.3.2.4 Asymptotic limit

In the asymptotic limit, one can work in the flat spacetime coordinates, which are shown in (2.67). This implies that

$$v_r = \frac{1}{\sqrt{g_{rr}}} \partial_r b_\pm = \partial_r b_\pm. \quad (2.88)$$

In this limit,

$$D \approx r^4 \sin^2\theta \cos^2\theta, \quad (2.89)$$

and therefore

$$\Delta \approx \frac{4}{r^2 \sin^2\theta \cos^2\theta} \left(\cos^2\theta b_1^2 + \sin^2\theta b_2^2 \right). \quad (2.90)$$

By using this, we obtain

$$b_\pm = \pm \frac{1}{r \sin\theta \cos\theta} \sqrt{\cos^2\theta b_1^2 + \sin^2\theta b_2^2}, \quad (2.91)$$

and finally calculate

$$v_{r,\pm} = \mp \frac{1}{r^2 \sin\theta \cos\theta} \sqrt{\cos^2\theta b_1^2 + \sin^2\theta b_2^2}. \tag{2.92}$$

Since $\theta \in \left[0, \frac{\pi}{2}\right]$, $\sin\theta\cos\theta > 0$. In the asymptotic limit, $r \to \infty$,

$$\text{sign}\left(v_{r,\pm}\right)|_\infty = \mp 1. \tag{2.93}$$

The angular component changes sign as in the equal momenta case and contributes a negative half winding. The general behavior of the vector field around the light ring is plotted in Figs. 2.4, 2.5.

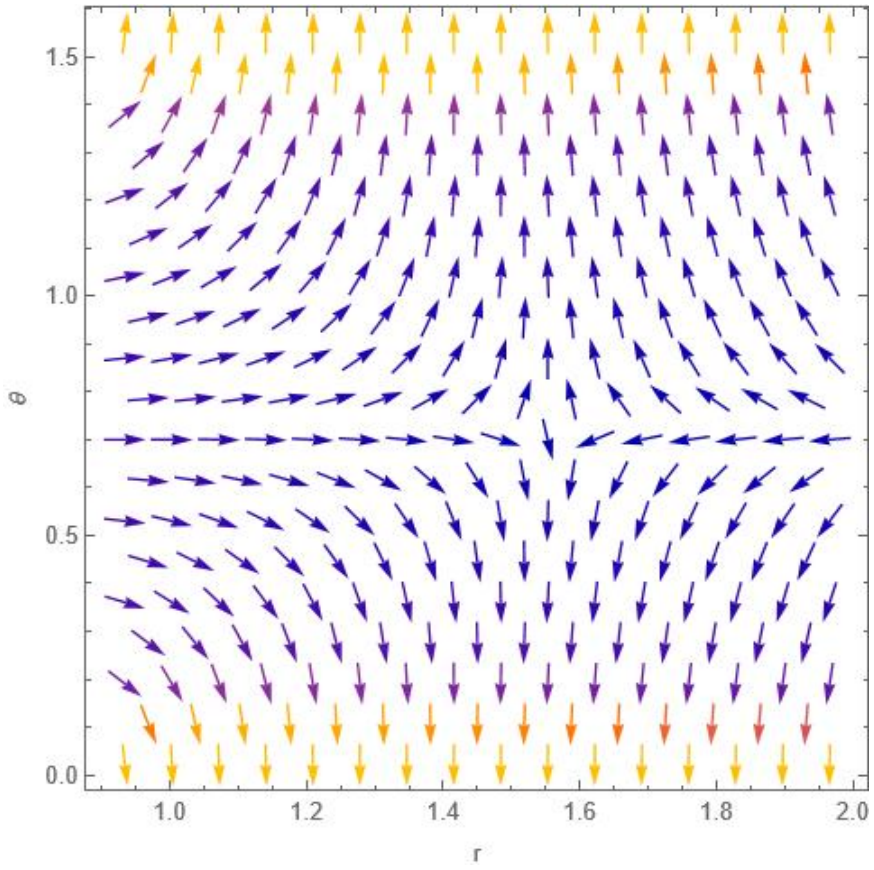

Figure 2.4: **Black hole case** The vector field, $\vec{v}$, obtained by using the impact parameter b_+ as given in (2.74), (2.75), (2.76), can be seen in the neighborhood of the standard light ring for the Myers-Perry black hole with two distinct angular momenta. For this plot, we assumed that the mass term is $\mu = 1$, the rotation parameters are $a = 0.1$ and $b = 0.4$ and the angular momenta of the photon are $\Phi_1 = 1.1$ and $\Phi_2 = 1.5$. The horizon is located at $r_H = 0.83$.

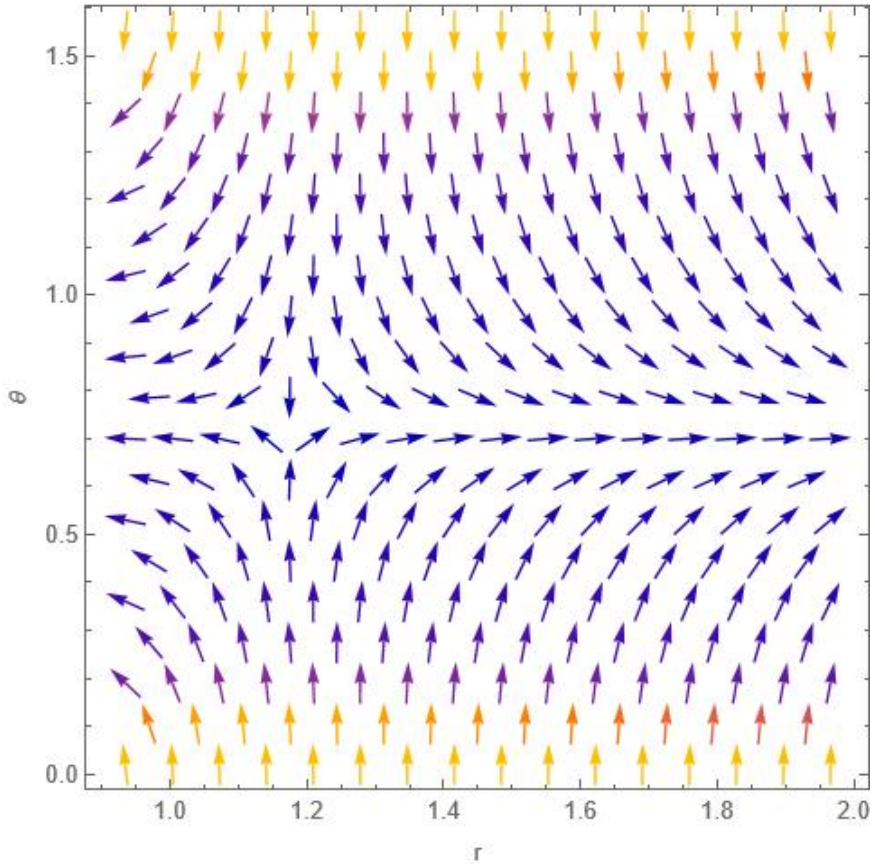

Figure 2.5: **Black hole case** The vector field, $\vec{v}$, obtained by using the impact parameter b_{-} as given in (2.74), (2.75), (2.76), can be seen in the neighborhood of the standard light ring for the Myers-Perry black hole with two distinct angular momenta. We took $\mu = 1$, $a = 0.1$ and $b = 0.4$ and the angular momenta of the photon are $\Phi_1 = 1.1$ and $\Phi_2 = 1.5$. The horizon is located at $r_H = 0.83$.

2.4 Naked Singularity, Cosmic Censorship and Light Rings

In the discussions so far, we have assumed the existence of a Killing horizon that hides the singularity in the spacetime as is expected according to the cosmic censorship hypothesis [14]. But, one could ask if this hypothesis can be tested using the light ring structure and the corresponding shadow. This problem will be addressed in full in Chapter 3. Here, we would like to point out that when the horizon disappears, the rotating solution loses one of its light rings as shown in Figs. (2.6, 2.7): there remains a single light ring around the naked singularity.

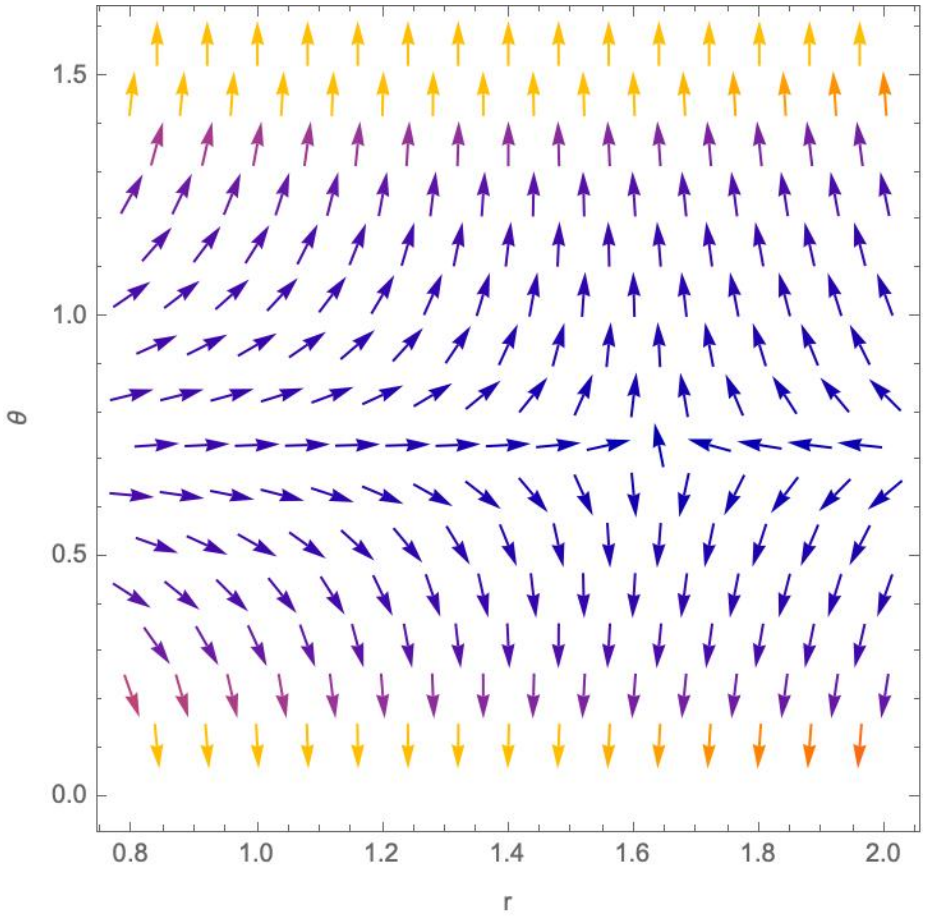

Figure 2.6: **No Horizon case** The vector field, $\vec{v}$, obtained by using the impact parameter b_+ as given in (2.74), (2.75), (2.76) can be seen in the neighborhood of the single light ring for the naked singularity. So, this light ring survives. For this plot, we assumed that the mass term is $\mu = 1$, the rotation parameters are $a = 0.3$ and $b = 0.8$ and the angular momenta of the photon are $\Phi_1 = 1.1$ and $\Phi_2 = 1.5$.

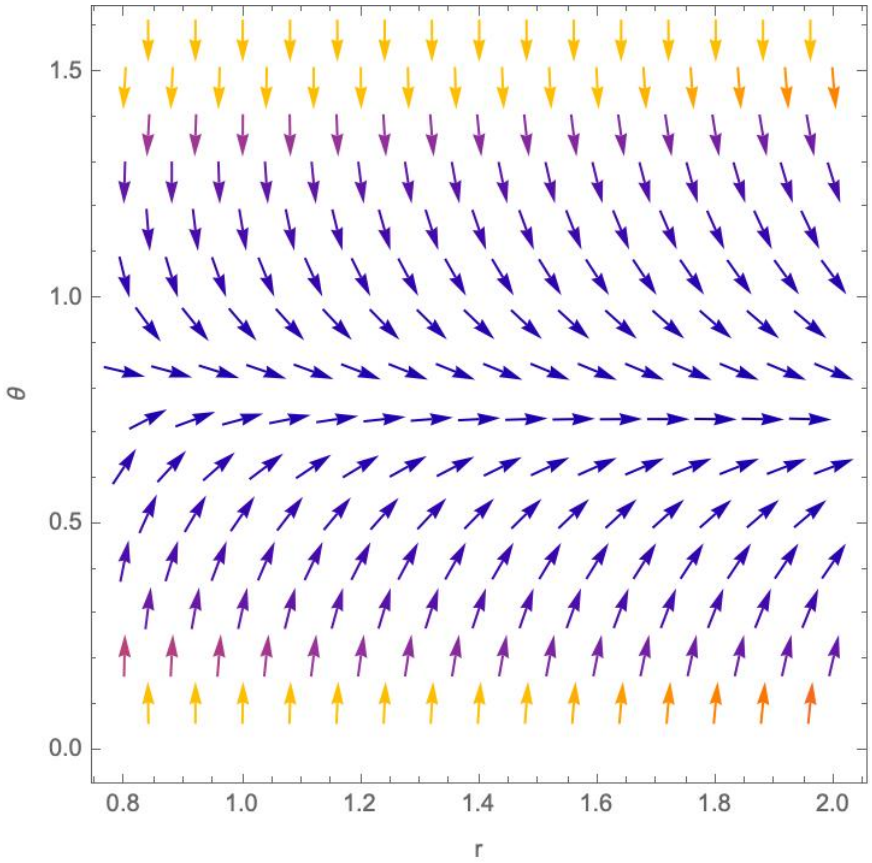

Figure 2.7: **No Horizon case** The vector field, $\vec{v}$, obtained by using the impact parameter b_- as given in (2.74), (2.75), (2.76) has no winding as can be seen. The light ring with b_- disappears for the naked singularity case. We took $\mu = 1$, $a = 0.3$ and $b = 0.8$ and the angular momenta of the photon are $\Phi_1 = 1.1$ and $\Phi_2 = 1.5$.

In this work, we have shown this in 4+1 dimensions, but the same phenomenon also appears in the 3+1 dimensional Kerr black hole. Let us show this analytically. There are two light rings outside the event horizon of a Kerr black hole (with mass m and the dimensionless rotation parameter $u = a^2/m^2$) which are located in the equatorial plane at the radii ($r_\pm = m x_\pm$) [12]

$$x_\pm = 2 + 2\cos\left(\frac{2}{3}\cos^{-1}(\pm\sqrt{u})\right), \tag{2.94}$$

where x_+ is the retrograde orbit satisfying $3 \leq x_+ \leq 4$, while x_- is the prograde orbit satisfying $2 \leq x_- \leq 3$. The event horizon is located at

$$x_{\rm H} = 1 + (1-u)^{1/2}, \tag{2.95}$$

for $0 \leq u \leq 1$ and disappears for larger values of u. For any value of $u > 1$, the retrograde orbit x_+ remains but the prograde orbit x_- disappears. That means compared to the Kerr black hole with a horizon, the naked singularity has only a single light ring. This could allow us to test the cosmic censorship hypothesis.

CHAPTER 3

INSTABILITY OF A KERR-TYPE NAKED SINGULARITY DUE TO LIGHT AND MATTER ACCRETION AND ITS SHADOW

3.1 Constant radii null geodesics around the Kerr-type naked singularity

A rotating, massive naked singularity can be obtained from the Kerr metric in the Boyer-Lindquist coordinates (t, r, θ, ϕ) which reads (in the $G = c = 1$ units) as

$$\begin{aligned} ds^2 = &-\Big(1 - \frac{2mr}{\Sigma}\Big)dt^2 - \frac{4mar\sin^2\theta}{\Sigma}dtd\phi + \frac{\Sigma}{\Delta}dr^2 \\ &+\Sigma\, d\theta^2 + \Big(r^2 + a^2 + \frac{2ma^2r\sin^2\theta}{\Sigma}\Big)\sin^2\theta d\phi^2, \end{aligned} \tag{3.1}$$

where $a := \frac{J}{m}$ is the dimensionfull rotation parameter which we shall take to be $a > m$. The two functions appearing in the metric are given as

$$\Delta := r^2 - 2mr + a^2, \qquad \Sigma := r^2 + a^2\cos^2\theta. \tag{3.2}$$

For $a < m$, the larger root of $\Delta = 0$ is the event horizon located at $r_{\rm H} = m + (m^2 - a^2)^{1/2}$, but in this work, $\Delta \neq 0$ and hence we have a naked rotating singularity. Our first task is to calculate the constant radii null and time-like geodesics in this background. The constant radii null geodesics are particularly important because they are unstable and carry away information about the environment of this strong gravitational region. In practice one computes the shadow of this region as seen by a distant observer. Time-like geodesics are also important as they are traced by massive particles that constitute the accretion disk and change both the mass and the spin of the central object. Studying the evolution of the rotation parameter due to the accretion of matter is our second task.

For the spherical photon orbits, assuming $E \neq 0$ and defining $x := r/m$, the relevant

part of the geodesic equation can be recast as

$$\Sigma \frac{dx}{d\lambda} = \pm\sqrt{m^2E^2\mathbf{R}(x)}, \tag{3.3}$$

where λ is an affine parameter along the null geodesics and the dimensionless radial function in terms of dimensionless parameters is

$$\mathbf{R}(x) := x^4 + (\alpha^2 - l^2 - q)x^2 + 2x((\alpha - l)^2 + q) - \alpha^2 q. \tag{3.4}$$

Here $\alpha := a/m$, and $l := \frac{L_z}{mE}$ where E is the conserved energy of the photon corresponding to the time-like Killing vector $\xi_{(t)} = \frac{\partial}{\partial t}$; and L_z is the conserved z-component of the angular momentum of the photon related to the $\xi_{(\varphi)} = \frac{\partial}{\partial \varphi}$ Killing vector, while $q := \frac{\mathcal{Q}}{m^2E^2}$ where $\mathcal{Q}$ is the Carter's constant related to a symmetric rank two Killing tensor. Explicitly, it reads

$$\mathcal{Q} := p_\theta^2 + \cos^2\theta\left(\frac{L_z^2}{\sin^2\theta} - a^2E^2\right), \tag{3.5}$$

and, as a result,

$$q = \frac{p_\theta^2}{m^2E^2} + \cos^2\theta\left(\frac{l^2}{\sin^2\theta} - \alpha^2\right). \tag{3.6}$$

For constant radii orbits, $\mathcal{Q} \geq 0$, and the bound is satisfied for equatorial orbits [48, 11, 49]. There are two conditions on $\mathbf{R}(x)$ for spherical orbits

$$\mathbf{R}(x) = 0, \qquad \frac{d\mathbf{R}(x)}{dx} = 0, \tag{3.7}$$

which yield two physically viable equations [12] [1]:

$$l = -\frac{x^3 - 3x^2 + \alpha^2 x + \alpha^2}{\alpha(x-1)}, \tag{3.8}$$

$$q = -\frac{x^3\left(x^3 - 6x^2 + 9x - 4\alpha^2\right)}{\alpha^2(x-1)^2}. \tag{3.9}$$

Now, we would like to investigate these two equations under various circumstances for $\alpha > 1$.

3.1.1 Equatorial null Orbits

On the equatorial plane, particles with a vanishing q can orbit [2]. For black holes with a rotation parameter $\alpha < 1$, it is known that there are 3 solutions [12]. One of

[1] As discussed in [11], there is another solution to constant radii conditions which turns out to be unphysical.

these lies inside the event horizon while the others are outside the horizon; and the latters correspond to prograde and retrograde orbits. On the other hand, for the naked singularity with a rotation parameter $\alpha > 1$, the only real and non-zero solution of (3.9) for $q = 0$ is [2]

$$x_{-} = 2 + \left(\alpha + \sqrt{\alpha^2 - 1}\right)^{2/3} + \left(\alpha + \sqrt{\alpha^2 - 1}\right)^{-2/3} \tag{3.10}$$

which can be seen in Fig. (3.1). The photons that follow this orbit have a negative l value as shown in Fig. (3.2), and therefore x_{-} is a retrograde orbit. The equatorial orbits set the *innermost* and the *outermost* limits of the generic spherical photon orbits. Hence, non-equatorial null orbits can exist only for the interval $0 < x < x_{-}$ in this naked singularity spacetime.

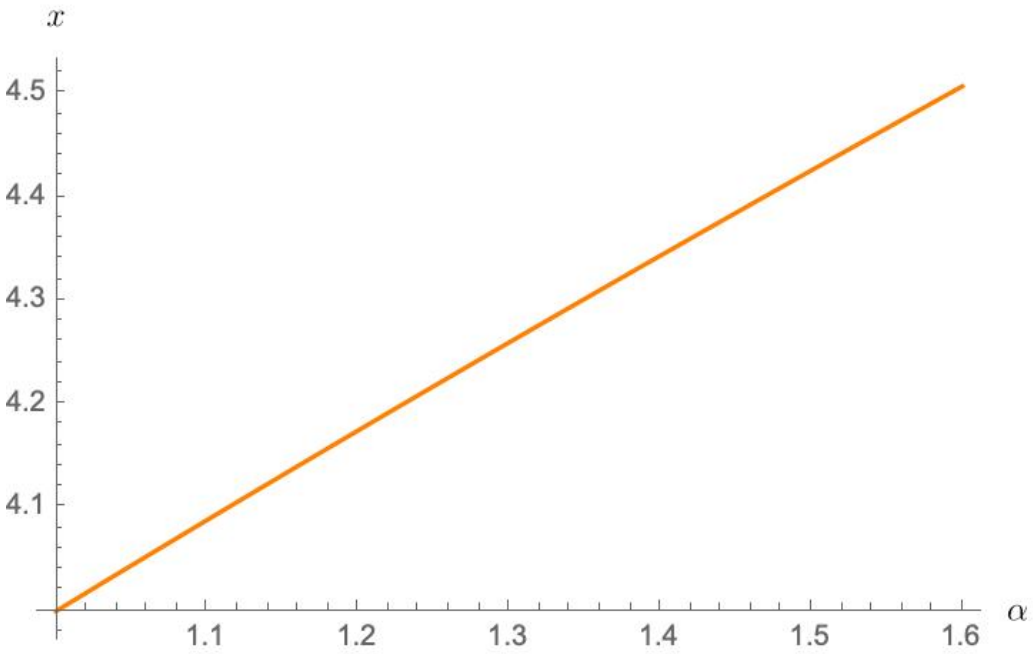

Figure 3.1: The orbit in the equatorial plane is plotted as a function of the rotation parameter for the interval $1 < \alpha < 1.6$ using (3.10). The radius of the orbit increases as the rotation parameter increases, which is an expected result for a retrograde orbit.

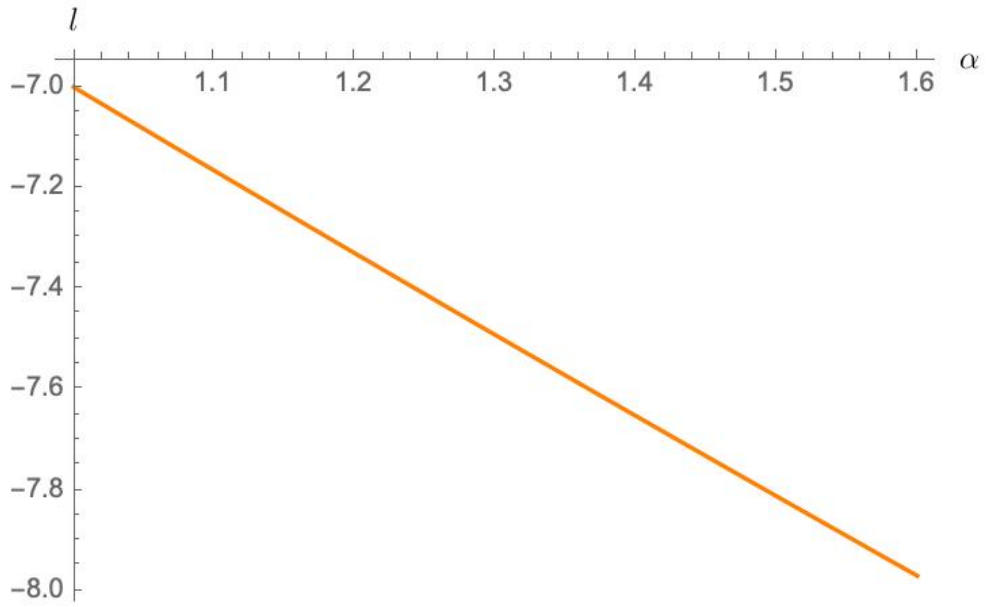

Figure 3.2: The l value of the equatorial orbit is plotted as a function of the rotation parameter for the interval $1 < \alpha < 1.6$ using (3.8). The negative l value confirms that this is a retrograde orbit.

3.1.2 Polar Null Orbits

Photons with a vanishing l and a positive q can have orbits on the polar plane. For a black hole with $\alpha < 1$, we have already shown that there are 3 polar circular null orbits [12]. One of them corresponds to an orbit with a negative radius and, therefore physically nonviable. The second solution lies inside the event horizon. The third solution lies outside the event horizon and corresponds to retrograde orbits. For the case of a naked singularity, (3.8) for $l = 0$ yields

$$\alpha(x) = \frac{x\sqrt{3-x}}{\sqrt{x+1}}, \tag{3.11}$$

which vanishes at $x = 0$ and $x = 3$, and has a local maximum at $x = \sqrt{3}$ as shown in Fig. (3.3). The maximum value of the rotation parameter is $\alpha_{max} = \sqrt{6\sqrt{3}-9} = 1.17996$ as was also found in [2]. The second derivative ($\frac{d^2\mathbf{R}(x)}{dx^2}$) for the physically viable orbits shows that while one of them is stable, the other one is unstable.

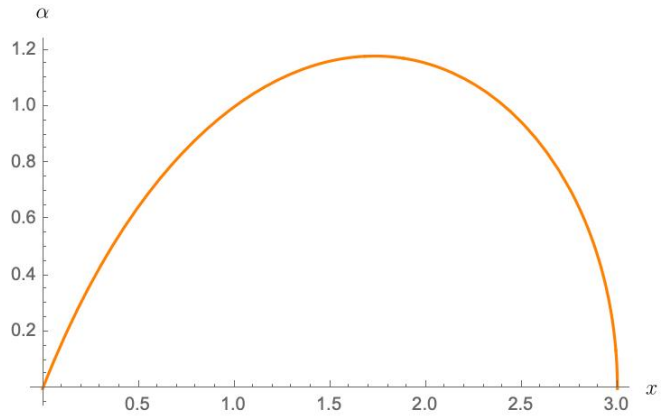

Figure 3.3: For the vanishing l value, the corresponding rotation parameter as a function of radius is plotted for the interval $0 < \alpha < 3$ using (3.11). The maximum value of the rotation parameter is $\alpha_{max} = \sqrt{6\sqrt{3} - 9}$. For higher values of rotation parameters, photons cannot reach to the polar plane.

In Fig. (3.4), the orbits on the polar plane are plotted as a function of the rotation parameter for the interval $1 < \alpha < 1.2$. Note that there are no polar orbits for the spacetimes with $\alpha > \sqrt{6\sqrt{3} - 9}$.

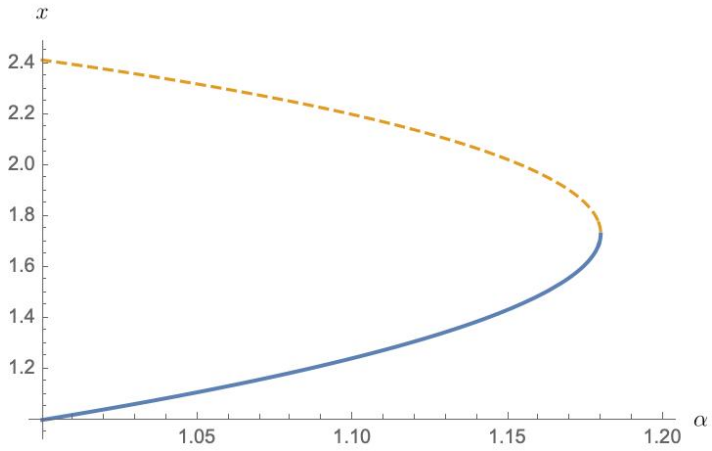

Figure 3.4: The polar orbits are drawn as a function of the rotation parameter in the interval $1 < \alpha < 1.2$. See that there are no polar orbits that have $\alpha > \sqrt{6\sqrt{3} - 9}$.

Let us note that the value $\sqrt{6\sqrt{3} - 9}$ is an important limit on the rotation parameter: in the interval $1 < \alpha < \sqrt{6\sqrt{3} - 9}$, for generic spherical null orbits, the l value can be positive. This means that prograde, as well as retrograde, orbits are allowed. For a naked singularity with a rotation parameter higher than the maximum rotation

parameter, $\alpha > \sqrt{6\sqrt{3}-9}$, there are only retrograde orbits, prograde orbits simply disappear. This will have an observable consequence in the shadow of the naked singularity as we shall see.

3.1.3 Marginally Stable null Orbits

Marginally stable orbits are defined by the condition on the radial function as $\frac{d^2\mathbf{R}}{dx^2} = 0$ augmented with the conditions (3.7). On these orbits, one finds [2]

$$\alpha(x) := \sqrt{(x-3)x^2+3x}, \tag{3.12}$$

or

$$x_M = 1 + (\alpha^2 - 1)^{\frac{1}{3}}, \tag{3.13}$$

which is plotted in Fig.(3.5). Therefore, orbits with $x < x_M$ are stable and orbits with $x > x_M$ are unstable. The photons we can observe originate as a result of slight perturbations of the unstable orbits. Hence, stable orbits are not relevant for the shadow imaging. This has an important consequence. The orbits around the naked singularity located at $x = 0$ and the orbits around $x = 1$ cannot have any visible effects on the image and the shadow.

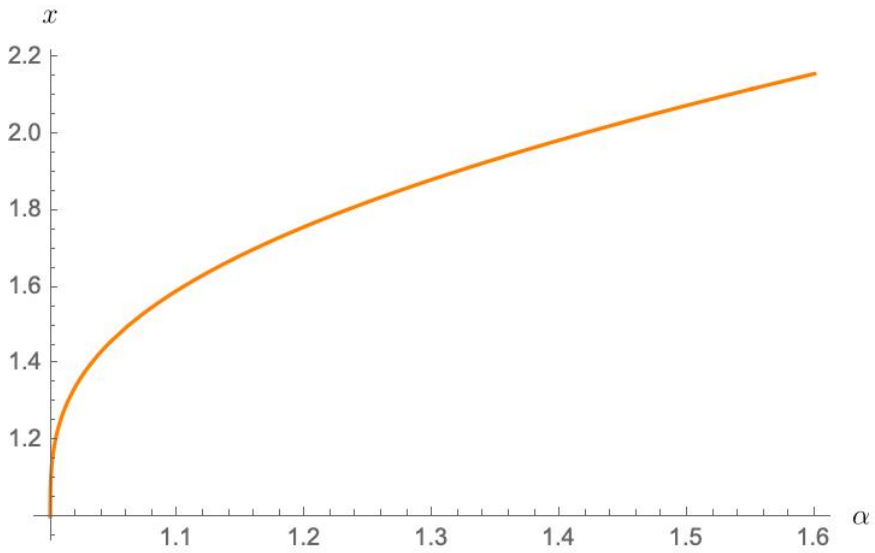

Figure 3.5: The marginally stable orbit as a function of the rotation parameter is plotted for the interval $1 < \alpha < 1.6$ using (3.13).

3.2 Shadow of a naked singularity

To obtain the shadow, we will use the conventions of [50], [51]. For light rays with parameters l and q, we assume that there is an observer located at a point far away from the black hole with coordinates (r_0, θ_0, ϕ_0) measuring the directions of these light rays. The coordinate ϕ_0 can be taken as 0 using the axial symmetry of the spacetime for simplicity. θ_0 is called the inclination angle of the observer. At large distances, for light rays one has

$$\frac{d\phi}{dt} \approx \frac{l}{r_0^2 \sin^2 \theta_0}, \tag{3.14}$$

and

$$\frac{d\theta}{dt} \approx \pm \frac{1}{r_0^2} \sqrt{q + \alpha^2 \cos^2 \theta_0 - l^2 \cot^2 \theta_0}. \tag{3.15}$$

Observe that the affine parameter is eliminated and the coordinate time t is used. Therefore, on the 2 dimensional image plane of the observer, we can define the impact parameters, following [52] as

$$X := -\frac{l}{\sin \theta_0}, \tag{3.16}$$

and

$$Y := \pm \sqrt{q + \alpha^2 \cos^2 \theta_0 - l^2 \cot^2 \theta_0}. \tag{3.17}$$

Each photon coming from an orbit around the black hole due to a slight perturbation determines a point on the (X, Y) plane of the image taken by the observer.

3.2.1 Two Exemplary Cases

3.2.1.1 Naked singularity with $\alpha = 1.1 < \alpha_{max}$

For $\alpha = 1.1$, using the results of previous sections, we can find spherical photon orbits with a radius in the interval

$$0 < x < 4.08808. \tag{3.18}$$

The marginally stable orbit is located at

$$x_M = 1.59439, \tag{3.19}$$

so the unstable spherical photon orbits will be in the interval

$$1.59439 < x < 4.08808. \tag{3.20}$$

Because we have a rotation parameter that is smaller than $\alpha_{max} = \sqrt{6\sqrt{3} - 9}$, we can expect prograde orbits as well as retrograde orbits. The prograde orbits exist in the interval

$$1.59439 < x < 2.2, \tag{3.21}$$

while the retrograde orbits are in the interval

$$2.2 < x < 4.08808. \tag{3.22}$$

The shadow of the black hole is shown in Fig. (3.6). It is important to note that an observer located at the polar plane, $\theta_0 = 0$, cannot decide whether this is a Kerr black hole or Kerr-type naked singularity.

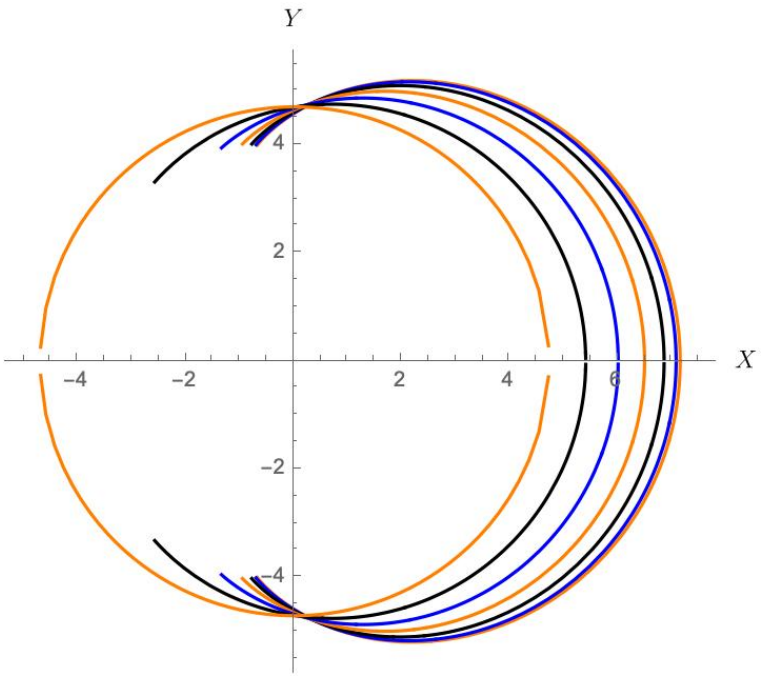

Figure 3.6: The shadow image of the Kerr-type naked singularity located at the origin, with a rotation parameter $\alpha = 1.1$ for observers with different angles $0 < \theta_0 < \frac{\pi}{2}$. An observer located at the polar plane, $\theta_0 = 0$, cannot decide whether this is a Kerr black hole or Kerr-type naked singularity considering only the light emanating from the unstable photon orbits. See also [51].

3.2.1.2 Naked singularity with $\alpha_{max} < \alpha = 1.5$

For $\alpha = 1.5$, we can find spherical photon orbits with a radius in the interval

$$0 < x < 4.4260. \tag{3.23}$$

The marginally stable orbit is located at $x_M = 2.0772$, so the unstable spherical orbits will be in the interval

$$2.0772 < x < 4.4260. \tag{3.24}$$

Because the rotation parameter is greater than $\alpha_{max} = \sqrt{6\sqrt{3} - 9}$, the l value can never change sign, there are no photons that can reach the polar plane, and all the orbits are retrograde. The shadow of the naked singularity is shown in Fig. (3.7).

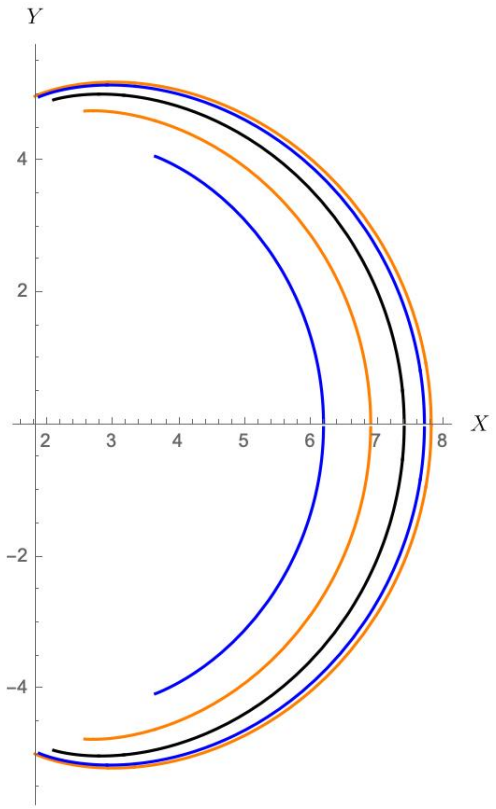

Figure 3.7: The shadow image of the Kerr-type naked singularity with a rotation parameter $\alpha = 1.5$ for observers with different inclination angles $0 < \theta_0 < \frac{\pi}{2}$. There is no prograde orbit for this spacetime. Therefore, changing the inclination angle only affects the arc shape in the image. See also [51].

3.3 Critical Inclination Angle for Null Orbits

In our previous work, [12], by combining the l (3.8) and q (3.9) expressions, we obtained a sextic polynomial and searched its analytical solutions for different conditions. In addition to the known equatorial and polar plane solutions, we found a new family of analytic solutions at the *critical inclination angle*. At this critical inclination angle, the sextic polynomial factors into a quadratic and a quartic part and becomes solvable by radicals. By using the same method, we can find the critical inclination angle solutions for the $\alpha > 1$ cases.

The mentioned sextic polynomial equation is

$$p(x) := x^6 - 6x^5 + (9 + 2\nu u)x^4 - 4ux^3 - \nu u(6-u)x^2 + 2\nu u^2 x + \nu u^2 = 0, \quad (3.25)$$

where we have defined the dimensionless variables

$$u := \alpha^2, \qquad \nu := \frac{q}{l^2 + q}. \quad (3.26)$$

In this section, we will call u to be the rotation parameter. One must solve this polynomial equation as $x = x(u, \nu)$ for the following intervals:

$$0 < x, \qquad 0 \leq \nu \leq 1, \qquad 1 < u. \quad (3.27)$$

To proceed further, it pays to define the following variables which will simplify the final expressions:

$$\nu := \frac{\xi}{u}, \qquad u := 1 + w^3, \quad (3.28)$$

with $0 \leq \xi \leq u$ and $w \geq 0$. Even though a generic radical solution to the sextic (3.25) is not possible, it can be shown that it reduces to quadratic times a quartic polynomial at the following critical point for $u > 1$:

$$\xi_{\text{cr}} = \frac{3(w+1)^3}{w(w+5)+7} \quad (3.29)$$

and it becomes solvable. The four real solutions of this sextic polynomial are plotted in Fig. (3.8).

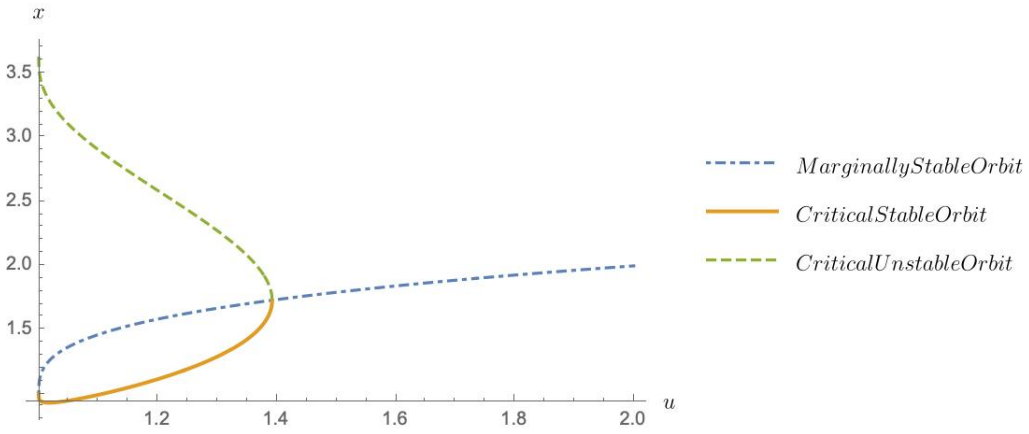

Figure 3.8: The solution of the sextic polynomial is plotted as a function of the rotation parameter for the interval $1 < u < 2$.

Two of the solutions are degenerate with a vanishing second derivative and they are marginally stable orbits. One of the remaining solutions has a negative second derivative and the other one has a positive second derivative, therefore they are stable and unstable critical orbits, respectively. The critical stable and unstable orbits are available only for spacetimes with a rotation parameter $u < u_{max} = 6\sqrt{3} - 9 = 1.3923$.

The l and q values of these solutions can be seen in Fig. (3.9) and Fig. (3.10), respectively. The marginally stable orbits have a turning point and they can be prograde or retrograde. Likewise, the stable orbit can be prograde or retrograde. Yet, the unstable orbit is always retrograde. The Carter's constants are non-zero, as expected.

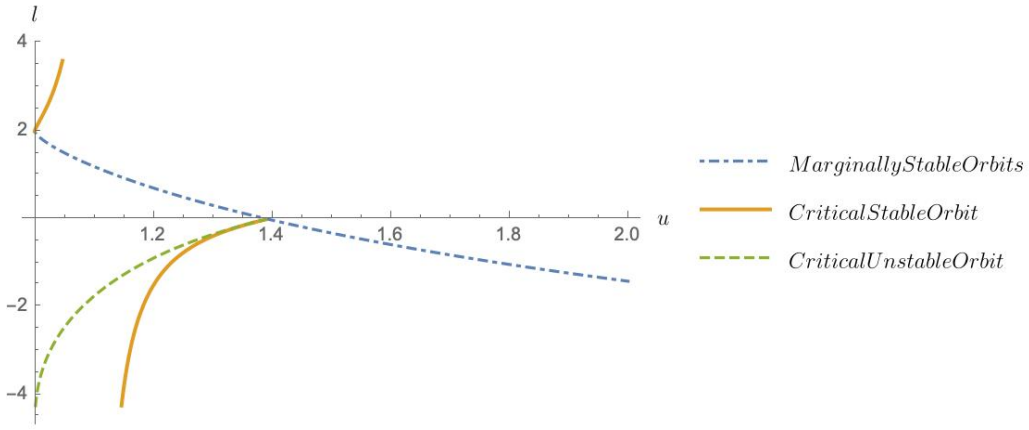

Figure 3.9: The l value of the critical inclination angle orbit is plotted as a function of the rotation parameter for the interval $1 < u < 2$.

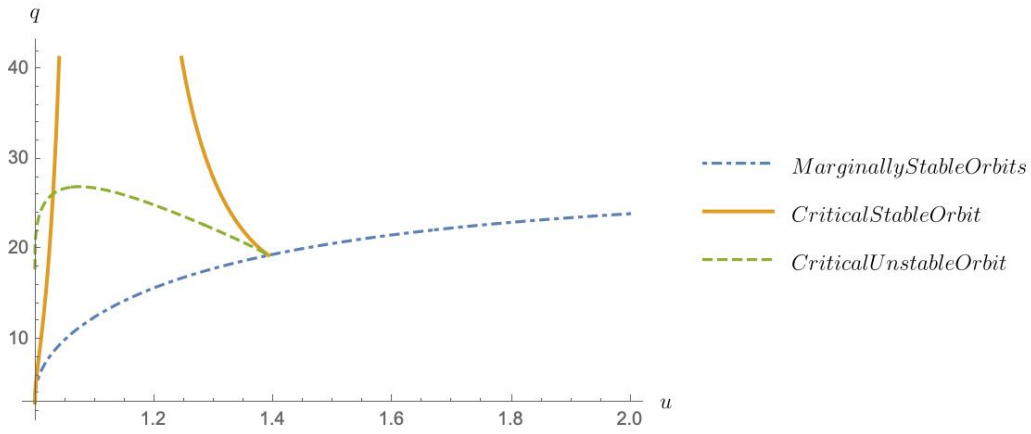

Figure 3.10: The Carter's constant of the critical inclination angle orbit as a function of the rotation parameter is plotted for the interval $1 < u < 2$.

3.4 Spherical Timelike Orbits around the naked singularity

Let us now consider a massive particle with mass μ that moves on a spherical timelike orbit in the vicinity of the naked singularity. For the spherical timelike orbits, [53], the relevant geodesic equation is

$$\Sigma \frac{dr}{d\tau} = \pm\sqrt{R(r)}, \tag{3.30}$$

where the radial function can be rearranged as $\mathbf{R}(x) := R(r)/(m^4\mu^2)$ which is given as

$$\begin{aligned}\mathbf{R}(x) := \quad & x^2\left(\alpha^2\left(\tilde{E}^2-1\right)-l^2-q\right)-\alpha^2 q+2x\left((\alpha\tilde{E}-l)^2+q\right)\\ & +\left(\tilde{E}^2-1\right)x^4+2x^3,\end{aligned} \tag{3.31}$$

with $l = \frac{L_z}{m\mu}$, $q = \frac{\mathcal{Q}}{m^2\mu^2}$ and $\tilde{E} = \frac{E}{\mu}$. Here, the Carter's constant $\mathcal{Q}$ was given in (3.5). Note that in contrast to the null geodesics, the energy of the orbit is important, but the mass of the particle is not, hence we scaled out the mass of the particle as well as the mass of the central body.

Two equations must be satisfied, $\mathbf{R}(x) = 0$ and $\frac{d\mathbf{R}(x)}{dx} = 0$, for constant radius geodesics. There is a bifurcation of solutions: for $x = 1$, one has the following solutions

$$l = \frac{2\left(\alpha^2+1\right)\tilde{E}^2-\alpha^2+1}{2\alpha\tilde{E}}, \tag{3.32}$$

and

$$q=\frac{\alpha^2-\left(2\tilde{E}^2+1\right)^2}{4\alpha^2\tilde{E}^2}. \tag{3.33}$$

On the other hand, for $x\neq 1$, one has

$$l=\frac{-\left[\alpha\tilde{E}(\alpha^2-x^2)+\left(x\left(\alpha^3+\alpha(x-2)x\right)^2\left(\left(\tilde{E}^2-1\right)x+1\right)\right)^{1/2}\right]}{\alpha^2(x-1)}, \tag{3.34}$$

and

$$\begin{aligned} q=\quad & \frac{x^2}{\alpha^3(-1+x)^2}\times\left[\alpha^3\left(\left(2\tilde{E}^2-1\right)x+1\right)\right. \\ & +2\tilde{E}\left(x\left(\alpha^3+\alpha(x-2)x\right)^2\left(\left(\tilde{E}^2-1\right)x+1\right)\right)^{1/2} \\ & \left.+\alpha x\left(x\left(\tilde{E}^2(-((x-4)x+5))+(x-5)x+8\right)-4\right)\right]. \end{aligned} \tag{3.35}$$

Next, we shall analyze the unit energy solutions for which the equations are more transparent.

3.4.1 Unit Energy Timelike Orbits

For unit energy particles, $\tilde{E}=1$, from (3.34) and (3.35) one can obtain for the equatorial plane, $q=0$,

$$x=2+\alpha\pm 2\sqrt{\alpha+1}, \tag{3.36}$$

and the plus solution is plotted in Fig. (3.11) for the interval $1<\alpha<2$. The l value for this orbit is plotted in Fig. (3.12) for the same interval and it shows that this orbit is retrograde. On the polar plane, $l=0$, we obtain

$$\alpha=\sqrt{2x^{3/2}-x^2}, \tag{3.37}$$

which vanishes at $x=0$ and $x=4$ as can be seen in Fig. (3.13). This rotation parameter has a maximum at $x_{max}=\frac{9}{4}$ with a value $\alpha_{max}=\frac{3\sqrt{3}}{4}=1.29904$. For naked singularities with a rotation parameter less than this value, there could be prograde orbits as well as retrograde orbits for generic spherical orbits. It is important to observe that massive particles with unit energy can co-rotate with the black hole for higher values of the rotation parameter than the photons whose maximum rotation parameter is $\alpha_{max}=\sqrt{6\sqrt{3}-9}$. The spherical timelike orbits of the polar plane can be seen in Fig. (3.14).

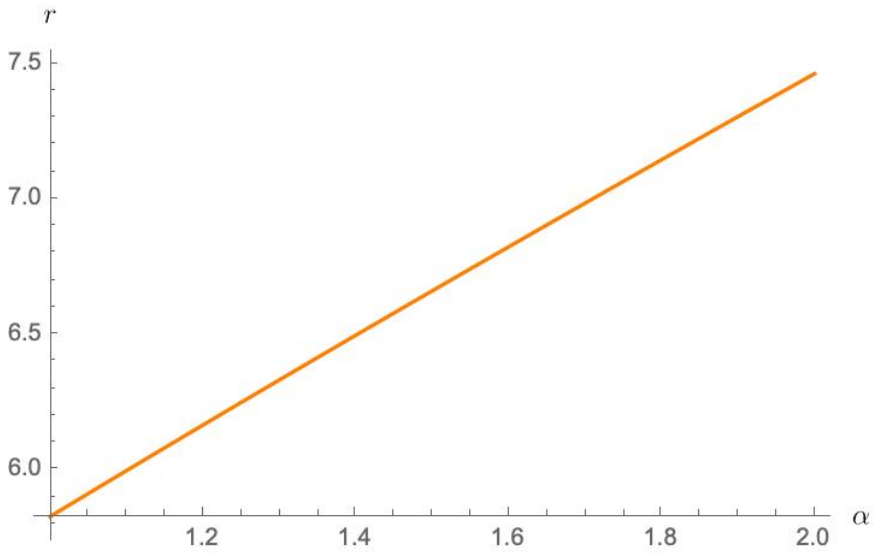

Figure 3.11: The radius of an equatorial retrograde orbit for a unit energy particle is plotted as a function of the rotation parameter for the interval $1 < \alpha < 2$ by using (3.36).

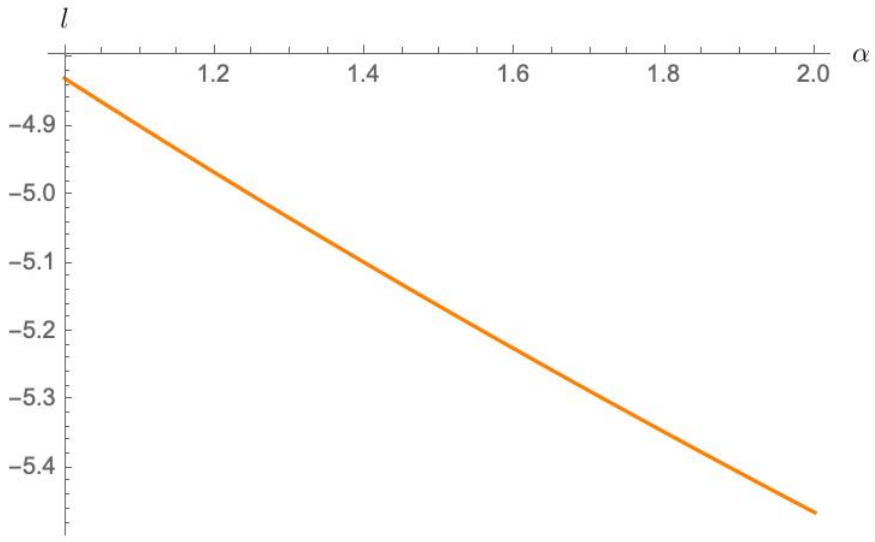

Figure 3.12: The l value of an equatorial orbit for a unit energy particle is plotted as a function of the rotation parameter for the interval $1 < \alpha < 2$. The negative l values imply that this is a retrograde orbit.

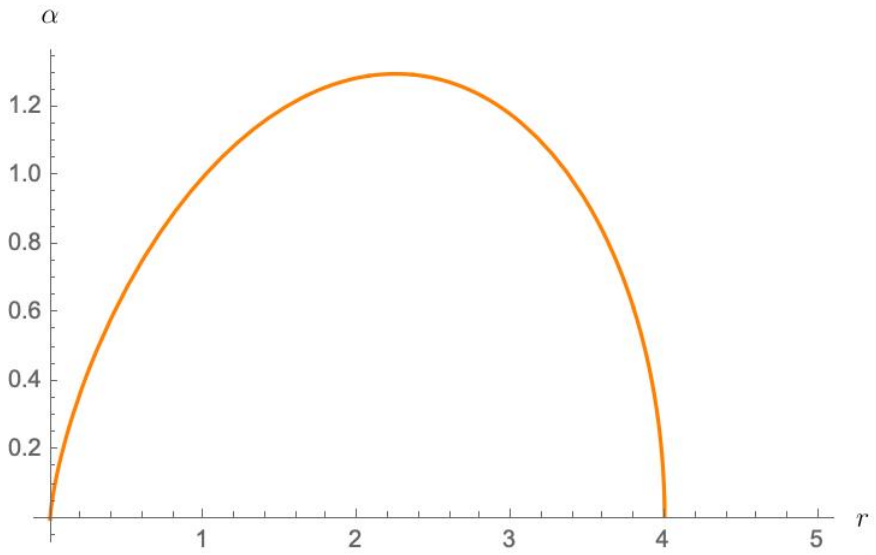

Figure 3.13: The rotation parameter as a function of the radius of the polar orbits is plotted for the interval $0 < r < 5$.

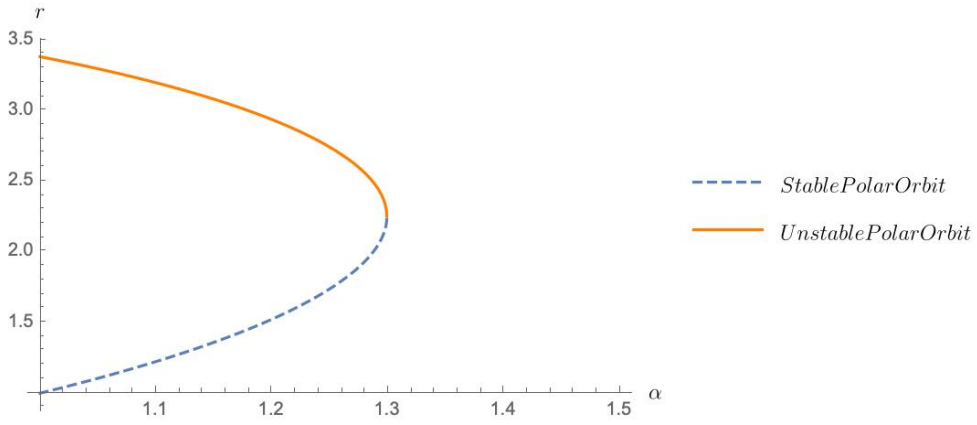

Figure 3.14: The polar orbits as a function of the rotation parameter are plotted for the interval $1 < \alpha < 1.5$.

3.4.2 Generic Energy orbits on the Equatorial Plane

When we solve the equation (3.35) for $q = 0$ concerning the rotation parameter without assuming the unit energy condition, we get

$$\alpha = \left[4x + x^2\left(2\tilde{E}^4 x + \tilde{E}^2(5-3x) + x - 4\right) - 2\left(2 + \left(\tilde{E}^2 - 1\right)x\right)\sqrt{\tilde{E}^2 x^3\left(\left(\tilde{E}^2 - 1\right)x + 1\right)}\right]^{\frac{1}{2}}. \quad (3.38)$$

Two conclusions can be drawn from this relation. Firstly, for higher rotation parameter values, the radius of the spherical timelike orbit for particles of constant energy on the equatorial plane increases. Secondly, higher energy particles follow closer orbits to the naked singularity with a constant rotation parameter than the lower energy particles. As an example, for $\alpha = 1.6$, the energy values as a function of the radius are plotted in Fig. (3.15).

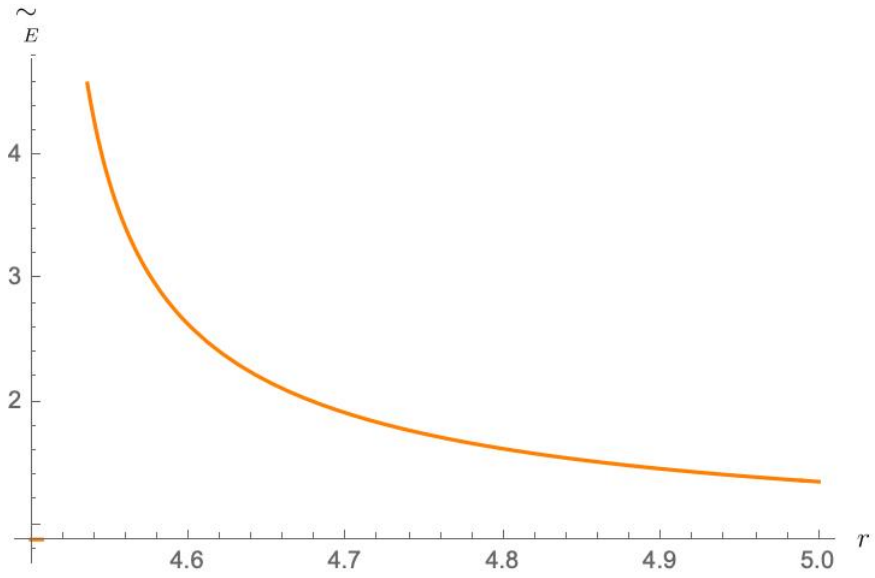

Figure 3.15: The energy of the particles is plotted as a function of the radius for the interval $4.5 < r < 5$ around a black hole with a rotation parameter $\alpha = 1.6$. Higher energy particles follow orbits with smaller radii.

3.4.3 Generic Energy orbits on the Polar Plane

The equation (3.34) for $l = 0$ yields

$$\alpha = \left(\frac{x^2 \left(\tilde{E}^2(-(x-1)) + x - 2 \right) + 2\sqrt{\tilde{E}^2 x^3 \left(\left(\tilde{E}^2 - 1 \right) x + 1 \right)}}{\tilde{E}^2(x+1) - x} \right)^{\frac{1}{2}} . \quad (3.39)$$

Then, by using this relation, one can investigate the rotation parameter for different energy values. We have already shown that for a unit energy particle, there is a maximum possible rotation parameter $\alpha_{max} = \frac{3\sqrt{3}}{4}$. For $\tilde{E} = 1.5$, one finds $\alpha_{max} = 1.21002$ and for $\tilde{E} = 2$, one finds $\alpha_{max} = 1.19495$. In conclusion, one can observe that for the high energy limit (for example $\tilde{E} = 100$), the maximum value of the rotation parameter approaches the maximum value of the photon case ($\alpha_{max} = \sqrt{6\sqrt{3} - 9}$) as expected.

3.5 Accretion into the naked singularity

3.5.1 Review of the $\alpha < 1$ Case

3.5.1.1 Special Circular Null and Timelike Orbits

Accretion of matter and radiation around both non-rotating and rotating black holes is an extremely important aspect of black hole physics in the strong field region, both from the vantage point of theory and observation. For rotating black holes, one can consider thin accretion disks around the equatorial plane. One may not be able to solve the whole disk plus the black hole system analytically in an exact form, but one can compute the effects of the accretion disk on the black hole by considering the properties of some special equatorial, circular null, and timelike orbits. As matter and radiation fall into the black hole, the mass and the spin of the black hole increase as discussed by Bardeen [54] (without taking into account the radiation) and later by Thorne [55] who considered the effects of the radiation. It turns out the retrograde photon orbits have a larger capture cross-section than that of prograde photon orbits, the latter generically spin up but the former spin down the black hole. Before inves-

tigating the accretion around a Kerr-type naked singularity, we would like to review the Kerr black hole case with $\alpha < 1$.

The radial timelike geodesic equation can be rewritten on the equatorial plane as

$$\frac{dr}{d\tau} = \pm r^{-3/2}\sqrt{R(r)}, \tag{3.40}$$

where the radial function can be rearrange to $\mathbf{R}(x) := R(r)/(m^4\mu^2)$ which is given as

$$\mathbf{R}(x) := \left(\tilde{E}^2 - 1\right) x^3 + \alpha^2 \left(\tilde{E}^2 - 1\right) x + 2(l - \alpha\tilde{E})^2 - l^2 x + 2x^2. \tag{3.41}$$

By using the circularity conditions, $\mathbf{R}(x) = 0$ and $\frac{d\mathbf{R}(x)}{dx} = 0$, one can get

$$\begin{aligned} l_\pm &= \pm\frac{\alpha^2 + x^2 \mp 2\alpha\sqrt{x}}{\sqrt{\pm 2\alpha x^{3/2} + (x-3)x^2}}, \\ \tilde{E}_\pm &= \frac{\pm\alpha + (x-2)\sqrt{x}}{\sqrt{\pm 2\alpha x^{3/2} + (x-3)x^2}}, \end{aligned} \tag{3.42}$$

where $+$ represents prograde orbits while $-$ represent retrograde orbits. It is important to state that circular orbit solutions exist on the equatorial plane only if $\pm 2\alpha x^{3/2} + (x-3)x^2 \geq 0$ and the equality is satisfied only by null orbits which is consistent with the left-hand side of the equations as these quantities represent angular momentum and energy per mass.

The stability of these circular orbits is determined by the second derivative test: $\frac{d^2\mathbf{R}(x)}{dx^2} > 0$ for unstable orbits, while $\frac{d^2\mathbf{R}(x)}{dx^2} < 0$ for stable ones. The special case $\frac{d^2\mathbf{R}(x)}{dx^2} = 0$ represents the innermost stable circular orbit (ISCO) or the marginally stable orbit. This ISCO condition yields

$$-3\alpha^2 + x^2 \pm 8\alpha\sqrt{x} - 6x = 0, \tag{3.43}$$

which has 4 solutions two of which are physically relevant and correspond to prograde and retrograde ISCOs.

Massive particles with $\tilde{E} > 1$ follow unstable circular orbits on the equatorial plane and under a slight perturbation, they may escape to infinity or fall into the black hole. Particles with $\tilde{E} < 1$, under a perturbation, can only fall into the black hole. The special unstable orbits with $\tilde{E} = 1$ are aptly called the *binding orbits*, and are located at

$$x_{bind,\pm} = \mp\alpha + 2\sqrt{1 \pm \alpha} + 2. \tag{3.44}$$

3.5.1.2 Change in the spin of the black hole due to accretion

Let us assume that there is a subextremal Kerr black hole with a thin accretion disk around its equator, and further assume that there is no gravitational or electromagnetic radiation from the disk. Particles fall into the black hole under slight perturbations from the ISCO. These particles feed the black hole with mass $\delta m = \tilde{E}_{ISCO}$, and angular momentum $\delta J = l_{ISCO}$. Under these assumptions, Bardeen [54] showed that a black hole that is initially static can be spun up by particles on the accretion disk until it reaches the extremal rotation parameter $\alpha = 1$. Later, Thorne [55] calculated the upper limit as $\alpha = 0.998$ by considering photons coming out of the accelerated particles. Here it turns out the capture cross-section of the retrograde orbits is larger than that of the prograde orbits and this fact does not allow the subextremal black hole to be spinned up to the extremal value.

3.5.2 Accretion around Kerr-type Naked Singularity

3.5.2.1 Special Circular Null and Timelike Orbits

When the circularity conditions are applied for the radial part of the geodesic equations, $\mathbf{R}(x) = 0$ and $\frac{d\mathbf{R}(x)}{dx} = 0$, for Kerr-type naked singularity spacetimes, $\alpha > 1$, one get

$$\tilde{E}_\epsilon = \frac{(x-2)\sqrt{x} + \epsilon\alpha}{\sqrt{(x-3)\,x^2 + 2\epsilon\alpha x^{3/2}}}, \tag{3.45}$$

and

$$l_\epsilon = \epsilon \frac{x^2 + \alpha^2 - 2\epsilon\alpha\sqrt{x}}{\sqrt{(x-3)\,x^2 + 2\epsilon\alpha x^{3/2}}}, \tag{3.46}$$

where $\epsilon = +1$ represents the prograde solutions while $\epsilon = -1$ represents retrograde solutions. Because the radial part of the geodesic equations has a quadratic dependence on $\tilde{E}$ and l, there should be a second solution. A straightforward calculation shows that the second solution is

$$\tilde{E}' = -\tilde{E}, \quad l' = -l. \tag{3.47}$$

As already mentioned, the circular orbits exist only if $(x-3)x^2 \pm 2\alpha x^{3/2} \geq 0$ and equality is satisfied only by null orbits. For spacetimes with $\alpha > 1$, the equality is

satisfied by a *single* orbit which is retrograde. In other words, there is no prograde null orbit on the equatorial plane.

At this point, let us concentrate on an interesting property of the Kerr-type naked singularity spacetimes, which was first shown in [56]. For rotation parameter values which can be given as

$$\alpha\left(x\right)=\left(2-x\right)\sqrt{x}, \tag{3.48}$$

the particles can rotate in their prograde orbits with zero energy. This is not possible for Kerr spacetimes because these orbits are located inside the event horizon. Yet, because there is no event horizon for naked singularity spacetimes, these orbits are relevant. Even more interestingly, there are orbits with radii smaller than zero energy orbits which are followed by particles with negative energy, [57]. By using 3.48, one can find that zero and negative energy orbits are possible in the range $1<\alpha<\sqrt{\frac{32}{27}}=1.08866$ as can be seen in Fig. (3.16).

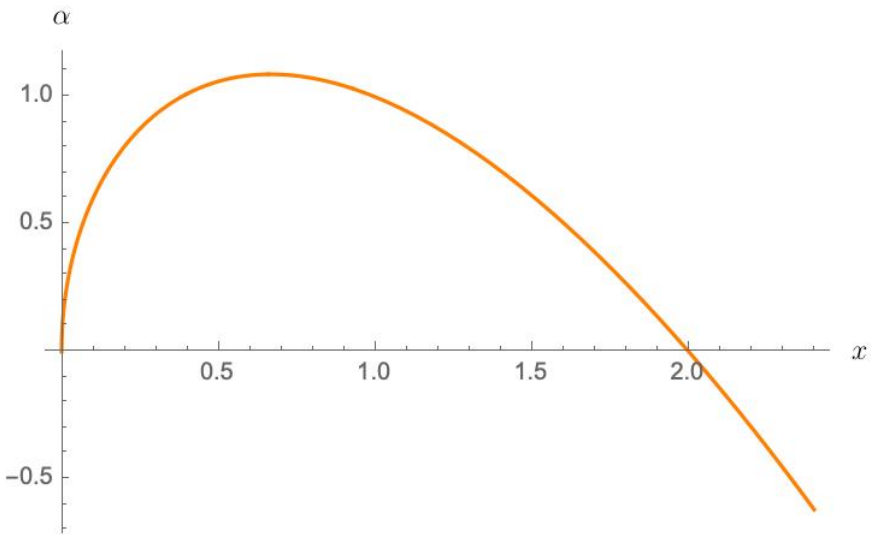

Figure 3.16: The rotation parameter relation (3.48) is plotted for the interval $0<x<2.4$. The maximum value of the rotation parameter is $\alpha=\sqrt{\frac{32}{27}}$ and this means that it is possible to find orbits with zero or negative energy for the interval $1<\alpha<\sqrt{\frac{32}{27}}$.

In addition to these zero energy orbits, zero angular momentum orbits or ZAMOs are also possible for Kerr-type naked singularity spacetimes as was shown in [56]. For rotation parameter values

$$\alpha\left(x\right)=\sqrt{x}\pm\sqrt{x-x^{2}}, \tag{3.49}$$

the particles can rotate in their orbits with zero angular momentum. The relation (3.49) can be seen in Fig. (3.17). The maximum of the rotation parameter can be calculated via 3.49 and it is $\alpha=\sqrt{\frac{27}{16}}=1.29904$. This means that it is possible to obtain orbits with zero or negative angular momenta for the interval $1<\alpha<\frac{3\sqrt{3}}{4}$.

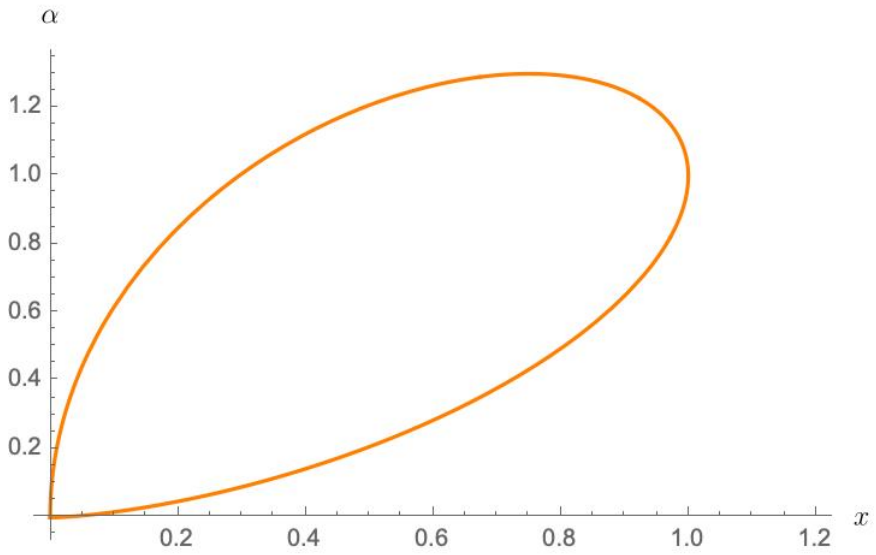

Figure 3.17: The rotation parameter relation (3.49) is plotted for the interval $0<x<1.2$. The maximum value of the rotation parameter is $\alpha=\frac{3\sqrt{3}}{4}$ and this means that it is possible to find orbits with zero or negative angular momentum for the interval $1<\alpha<\frac{3\sqrt{3}}{4}$.

The special case, the innermost stable circular orbits (ISCO), correspond to the orbits that satisfy the equation

$$-3\alpha^{2}+x^{2}\pm8\alpha\sqrt{x}-6x=0. \tag{3.50}$$

This condition accepts two solutions which correspond to prograde and retrograde ISCO. For the sake of simplicity, we will not provide the explicit expression here.

The other special case discussed for the Kerr black hole is the binding orbits. There

exist prograde and retrograde binding orbits for the Kerr-type naked singularity spacetime which can be given as

$$x_{bind,\pm} = 2 + \alpha \mp 2\sqrt{\alpha + 1}. \tag{3.51}$$

The prograde and retrograde ISCO and binding orbits as well as retrograde photon orbits can be seen in Fig. (3.18). All orbits on the equatorial plane for both intervals $0 < \alpha < 1$ and $1 < \alpha < 1.5$ are plotted in Fig. (3.19). The retrograde ISCO, binding orbit, and photon orbit continue to exist for the naked singularity spacetimes. The prograde ISCO, binding orbit, and the photon orbit merge at $\alpha = 1$. The prograde photon orbit does not exist for $\alpha > 1$. The prograde ISCO continues to exist but starts to move away from the singularity with an increasing rotation parameter. For the rotation parameter $\alpha = \frac{3\sqrt{3}}{4}$, the particles on the prograde ISCO has $l = 0$. The prograde binding orbit also continues to exist but there is a discontinuity at $\alpha = 1$ as can be seen in (3.19).

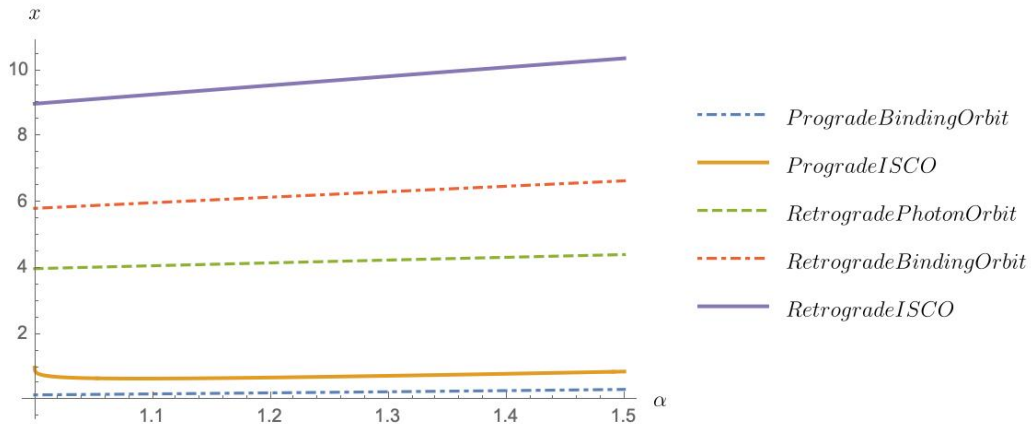

Figure 3.18: The prograde and retrograde ISCO and binding orbits, and retrograde photon orbit are plotted as a function of the rotation parameter for the interval $1 < \alpha < 1.5$. Observe that the prograde orbits are closer to the naked singularity than the retrograde orbits which means the latter have a larger capture cross-section. This fact plays an important role in the spinning-down effect.

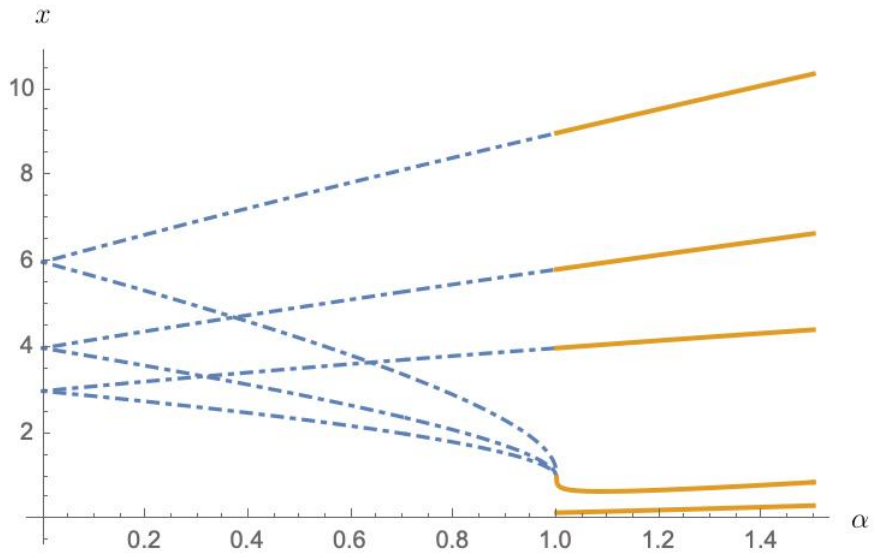

Figure 3.19: All equatorial orbits are plotted as a function of the rotation parameter for the interval $0 < \alpha < 1.5$. The dashed lines indicate orbits around the Kerr black hole, while solid lines indicate the orbits around Kerr-type naked singularity. The legends provided for Fig. 18 apply verbatim to this figure.

3.5.2.2 Spinning down the Singularity

An approach similar to the one developed by Bardeen [54] to investigate the effect of the particles in the accretion disk on the Kerr black hole can be developed for the Kerr-type naked singularity. Let us assume there is a Kerr-type naked singularity with an accretion disk with a negligible thickness on the equatorial plane. Let us also assume gravitational and electromagnetic radiation of this disk is negligible. The gravitational field of the disk itself is much smaller than the gravitational field of the singularity and therefore it is negligible. As a result, it can be assumed that particles on the disk follow circular orbits as already discussed in the previous section.

As a starting point, the change in the mass and the angular momentum of the Kerr-type naked singularity can be written as

$$\frac{\delta J}{\delta m} = mf\left(\alpha\right) \tag{3.52}$$

to denote their relation with the rotation parameter. Before starting the calculation, to

avoid complicated equations, let us define

$$\tilde{x} := \sqrt{x_{ISCO}}. \tag{3.53}$$

In what follows, we will prove the following fact

$$\delta\left(\ln \tilde{x}\right) \;=\; -\delta\left(\ln m\right), \tag{3.54}$$

which can also be succinctly written as [2]

$$\delta\left(m r_{ISCO}\right) \;=\; 0. \tag{3.55}$$

In the previous section, it was shown that, on the innermost stable circular orbit, the condition

$$\tilde{x}^4 - 6\tilde{x}^2 + 8\epsilon\alpha\tilde{x} - 3\alpha^2 = 0 \tag{3.56}$$

should be satisfied. One can solve this equation with respect to the rotation parameter, α. For retrograde orbits for which $\epsilon = -1$, there are two solutions, one of which provides negative rotation parameter values and can be ignored. The physically viable retrograde solution is

$$\alpha_r\left(\tilde{x}\right) = \frac{1}{3}\tilde{x}\left(\sqrt{3\tilde{x}^2 - 2} - 4\right). \tag{3.57}$$

Note that for $\tilde{x} \geq 3$, one has $\alpha \geq 1$. For prograde orbits for which $\epsilon = +1$, there are two solutions and both of them are physically viable in their corresponding ranges. For the prograde orbit which already appeared in [54],

$$\alpha_{p,1}\left(\tilde{x}\right) = \frac{1}{3}\tilde{x}\left(4 - \sqrt{3\tilde{x}^2 - 2}\right), \tag{3.58}$$

the corresponding range becomes $\sqrt{2/3} \leq \tilde{x} \leq 1$, and this range ensures that the rotation parameter is $1 \leq \alpha \leq \sqrt{\frac{32}{27}}$. The other prograde orbit is

$$\alpha_{p,2}\left(\tilde{x}\right) = \frac{1}{3}\tilde{x}\left(4 + \sqrt{3\tilde{x}^2 - 2}\right), \tag{3.59}$$

and it exists for $\sqrt{2/3} \leq \tilde{x}$ with a rotation parameter value $\sqrt{\frac{32}{27}} \leq \alpha$. Both rotation parameter solutions corresponding to prograde orbit can be seen in Fig. (3.20).

[2] This form was suggested to us by a very conscientious referee who also went over all the computations throughout this work.

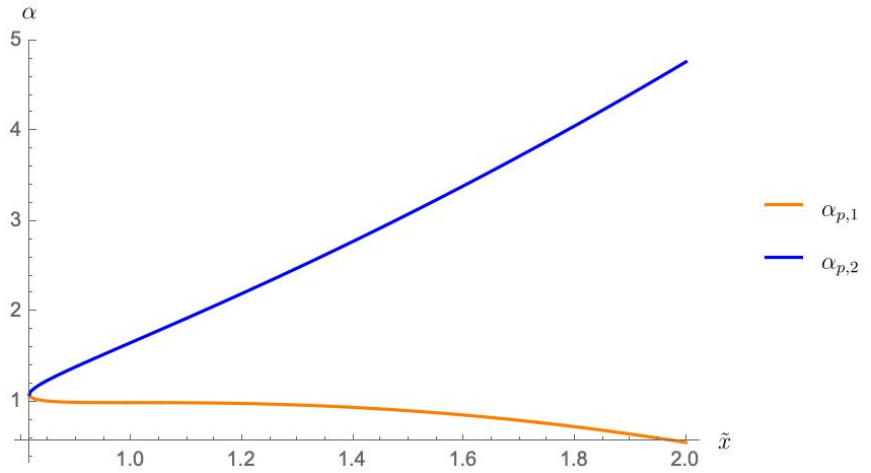

Figure 3.20: Two rotation parameters, $\alpha_{p,1}$ and $\alpha_{p,2}$, corresponding to prograde orbit are plotted as a function of $\tilde{x}$ for the interval $\sqrt{2/3} \leq \tilde{x} \leq 2$.

At this point, we assume that the infinitesimal changes in the mass and the angular momentum of the naked singularity are equal to those of particles coming from the innermost stable orbit. In other words, we assume that $\delta m = \tilde{E}_{ISCO}$ and $\delta J = l_{ISCO}$. One has

$$f(\alpha) = \frac{1}{m}\frac{\delta J}{\delta m} = \left.\frac{l_{\pm}}{\tilde{E}_{\pm}}\right|_{\tilde{x}}. \tag{3.60}$$

Let us start calculating the function $f(\alpha)$ for the retrograde orbits first.

$$f(\alpha) = \left.\frac{l_{-}}{\tilde{E}_{-}}\right|_{\tilde{x}} = -\frac{2\tilde{x}}{3}\left(2 + \frac{1}{\sqrt{3\tilde{x}^2 - 2}}\right), \tag{3.61}$$

where $\tilde{E}_{-}$ was given as 3.45, l_{-} was given as 3.46 and α was given as 3.57. By using the relation $J = \alpha m^2$, one can get

$$f(\alpha) = \frac{1}{m}\frac{\delta J}{\delta m} = \frac{\delta \alpha}{\delta(\ln m)} + 2\alpha. \tag{3.62}$$

With the help of 3.57, one has

$$\delta\alpha_r = \left(\frac{2}{3}\left(\frac{3\tilde{x}^2 - 1}{\sqrt{3\tilde{x}^2 - 2}} - 2\right)\right)\delta\tilde{x}. \tag{3.63}$$

Hence,

$$\begin{aligned} f(\alpha) - 2\alpha &= -\frac{2\tilde{x}}{3}\left(2 + \frac{1}{\sqrt{3\tilde{x}^2 - 2}}\right) - 2\alpha \\ &= -\frac{2\tilde{x}}{3}\left(-2 + \frac{1}{\sqrt{3\tilde{x}^2 - 2}} + \sqrt{3\tilde{x}^2 - 2}\right), \end{aligned} \tag{3.64}$$

and

$$\frac{\delta\alpha}{\delta\left(\ln m\right)} = \frac{2}{3}\left(\frac{3\tilde{x}^2-1}{\sqrt{3\tilde{x}^2-2}}-2\right)\frac{\delta\tilde{x}}{\delta\left(\ln m\right)}, \tag{3.65}$$

and by using 3.62 one can get

$$\delta\left(\ln\tilde{x}\right) = -\delta\left(\ln m\right), \tag{3.66}$$

of which the solution is $\tilde{x} = C/m$ where C is a positive constant and (3.57) becomes

$$\alpha_r\left(m\right) = \frac{C}{3m}\left(\sqrt{3\frac{C^2}{m^2}-2}-4\right). \tag{3.67}$$

The constant C can be found from the initial conditions with initial mass m_0 and the initial rotation parameter α_0. For instance, the retrograde ISCO is located at $x = 10.3759$ for $\alpha_0 = 1.5$; and hence $\tilde{x} = 3.22116$. So one finds $C = 3.22116m_0$. After the falling of matter, at a later time, the relation turns into

$$\tilde{x} = \frac{3.22116m_0}{m}. \tag{3.68}$$

Therefore, one can write the rotation parameter relation (3.57) as a function of the mass of the singularity

$$\alpha\left(m\right) = \frac{1.07372m_0}{m}\left(\sqrt{\frac{31.1277m_0^2}{m^2}-2}-4\right), \tag{3.69}$$

and this relation is valid for $1.07372 \geq \frac{m}{m_0}$. So after accreting a mass of $\delta m = 0.07372m_0$ the rotation parameter is reduced to $\alpha_r = 1$ from its initial value of $\alpha_r = 1.5$. Thus the particles following the retrograde ISCO quickly slow down the rotation of the singularity. This is a rather remarkable result: for example, naked singularity with mass $m_0 = 1$ kg and $\alpha_0 = 1.5$ only requires less than 74 grams of matter to reduce α to the extremal rotation with an event horizon. The results can be seen in the Fig. (3.21). See also the Appendix for an estimate.

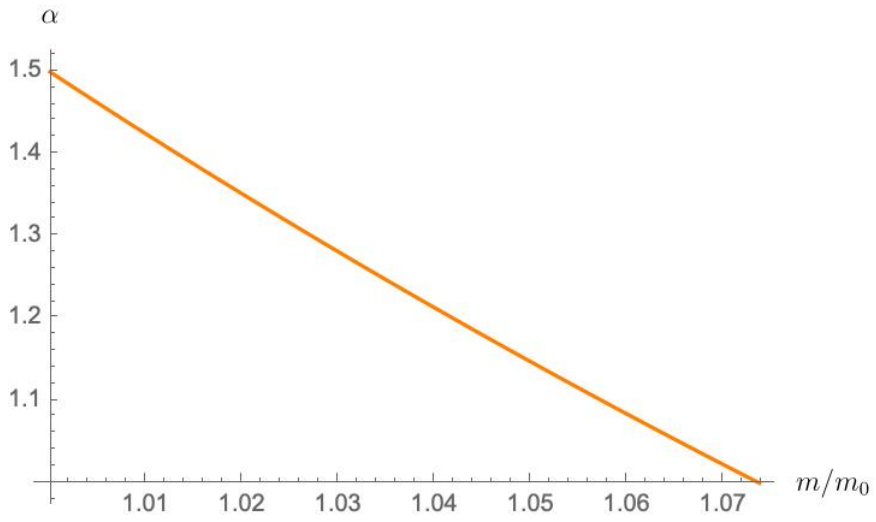

Figure 3.21: The rotation parameter is plotted as a function of the m/m_0 for the interval $1 \leq \frac{m}{m_0} \leq 1.07372$.

Now, we can concentrate on the prograde orbit. For prograde ISCO, from (3.60), one has

$$f\left(\alpha_{p,1}\right) = \frac{1}{m}\frac{l_+}{\tilde{E}_+}\bigg|_{\tilde{x}} = \frac{2\tilde{x}}{3}\left(2+\frac{1}{\sqrt{3\tilde{x}^2-2}}\right), \tag{3.70}$$

and

$$f\left(\alpha_{p,2}\right) = \frac{1}{m}\frac{l_+}{\tilde{E}_+}\bigg|_{\tilde{x}} = \frac{2\tilde{x}}{3}\left(2-\frac{1}{\sqrt{3\tilde{x}^2-2}}\right). \tag{3.71}$$

Let us first study the first prograde solution. Doing the computations as in the retrograde orbit case verbatim, we have

$$\begin{aligned} f\left(\alpha_{p,1}\right)-2\alpha_{p,1} &= \frac{2\tilde{x}}{3}\left(2+\frac{1}{\sqrt{3\tilde{x}^2-2}}\right)-2\alpha_{p,1} \\ &= \frac{2\tilde{x}}{3}\left(\frac{3\tilde{x}^2-1-2\sqrt{3\tilde{x}^2-2}}{\sqrt{3\tilde{x}^2-2}}\right). \end{aligned} \tag{3.72}$$

One can also find that

$$f\left(\alpha_{p,1}\right)-2\alpha_{p,1} = \frac{\delta\alpha}{\delta\left(\ln m\right)} = -\frac{2}{3}\left(\frac{3\tilde{x}^2-1-2\sqrt{3\tilde{x}^2-2}}{\sqrt{3\tilde{x}^2-2}}\right)\frac{\delta\tilde{x}}{\delta\left(\ln m\right)}. \tag{3.73}$$

These two equations give

$$\delta\left(\ln\tilde{x}\right) = -\delta\left(\ln m\right), \tag{3.74}$$

of which the solution is $\tilde{x} = C/m$ which is valid in the interval $\sqrt{2/3} \leq \tilde{x} \leq 1$. Let us consider a Kerr-type naked singularity with initial mass m_0 and initial rotation

parameter $\alpha_0 = 1.01$. The prograde ISCO is represented by $\alpha_{p,1}$ for this case and it is located at $x = 0.75192$ and hence $\tilde{x} = 0.867133$. As a result, $C = 0.867133 m_0$. After matter accretion, the relation evolves to

$$\tilde{x} = \frac{0.867133 m_0}{m}. \tag{3.75}$$

As a consequence, the rotation parameter as a function of mass becomes

$$\alpha_{p,1}(m) = \frac{0.289044 m_0}{m}\left(4 - \sqrt{\frac{2.25576 m_0^2}{m^2} - 2}\right), \tag{3.76}$$

which is valid in the interval $0.867133 \leq \frac{m}{m_0} \leq 1.06202$. But accretion will not lead to a decrease in mass, so one should restrict this interval to $1 \leq \frac{m}{m_0} \leq 1.06202$. The evolution of the rotation parameter can be seen in Fig. (3.22). As can be seen, this prograde orbit tries to increase the rotation parameter value up to $\alpha = \sqrt{\frac{32}{27}}$.

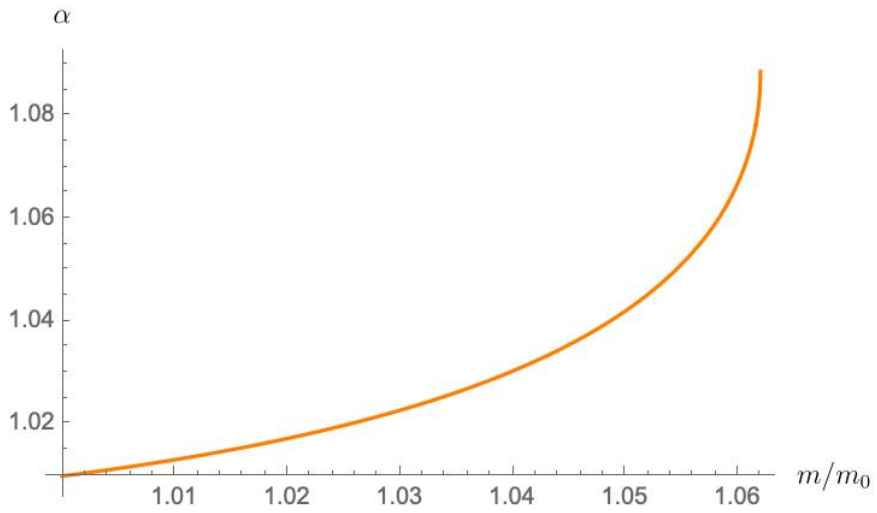

Figure 3.22: The rotation parameter is plotted with respect to $\frac{m}{m_0}$ for the interval $1 \leq \frac{m}{m_0} \leq 1.06202$.

Now, as a final case, we would like to investigate the second prograde solution. Following similar steps, one arrives at $\tilde{x} = C/m$. Assuming there is a Kerr-type naked singularity with an initial mass m_0 and an initial rotation parameter $\alpha_0 = 1.5$, the prograde ISCO can be found at $x = 0.879352$ and hence $\tilde{x} = 0.937738$ and $C = 0.937738 m_0$. So one has

$$\tilde{x} = \frac{0.937738 m_0}{m}. \tag{3.77}$$

As a consequence, the rotation parameter relation becomes

$$\alpha_{p,2}\left(m\right) = \frac{0.312579 m_0}{m}\left(4 + \sqrt{\frac{2.63806 m_0^2}{m^2} - 2}\right), \tag{3.78}$$

which is valid for $1.14849 \geq \frac{m}{m_0}$. The evolution of the rotation parameter can be seen in Fig. (3.23). It is interesting to observe that the particles coming from a prograde orbit slow down the rotation. The final rotation parameter value of this process is $\alpha = 1.08866$. After that value, the volution is governed by the solution of the second interval.

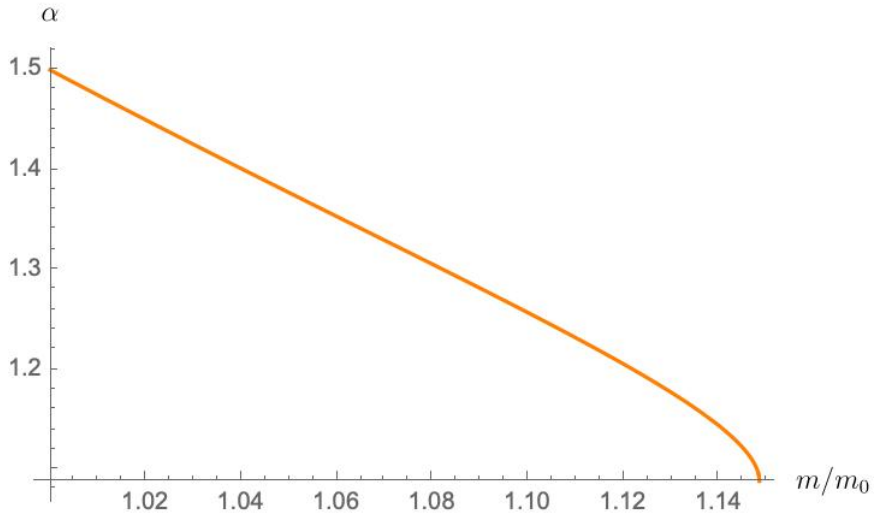

Figure 3.23: The rotation parameter is plotted as a function of $\frac{m}{m_0}$ for the interval $1 < \frac{m}{m_0} < 1.14849$.

To sum up, a Kerr-type naked singularity with an initial mass m_0 and an initial rotation parameter $\alpha_0 = 1.5$ is slowed down by all falling particles. For the retrograde particles, this is easy to understand. Yet, for the prograde particles, it is not: each orbiting particle brings its angular momentum and energy; if the prograde orbit has a higher energy contribution than its angular momentum contribution, then the dimensionless spin is still reduced. This slowing down process continues until $\alpha = \sqrt{\frac{32}{27}}$. Below $\alpha = \sqrt{\frac{32}{27}}$, the particles from the prograde orbit start to spin the singularity up while the particles from the retrograde orbit continue to slow it down as can be seen in Fig. (3.24) and Fig. (3.25). Due to the larger capture cross-section of the retrograde orbits, in the end, they win over the prograde ones and slow the spin further down until the event horizon appears.

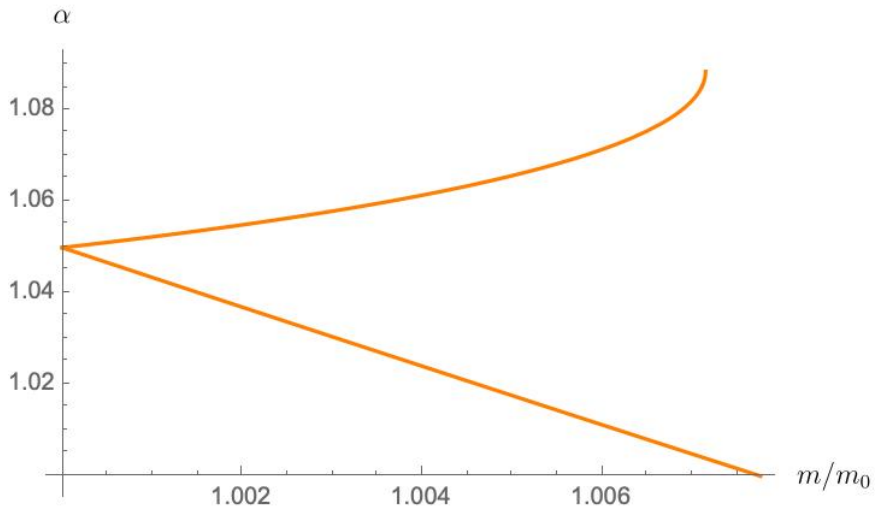

Figure 3.24: The rotation parameter of a naked singularity with initial mass m_0 and rotation parameter $\alpha_0 = 1.05$ is plotted for both prograde and retrograde orbits as a function of $\frac{m}{m_0}$ for the interval $1 < \frac{m}{m_0} < 1.00776$.

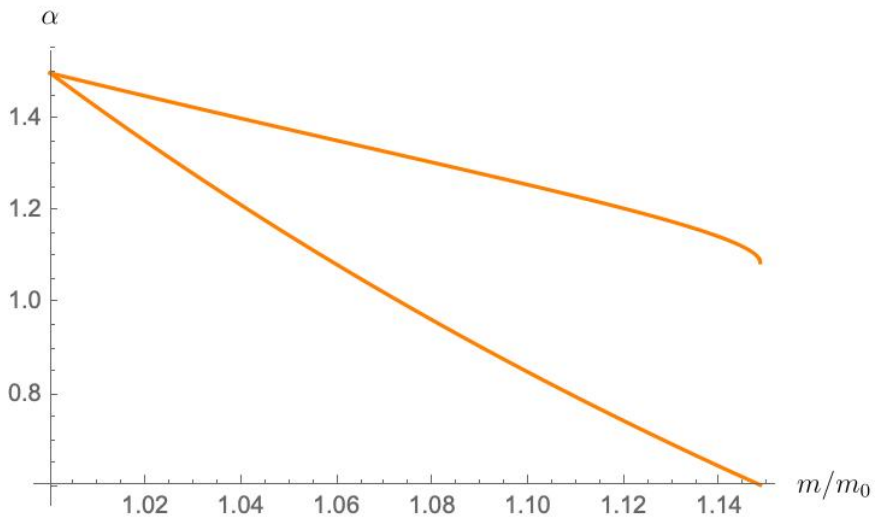

Figure 3.25: The rotation parameter of a naked singularity with initial mass m_0 and rotation parameter $\alpha_0 = 1.5$ is plotted for both prograde and retrograde orbits as a function of $\frac{m}{m_0}$ for the interval $1 < \frac{m}{m_0} < 1.14849$. Observe that the retrograde orbits continue to spin down the central object even after the event horizon is formed.

3.5.3 Remarks on earlier works

Let us remark on some of the earlier works about and complementing our discussion in this paper, especially in the context of the time evolution of the parameters of the naked singularity. In [58], the optical properties of the "silhouette" and the accretion disc around the Kerr "superspinars" were investigated in depth where constructing the image of the Kerr superspinar was done first, and then, the work focused on the optical properties of the accretion discs around it. While performing the analysis, they provided the Kerr naked singularity and Kerr black hole results for comparison. In another work [59], a comparison of the effects of counterrotating and corotating orbits around a Kerr superspinar was done. The authors discuss the accumulated mass from both orbits, the conversion times of both orbits and the radiated energy from both orbits. Their conclusion about the conversion time, the time needed to convert a Kerr superspinar into a near-extreme Kerr black hole, is much smaller for counterrotating orbit with respect to corotating orbit. Yet, the energy radiated from the corotating orbit is much higher than the counterrotating orbit. In other words, various Kerr superspinar properties were investigated. For instance, in [60], radial and vertical epicyclic frequencies of Keplerian motion in the field of Kerr naked singularities were studied; and in [61], observational properties of Kerr superspinars were demonstrated.

In [62] the question of obtaining the spin parameter and the inclination angle via the shadow of the Kerr black hole and the Kerr-type naked singularity was studied. For various inclination angles, the appearances of both a Kerr black hole and a rotating singularity are plotted. Our shadow discussion confirms the findings of this earlier work. Even though our discussion confirms the results of this work, we also discuss the analytically solvable case of the critical inclination angle which was more recently discovered in our earlier work [12].

A similar shadow analysis, that was used for the Kerr black hole, Kerr-type naked singularity, and Kerr superspinars, can be performed for many other models. For instance, in [63], the shadows of rotating black holes in the Randall-Sundrum type-II models have been investigated thoroughly. The interesting feature of this work is that they consider not only the near region of the black hole but also the linearized metric in the far region.

Another interesting paper, [64], provides a shadow analysis for three rotating regular no-horizon spacetimes, namely, Bardeen, charged Hayward, and nonsingular spacetimes. In that paper, the results were compared with Kerr black hole and Kerr-type naked singularity and they reached a remarkable result: unlike Kerr-type naked singularity spacetimes, which has not a closed shadow, there could be a closed shadow for no-horizon spacetimes as in the Kerr black hole.

CHAPTER 4

PARTITION FUNCTION OF A VOLUME OF SPACE IN A HIGHER CURVATURE THEORY

4.1 Partition Function for a Fixed Volume of Space

The quantum gravity partition function with a constraint in the general form can be written as

$$\mathcal{Z} = \int \mathcal{D}g e^{-I_E(g)} = \int \mathcal{D}\mu \int \mathcal{D}\xi \int \mathcal{D}g e^{-I_E(g)+\frac{1}{\hbar}\int d\phi \xi(\phi)(C(g)-\mu)}, \quad (4.1)$$

where $I_E(g)$ represents the Euclidean action that is under investigation, ξ is the Lagrange multiplier, and $C(g) - \mu = 0$ is the constraint equation. We shall consider the three-dimensional gravity introduced in [65]. In $2+1$ dimensions, Einstein's gravity with or without a cosmological constant has no local degrees of freedom. Hence, it has no resemblance to four-dimensional Einstein theory. In [66], a massive three-dimensional gravity theory was introduced which has two propagating degrees of freedom, just like four-dimensional Einstein gravity. The action of this new massive gravity theory (NMG) is

$$I_{NMG} = \frac{1}{\kappa^2}\int d^3x\sqrt{-g}\left[\sigma R + \frac{1}{m^2}\left(R_{\mu\nu}R^{\mu\nu} - \frac{3}{8}R^2\right) - 2\lambda_0 m^2\right], \quad (4.2)$$

where $\sigma = \pm 1$. Here, λ_0 is the bare dimensionless cosmological constant. In [65], this theory was extended in principle to infinite powers in the curvature expansion, and the new action is defined as

$$I_{BI-NMG} = -\frac{4m^2}{\kappa^2}\int d^3x\left[\sqrt{-\det\left(g + \frac{\sigma}{m^2}G\right)} - \left(1 - \frac{\lambda_0}{2}\right)\sqrt{-g}\right], \quad (4.3)$$

where $G_{\mu\nu} = R_{\mu\nu} - \frac{1}{2}g_{\mu\nu}R$. This theory has the following rather nice properties which we take from [67].

1. For $\lambda_0 \neq 0$, unlike any generic finite-order theory besides Einstein's gravity with a cosmological constant, it has a *unique* maximally symmetric vacuum with an effective cosmological constant $\Lambda = m^2\lambda$ given as [68, 69]

$$\lambda = -\sigma\lambda_0\left(1 - \frac{\lambda_0}{4}\right), \quad \lambda_0 < 2. \tag{4.4}$$

   For $\lambda_0 = 0$, the flat space is the unique vacuum. The uniqueness of the vacuum in this higher derivative theory is the same as in general relativity. This uniqueness property is not easily achievable in higher curvature gravity theories: For example, NMG has two maximally symmetric vacua.

2. The theory has a unitary massive spin-2 degree of freedom (with ± 2 modes) in flat space with mass $m_g = m$ and with mass $m_g = m\sqrt{1+\lambda}$ around the anti-de Sitter (AdS) backgrounds. This provides an infinite-order extension of the quadratic NMG which has the same perturbative properties.

3. In three dimensions, the Riemann and the Ricci tensors both carry six independent components; hence, a generic gravity theory built from the contractions and the powers of the Ricci curvature is of the form [70]

$$I = \int d^3x\sqrt{-g}\left[\frac{1}{\kappa}\left(R - 2\Lambda_0\right) + \sum_{n=2}^{\infty}\sum_{\substack{i=0\\ i\neq 1}}^{n}\sum_{j} a^j_{ni}\left(R^\mu_\nu\right)^i_j R^{n-i}\right], \tag{4.5}$$

   where i in $\left(R^\mu_\nu\right)^i_j$ represents the number of Ricci tensors, and j represents the number of possible ways to contract the i number of Ricci tensors. Generically, each higher curvature combination has a different dimensionful coupling constant denoted by a^j_{ni}. This theory generically has many maximally symmetric vacua, many massive degrees of freedom, and is nonunitary at the tree level about its constant curvature vacua. However, due to the determinantal nature of the Lagrangian, BINMG (4.3) as a very specific example of the generic theory (4.5) is consistent at infinite order or at any finite truncation in powers of curvature. By consistency, we mean it reproduces, up to desired order in the curvature expansion, the extended NMG theories that are consistent with the AdS/CFT duality and that have a c-function [68, 71, 72]. See [73] for details of these calculations.

4. The BINMG action appears as a counterterm in AdS_4 [74] and might have a supersymmetric extension [75].

All these considerations encourage us to study the Euclidean version of the BINMG theory following [3].

Going back to the partition function, for the spatial volume constraint (here it is actually an area of the disk, yet we will use the word volume to conform with the higher-dimensional cases) we have $C(g) = \int d^2x\sqrt{\gamma}$ and $\mu = V$ where the induced metric on the spatial disk is

$$\gamma_{\mu\nu} := g_{\mu\nu} - N^2 \left(\partial_\mu \phi\right)\left(\partial_\nu \phi\right), \qquad N := \left(g^{\mu\nu}\left(\partial_\mu \phi\right)\left(\partial_\nu \phi\right)\right)^{-\frac{1}{2}}. \tag{4.6}$$

Therefore, in the end, the constraint can be written as

$$\frac{1}{\hbar}\int d\phi \xi(\phi)\left(\int d^2x\sqrt{\gamma}\left(-V\right)\right), \tag{4.7}$$

which reduces the partition function to

$$\mathcal{Z}(V,\Lambda,m^2) = \int\int \mathcal{D}g\mathcal{D}\xi e^{-I_E(g)+\frac{1}{\hbar}\int d\phi\xi(\phi)\left(\int d^2x\sqrt{\gamma}(-V)\right)}. \tag{4.8}$$

In the next section, we will evaluate this partition function in the saddle point approximation, which is dominated by constrained instantons. For this purpose, we first need to find the field equations.

4.1.1 Field equations

When the constraint equation is satisfied, $C(g) = V$, the field equations can be obtained from the variation of the action at the saddle point approximation,

$$\delta I_E(g) - \frac{1}{\hbar}\int d\phi\xi(\phi)\delta(C(g)-\mu) = 0. \tag{4.9}$$

From the constraint equation, we get

$$\delta\left(\frac{1}{\hbar}\int d\phi\xi(\phi)(C(g)-\mu)\right) = \frac{1}{\hbar}\int d\phi\xi(\phi)\delta C(g) \tag{4.10}$$

and

$$\delta C(g) \;=\; \int d^2x\delta(\sqrt{\gamma}) = \int d^2x\left(-\frac{1}{2N}\sqrt{g}\gamma_{\mu\nu}\delta g^{\mu\nu}\right). \tag{4.11}$$

The field equations of BINMG are rather cumbersome, but fortunately, they were found in [68]. Following that computation verbatim, one first writes the Euclidean form of the BINMG action (4.3) in a more convenient way as

$$I_E = -\frac{4m^2}{\kappa^2}\int d^3x\sqrt{g}F(R,K,S), \tag{4.12}$$

where the Lagrangian is

$$F(R,K,S) \;:=\; \sqrt{1-\frac{\sigma}{2m^2}\left(R+\frac{\sigma}{m^2}K-\frac{1}{12m^4}S\right)}-\left(1-\frac{\lambda_0}{2}\right), \tag{4.13}$$

and the curvature invariants are defined as

$$K := R_{\mu\nu}R^{\mu\nu}-\frac{1}{2}R^2, \qquad\qquad S := 8R^{\mu\nu}R_{\mu\alpha}R^{\alpha}_{\nu}-6RR_{\mu\nu}R^{\mu\nu}+R^2. \tag{4.14}$$

Hence, one can get the variation of the action as

$$\begin{aligned}\delta I_E(g) &= -\frac{4m^2}{\kappa^2}\int d^3x\left(\delta\sqrt{g}F+\sqrt{g}\delta F\right) \qquad (4.15)\\ &= -\frac{4m^2}{\kappa^2}\int d^3x\sqrt{g}\left(-\frac{1}{2}g_{\mu\nu}F\delta g^{\mu\nu}+\frac{\partial F}{\partial R}\delta R+\frac{\partial F}{\partial K}\delta K+\frac{\partial F}{\partial S}\delta S\right).\end{aligned}$$

The final form of the action variation including the constraint part is

$$\begin{aligned}\delta I_E(g) &= -\frac{4m^2}{\kappa^2}\int d^3x\sqrt{g}\delta g^{\mu\nu} \qquad (4.16)\\ &\quad\times\left(-\frac{1}{2}g_{\mu\nu}F+\frac{\partial F}{\partial R}\frac{\delta R}{\delta g^{\mu\nu}}+\frac{\partial F}{\partial K}\frac{\delta K}{\delta g^{\mu\nu}}+\frac{\partial F}{\partial S}\frac{\delta S}{\delta g^{\mu\nu}}-\frac{\kappa^2}{8m^2\hbar}\frac{\xi(\phi)}{N}\gamma_{\mu\nu}\right),\end{aligned}$$

which yields the field equations

$$\mathcal{E}_{\mu\nu} = \frac{\kappa^2}{8m^2\hbar}T_{\mu\nu}, \tag{4.17}$$

where

$$\mathcal{E}_{\mu\nu} := -\frac{1}{2}g_{\mu\nu}F+\frac{\partial F}{\partial R}\frac{\delta R}{\delta g^{\mu\nu}}+\frac{\partial F}{\partial K}\frac{\delta K}{\delta g^{\mu\nu}}+\frac{\partial F}{\partial S}\frac{\delta S}{\delta g^{\mu\nu}}, \tag{4.18}$$

and the constraint acts as a source of perfect fluid without an energy density but with pressure

$$T_{\mu\nu} := \frac{\xi(\phi)}{N}\gamma_{\mu\nu}. \tag{4.19}$$

To be able to find the constrained instanton solution, we still need the explicit form of the field equations which were given in [68] as

$$\begin{aligned}\frac{\kappa^2}{8m^2\hbar^2}T_{\mu\nu} = \quad & -\frac{1}{2}Fg_{\mu\nu} + \left(g_{\mu\nu}\Box - \nabla_\mu\nabla_\nu\right)F_R + F_R R_{\mu\nu} \\ & -\frac{\sigma}{m^2}\left\{2\nabla_\alpha\nabla_\mu\left(F_R R^\alpha{}_\nu\right) - g_{\mu\nu}\nabla_\beta\nabla_\alpha\left(F_R R^{\alpha\beta}\right)\right. \\ & -\Box\left(F_R R_{\mu\nu}\right) - 2F_R R_\nu{}^\alpha R_{\mu\alpha} + g_{\mu\nu}\Box\left(F_R R\right) \\ & \left.-\nabla_\mu\nabla_\nu\left(F_R R\right) + F_R R R_{\mu\nu}\right\} - \frac{1}{2m^4}\left\{4F_R R^\rho{}_\mu R_{\rho\alpha}R^\alpha{}_\nu\right. \\ & +2g_{\mu\nu}\nabla_\alpha\nabla_\beta\left(F_R R^{\beta\rho}R^\alpha{}_\rho\right) + 2\Box\left(F_R R_\nu{}^\rho R_{\mu\rho}\right) \\ & -4\nabla_\alpha\nabla_\mu\left(F_R R_\nu{}^\rho R^\alpha{}_\rho\right) + 2\nabla_\alpha\nabla_\mu\left(F_R R R^\alpha{}_\nu\right) \\ & -g_{\mu\nu}\nabla_\alpha\nabla_\beta\left(F_R R R^{\alpha\beta}\right) - \Box\left(F_R R R_{\mu\nu}\right) - 2F_R R R_\nu{}^\rho R_{\mu\rho} \\ & -g_{\mu\nu}\Box\left(F_R R^2_{\alpha\beta}\right) + \nabla_\nu\nabla_\mu\left(F_R R^2_{\alpha\beta}\right) - F_R R^2_{\alpha\beta}R_{\mu\nu} \\ & \left.+\frac{1}{2}g_{\mu\nu}\Box\left(F_R R^2\right) - \frac{1}{2}\nabla_\mu\nabla_\nu\left(F_R R^2\right) + \frac{1}{2}F_R R^2 R_{\mu\nu}\right\},\end{aligned} \tag{4.20}$$

where

$$F_R := \frac{\partial F}{\partial R} = -\frac{\sigma}{4m^2\left[F + \left(1 - \frac{\lambda_0}{2}\right)\right]}. \tag{4.21}$$

Next, we will solve these equations for a particular saddle point that has two Killing symmetries. From now on, we will work in the units for which $\hbar = c = 1$.

4.1.2 Saddle point metric

Let us consider a metric with ϕ and θ as Killing coordinates such that $\xi(\phi) = \xi$:

$$ds^2 := N^2(r)d\phi^2 + h(r)dr^2 + r^2 d\theta^2. \tag{4.22}$$

$N(r)$ and $h(r)$ are to be determined from (4.20) and the boundary conditions to be discussed. When (4.22) is plugged into (4.20), the resulting differential equations are still highly complicated. Therefore, guided by the discussion in [3], we take the following ansatz:

$$h(r) \;:=\; \frac{1}{1 - \frac{r^2}{L^2}} = \frac{1}{1 - \Lambda r^2}, \tag{4.23}$$

where L is the dS radius defined as $L^2 = 1/\Lambda$. Given this $h(r)$ in this saddle point metric, one can determine $N(r)$, but the ordinary differential equation is still highly

nonlinear, and it pays to discuss the boundary conditions first. We expect the lapse function $N(r)$ to vanish on the surface of the constraint volume $N(R_V) = 0$, where R_V can be found by using the constraint equation $\int d^2x\sqrt{\gamma} = V$. Analogous to the discussion given in [3], to remove the canonical singularity at the surface of the constraint boundary, we impose

$$\left.\frac{dN}{dl}\right|_{l=0} = 1, \tag{4.24}$$

where l is the distance from the horizon, i.e., the constraint volume surface $l = R_V - r$.

4.2 $\lambda_0 = 0$ Solution

For the flat spacetime, $\lambda_0 = 0$, $\Lambda = 0$ and $h(r) = 1$. When we insert (4.22) into (4.20), one finds that in order to obtain $\mathcal{E}_{\phi\phi} = 0$ since $T_{\phi\phi} = 0$, the lapse function should be of the form $N(r) = \alpha r^2 + \beta$, where α and β are to be found from the boundary conditions. The first boundary condition, namely, the lapse function should vanish on the surface of the volume constraint, gives $N(r) = \alpha\,(r^2 - R_V^2)$. For the second boundary condition, we have

$$\left.\frac{dN(l)}{dl}\right|_{l=0} = (2\alpha l - 2\alpha R_V)_{l=0} = -2\alpha R_V = 1 \tag{4.25}$$

yielding $N(r) = \frac{1}{2R_V}\,(R_V^2 - r^2)$. From the constraint equation, we have

$$\int d^2x\sqrt{\gamma} = \int_0^{R_V}\int_0^{2\pi} dr d\theta\, r = \pi R_V^2 = V, \tag{4.26}$$

so $R_V = \sqrt{\frac{V}{\pi}}$. In conclusion, the metric we obtained for the flat spacetime at the Euclidean saddle becomes

$$ds^2 \;=\; \frac{1}{4R_V^2}\left(R_V^2 - r^2\right)^2 d\phi^2 + dr^2 + r^2 d\theta^2. \tag{4.27}$$

Finally, for this constrained instanton, we get

$$\sqrt{\det(g + \frac{\sigma}{m^2}G)} = \frac{r\left(r^2 - R_V^2 + \frac{2}{m^2}\right)}{2R_V},\;\; \sqrt{g} = \frac{r\,(r - R_V)\,(r + R_V)}{2R_V}, \tag{4.28}$$

and the action becomes

$$I_E = -\frac{4m^2}{\kappa^2}\int d^3x\left[\sqrt{\det(g + \frac{\sigma}{m^2}G)} - \sqrt{g}\right] = -\frac{8\pi^2}{\kappa^2}R_V. \tag{4.29}$$

The circumference of the disk has the "area" $A_V = 2\pi R_V$. As a result, the action in terms of the area can be written as

$$I_E = -\frac{8\pi^2}{\kappa^2} R_V = \left(-\frac{4\pi}{\kappa^2}\right) A_V = -\frac{A_V}{4G_3}, \tag{4.30}$$

where in the last equality, we introduced the three-dimensional Newton's constant G_3 as

$$G_3 = \frac{\kappa^2}{16\pi}. \tag{4.31}$$

This result is the same as the Bekenstein-Hawking or Gibbons-Hawking results, except here we calculated not for a black hole or de Sitter horizon but for a bounded disk. Hence, the dimension of the Hilbert space is $\mathcal{Z} = \exp\left(\frac{A_V}{4G_3}\right)$.

As a final step, for completeness, let us calculate the Lagrange multiplier ξ. We know that

$$\mathcal{E}_{rr} = \frac{1}{m^2\left(R_V^2 - r^2\right)}, \qquad T_{rr} = \frac{2R_V}{R_V^2 - r^2}\xi. \tag{4.32}$$

This component of the field equations yields

$$\xi \;=\; \frac{1}{4\pi G_3 R_V}. \tag{4.33}$$

4.3 $\lambda_0 \neq 0$ Solution

We again take the metric as (4.22) with $h(r) = \frac{1}{1-\frac{r^2}{L^2}}$. Let us make a change of variables to simplify the ensuing discussion and define $r = L\sin\chi$ and $u = \sin\chi$ for which the metric becomes

$$ds^2 = L^2 N^2(u)\, d\phi^2 + \frac{L^2}{1-u^2} du^2 + L^2 u^2 d\theta^2. \tag{4.34}$$

We assume $N(\chi) = \alpha\cos\chi + \beta$. The first boundary condition on the lapse function discussed in the previous section gives $N(\chi) = \alpha(\cos\chi - \cos\chi_V)$. From the second boundary condition, one determines $\alpha = \frac{1}{\sin\chi_V}$. As a result, the lapse function becomes

$$N(\chi) = \frac{\cos\chi - \cos\chi_V}{\sin\chi_V}, \qquad \text{so} \qquad N(u) = \frac{\sqrt{1-u^2} - \sqrt{1-u_V^2}}{u_V}, \tag{4.35}$$

and the metric becomes

$$ds^2 = L^2\left(\frac{\sqrt{1-u^2} - \sqrt{1-u_V^2}}{u_V}\right)^2 d\phi^2 + \frac{L^2}{1-u^2} du^2 + L^2 u^2 d\theta^2. \tag{4.36}$$

We still need to determine the relation between L^2, m^2, and the bare cosmological constant λ_0. This follows from $\mathcal{E}_{\phi\phi} = \frac{\kappa^2}{8m^2\hbar} T_{\phi\phi} = 0$, and we get

$$\lambda_0 = -\frac{2Lm}{\sqrt{L^2m^2 - \sigma}} + \frac{2\sigma}{Lm\sqrt{L^2m^2 - \sigma}} + 2, \tag{4.37}$$

or in a more compact form,

$$\frac{1}{L^2} = \Lambda = m^2\sigma\lambda_0 \left(1 - \frac{\lambda_0}{4}\right), \tag{4.38}$$

which is the same result obtained in [68]. The next order of business is to evaluate the action of the constrained instanton metric (4.36). In the u coordinate the action looks a little cumbersome, but in the χ coordinate, it becomes

$$\begin{aligned} I_E &= -\frac{4m^2}{\kappa^2} \int d^3x \left[-\frac{\sigma \sin\chi \sqrt{L^2m^2 - \sigma}}{m^3 \sin\chi_V} \right] \\ &= \frac{4\sigma\sqrt{L^2m^2 - \sigma}}{\kappa^2 m \sin\chi_V} \int_0^{2\pi} \int_0^{\chi_V} \int_0^{2\pi} d\phi d\chi d\theta \sin\chi \\ &= \frac{\pi\sigma\sqrt{L^2m^2 - \sigma}}{mG_3 \sin\chi_V} \left(1 - \cos\chi_V\right), \end{aligned} \tag{4.39}$$

where in the last equality we used $\kappa^2 = 16\pi G_3$. Now, we can turn to our constraint equation and calculate the "volume" and area of the disk. For the volume of the boundary, one has

$$V = \int d^2x\sqrt{\gamma} = 2\pi L^2 \left(1 - \cos\chi_V\right), \tag{4.40}$$

and the area of the boundary becomes

$$A_V = \int_0^{2\pi} d\theta L \sin\chi_V = 2\pi L \sin\chi_V. \tag{4.41}$$

In terms of these, the action (4.39) becomes

$$I_E = \left(\frac{\pi}{G_3}\frac{V}{A_V}\right) \sigma \sqrt{1 - \frac{\sigma}{L^2m^2}}. \tag{4.42}$$

For a generic n-ball, one has $V = \frac{R_V}{2} A_V = \frac{L\sin\chi_V}{2} A_V$. Therefore, (4.42) becomes

$$I_E = \frac{A_V}{4G_3} \sigma \sqrt{1 - \frac{\sigma\Lambda}{m^2}}. \tag{4.43}$$

This is an interesting result: For $\Lambda = 0$ and $\sigma = -1$, it reduces to (4.30). Therefore, from now on we set $\sigma = -1$. For $\Lambda \neq 0$, this is exactly the same as the Wald entropy [76] defined as

$$S_W = -2\pi \oint \left(\frac{\partial L}{\partial R_{\rho\sigma}} g^{\mu\nu} \varepsilon_{\mu\rho} \varepsilon_{\nu\sigma}\right) d^3x, \tag{4.44}$$

where $\varepsilon_{\mu\rho}$ is the binormal vector to the constraint boundary surface. It is shown in [77] that the Wald entropy for the BINMG in the de Sitter spacetime becomes [1]

$$S_W = \frac{A}{4}\frac{1}{G_3}\sqrt{1+\frac{\Lambda}{m^2}}. \tag{4.45}$$

Therefore, the Euclidean action of the constrained instanton is exactly equal to the minus of the Wald entropy evaluated not at the de Sitter horizon but at the constraint boundary. Moreover, we can also relate the result to the Bekenstein-Hawking or Gibbons-Hawking result as follows. In the BINMG theory, one needs to define the effective gravitational constant as [77, 78]

$$\frac{1}{G_{\text{eff}}} := \frac{1}{G_3}\frac{\bar{R}_{\mu\nu}}{\bar{R}}\left(\frac{\partial\mathcal{L}}{\partial R_{\mu\nu}}\right)_{\bar{R}} = \frac{1}{G_3}\sqrt{1+\frac{\Lambda}{m^2}}. \tag{4.46}$$

Hence, as a result, the Wald entropy is just like the Bekenstein-Hawking entropy

$$S_W = \frac{A}{4G_{\text{eff}}}. \tag{4.47}$$

In conclusion, the entropy that we have calculated for the constrained volume is equivalent to the Wald or Bekenstein-Hawking entropies, and the dimension of the Hilbert space is given as

$$\mathcal{Z}\left(\Lambda, V, m^2\right) = e^{-I_E} = e^{\frac{A_V}{4G_3}\sqrt{1+\frac{\Lambda}{m^2}}} = e^{\frac{A_V}{4G_{\text{eff}}}}. \tag{4.48}$$

Let us note that, even though the constrained instanton has a finite action, as in the case of [3], for both $\lambda_0 = 0$ and $\lambda_0 \neq 0$ cases, there is a mild singularity at the boundary for the Ricci tensor and the stress-energy tensor.

As a final step, for completeness, let us calculate the Lagrange multiplier ξ. By using the relation

$$\mathcal{E}_{\mu\nu} = \frac{\kappa^2}{8m^2}T_{\mu\nu} = \frac{2\pi G_3}{m^2}\frac{\xi}{N(\chi)}\gamma_{\mu\nu}, \tag{4.49}$$

and the explicit forms of $\mathcal{E}_{rr}$ and γ_{rr}, one can find

$$\xi = -\frac{\cot\chi_V}{4\pi G_3\sqrt{L^2m^2+1}} = -\frac{1}{4\pi G_3}\frac{1}{mR_V}\frac{\cos\chi_V}{\sqrt{1+\frac{\Lambda}{m^2}}}. \tag{4.50}$$

[1] Note that in [77] the overall sign of the Wald entropy is opposite because the action in that work is written with the pseudo-Riemannian metric.

CHAPTER 5

REFINED THERMODYNAMICS OF BLACK HOLES WITH PROPER CONSERVED CHARGES

5.1 The Thermodynamics of Einstein Gravity with a cosmological constant

As the generic $D \geq 4$ dimensional computation becomes somewhat cumbersome, we first establish the definitions in the five-dimensional (5D) rotating black hole with two rotation parameters and then give the results of the generic dimensional cases.

5.1.1 Kerr-AdS black hole in five dimensions

In the units $\hbar = c = k_B = G = 1$ and $\Omega_3 = 2\pi^2$, the theory defined by the action

$$I = \frac{1}{4\Omega_3} \int d^5x \sqrt{-g} \left(R - 2\Lambda\right) \tag{5.1}$$

admits a three-parameter solution (the rotation parameters a, b and the mass parameter m), which in the coordinates $x^\mu = (t, r, \theta, \varphi, \psi)$ reads [32, 33, 34]

$$\begin{aligned} ds^2 &= -\frac{\Delta_\theta \left(1 - \frac{\Lambda r^2}{6}\right)}{\Xi_a \Xi_b} dt^2 + \frac{\rho^2}{\Delta_r} dr^2 + \frac{\rho^2}{\Delta_\theta} d\theta^2 + \frac{r^2 + a^2}{\Xi_a} \sin^2\theta d\varphi^2 \\ &\quad + \frac{r^2 + b^2}{\Xi_b} \cos^2\theta d\psi^2 + \frac{2m}{\rho^2} \left(\frac{\Delta_\theta}{\Xi_a \Xi_b} dt - \frac{a^2 \sin^2\theta}{\Xi_a} d\varphi - \frac{b^2 \cos^2\theta}{\Xi_b} d\psi\right)^2, \end{aligned} \tag{5.2}$$

where the metric functions are

$$\begin{aligned} \Delta_r &:= \frac{\left(r^2 + a^2\right)\left(r^2 + b^2\right)\left(1 - \frac{\Lambda r^2}{6}\right)}{r^2} - 2m, \\ \Delta_\theta &:= 1 + \frac{a^2\Lambda}{6} \cos^2\theta + \frac{b^2\Lambda}{6} \sin^2\theta, \\ \rho^2 &:= r^2 + a^2 \cos^2\theta + b^2 \sin^2\theta, \end{aligned} \tag{5.3}$$

and $\Xi_a = 1 + \frac{a^2\Lambda}{6}$, $\Xi_b = 1 + \frac{b^2\Lambda}{6}$. The (outer) event horizon is located at $r_{\rm H}$ at which the Killing vector $\xi_{\rm H} = \partial_t + \Omega_{\rm H}^{\varphi}\partial_\varphi + \Omega_{\rm H}^{\psi}\partial_\psi$ becomes null with the horizon angular velocities given as

$$\Omega_{\rm H}^{\varphi} = \frac{a\left(1 - \frac{\Lambda r_{\rm H}^2}{6}\right)}{(r_{\rm H}^2 + a^2)}, \quad \Omega_{\rm H}^{\psi} = \frac{b\left(1 - \frac{\Lambda r_{\rm H}^2}{6}\right)}{(r_{\rm H}^2 + b^2)}. \tag{5.4}$$

So $r_{\rm H}$ is given by the largest root of

$$(1 - \frac{\Lambda}{6}r_{\rm H}^2)(r_{\rm H}^2 + a^2)(r_{\rm H}^2 + b^2) - 2m{r_{\rm H}}^2 = 0. \tag{5.5}$$

These are sufficient to calculate the thermodynamical quantities of the solution. The entropy of this 5D rotating black hole is

$$S = \frac{\pi\left(r_{\rm H}^2 + a^2\right)\left(r_{\rm H}^2 + b^2\right)}{\Xi_a \Xi_b r_{\rm H}}, \tag{5.6}$$

while its temperature is [79]

$$T = \frac{r_{\rm H}^4\left(1 - \frac{\Lambda}{6}\left(2r_{\rm H}^2 + a^2 + b^2\right)\right) - a^2b^2}{2\pi r_{\rm H}\left(r_{\rm H}^2 + a^2\right)\left(r_{\rm H}^2 + b^2\right)}. \tag{5.7}$$

Please note that, due to the overall normalization of our action, the area law reads as $S = \frac{\pi}{\Omega_{D-2}}A$. To properly account for the cosmological constant in black hole thermodynamics, following [80], a rank-four totally antisymmetric gauge field is introduced [79] in such a way that the cosmological constant appears as a parameter of the solution and not a coupling constant defining the theory. This is also well-motivated in string or supergravity theories in which the cosmological constant appears as an expectation value of some potential, or appears after compactification [36]. The desired action reads

$$I = \int \frac{d^5x}{16\pi}\left(R \mp \frac{2}{5!}F^2 \pm \frac{4\nabla_\mu\left(A_{\mu_2\ldots\mu_5}F^{\mu\mu_2\cdots\mu_5}\right)}{4!}\right), \tag{5.8}$$

which has a $U(1)$ gauge symmetry: $A \to A + d\lambda(x)$ where $\lambda(x)$ is a totally antisymmetric three-form. The global part of this gauge symmetry yields, via the usual Noether's theorem, a conserved charge that is called the "cosmological charge" given as [81]

$$C := \pm\frac{\sqrt{|\Lambda|}}{2\pi^2}. \tag{5.9}$$

For this conserved charge, there exists a thermodynamical conjugate, the "cosmological potential" defined as a surface integral of the contraction of the hypersurface-generating null-Killing vector field with the gauge potential as

$$\Theta_{\rm H} := \oint_{\rm H} \xi_{\rm H} \cdot A, \tag{5.10}$$

where A is the cosmological gauge field $A_{\mu_1 \ldots \mu_4}$. This integral, for the 5D metric above, yields the cosmological potential

$$\Theta_{\mathrm{H}} = -\frac{\sqrt{|\Lambda|}\pi^2}{\Xi_a \Xi_b}\left(\frac{\left(r_{\mathrm{H}}^2 + a^2\right)\left(r_{\mathrm{H}}^2 + b^2\right)}{2} + \frac{m\left(a^2 + b^2 + \frac{\Lambda a^2 b^2}{3}\right)}{3\Xi_a \Xi_b}\right). \tag{5.11}$$

The mass and angular momenta of the solution can be computed from the following formula [82, 83] (which is given for generic D spacetime dimensions as is needed later):

$$Q\left(\bar{\xi}\right) = k\int_{\partial\bar{\Sigma}} d^{D-2}x\,\sqrt{\bar{\gamma}}\,\bar{\epsilon}_{\mu\nu}\left(R^{\nu\mu}{}_{\beta\sigma}\right)^{(1)}\bar{\mathcal{F}}^{\beta\sigma}, \tag{5.12}$$

where $k := \frac{(D-1)(D-2)}{8(D-3)\Lambda\Omega_{D-2}}$ and $\left(R^{\nu\mu}{}_{\beta\sigma}\right)^{(1)}$ is the linearized part of the Riemann tensor about the (A)dS background; while the antisymmetric two-form reads as $\bar{\mathcal{F}}^{\beta\sigma} = \bar{\nabla}^{\beta}\bar{\xi}^{\sigma}$ with $\bar{\xi}^{\sigma}$ being a background Killing vector corresponding to the relevant symmetry. The antisymmetric two-form $\bar{\epsilon}$ has the components $\bar{\epsilon}_{\mu\nu} := \frac{1}{2}\left(\bar{n}_{\mu}\bar{\sigma}_{\nu} - \bar{n}_{\nu}\bar{\sigma}_{\mu}\right)$, where $\bar{n}_{\mu}$ is a normal one-form on the boundary of spacetime, $\partial\bar{\mathscr{M}}$, $\bar{\sigma}_{\nu}$ is the unit normal one-form on the spatial boundary $\partial\bar{\Sigma}$, and $\bar{\gamma}$ is the induced metric on the boundary. For the metric (5.2), with $\bar{\xi} = -\partial_t$, $\bar{\xi} = \partial_{\varphi}$, and $\bar{\xi} = \partial_{\psi}$, one obtains, respectively [84], the following conserved charges:

$$E = \frac{m\left(2\Xi_a + 2\Xi_b - \Xi_a\Xi_b\right)}{2\Xi_a^2\Xi_b^2},\; J_{\varphi} = \frac{am}{\Xi_a^2\Xi_b},\; J_{\psi} = \frac{bm}{\Xi_b^2\Xi_a}. \tag{5.13}$$

Finally, using these thermodynamical coordinates and their conjugates (5.4), (5.6), (5.7), (5.9), (5.11), (5.13), one arrives at the first law of black hole thermodynamics:

$$\delta E = T\delta S + \Omega_{\mathrm{H}}^{\varphi}\delta J_{\varphi} + \Omega_{\mathrm{H}}^{\psi}\delta J_{\psi} + \Theta_{\mathrm{H}}\delta C, \tag{5.14}$$

and the following Smarr relation is satisfied:

$$E = 3TS + 3\Omega_{\mathrm{H}}^{\varphi}J_{\varphi} + 3\Omega_{\mathrm{H}}^{\psi}J_{\psi} - \Theta_{\mathrm{H}}C. \tag{5.15}$$

It is apt to note the following: with the necessary introduction of the cosmological constant as a conserved charge of the solution, the physical meaning E as energy changes: now it is the *gravitational enthalpy* of the solution, i.e., the energy needed to create this black hole with the given properties in a spacetime with the given cosmological constant. The cosmological constant (or here the cosmological charge) and the pressure can be identified while the cosmological potential defines an effective volume of the black hole that can be interpreted as the volume inside the event horizon,

or the difference of the renormalized volume of total spacetime when the difference refers to the difference of regularized volumes in the presence and the absence of the black hole [85, 86]. Therefore, the missing $P\delta V$ term in the conventional thermodynamics arises as $V\delta P$ in the black hole physics. This interpretation and the related thermodynamical volume of black holes has given rise to an interesting subbranch of black hole physics dubbed "black hole chemistry" [86, 87, 88, 89, 90]. Setting the negative heat capacity of black holes aside, the fact that these thermodynamical relations are satisfied by the pure gravitational field, that is, pure geometry, in a way similar to the thermodynamical relations of matter, gives one the following hint: thermodynamics, as our most crude description of a physical system, captures the gross features of a large cloud of gas not only before but also after it collapses into a black hole. Next, we generalize these results to generic $D \geq 4$ dimensions. The discussion bifurcates because of the special features of odd and even dimensions that allow different numbers of integration parameters. As the metric is somewhat cumbersome, we give the details of the computations in Appendix-C: Thermodynamic Quantities for Kerr-AdS Spacetimes and note the salient features here.

5.1.2 Kerr-AdS spacetimes in even dimensions

Taking the action to be $I = \frac{1}{4\Omega_{D-2}} \int d^D x \sqrt{-g}\,(R - 2\Lambda)$, with an even number of dimensions, $D = 2N + 2$, there are N distinct rotations; and the thermodynamic quantities become

$$
\begin{aligned}
E &= \frac{m}{\Xi} \sum_{i=1}^{N} \frac{1}{\Xi_i}, \quad J_i = \frac{m a_i}{\Xi_i \Xi}, \\
T &= \frac{r_{\rm H}\,(1 + g^2 r_{\rm H}^2)}{2\pi} \sum_{i=1}^{N} \frac{1}{r_{\rm H}^2 + a_i^2} - \frac{1 - g^2 r_{\rm H}^2}{4\pi r_{\rm H}}, \\
S &= \pi \prod_{i=1}^{N} \frac{r_{\rm H}^2 + a_i^2}{\Xi_i}, \quad \Omega_i = \frac{(1 + g^2 r_{\rm H}^2)\, a_i}{r_{\rm H}^2 + a_i^2}, \\
C &= \pm \frac{\sqrt{|\Lambda|}}{\Omega_{D-2}},
\end{aligned}
\tag{5.16}
$$

where $\Xi_i := 1 - g^2 a_i^2$, $g^2 := -\frac{2\Lambda}{(D-1)(D-2)}$, and $\Xi := \prod_{i=1}^{N} \Xi_i$. The event horizon is located at the largest root of the polynomial

$$\left(1 + g^2 r_{\rm H}^2\right) \prod_{i=1}^{N} \left(r_{\rm H}^2 + a_i^2\right) - 2m r_{\rm H} = 0. \tag{5.17}$$

These quantities satisfy the first law of black hole thermodynamics

$$\delta E = T\delta S + \sum_{i=1}^{N} \Omega_i \delta J_i + \Theta_{\rm H} \delta C \tag{5.18}$$

and the Smarr relation

$$(D-3)\, E = (D-2) \left(TS + \sum_{i=1}^{N} \Omega_i J_i \right) - \Theta_{\rm H} C. \tag{5.19}$$

5.1.3 The static limit

It pays to understand the no-rotation limit (the Schwarzschild-Tangherlini limit) and derive the isoperimetric ratio. Note that we still keep a nonzero cosmological constant. In the static limit, i.e., $a_i \to 0$, the thermodynamic quantities become

$$\begin{aligned}
\Xi_i &= 1, \quad \Xi = 1, \quad J_i = 0, \quad \Omega_i = 0, \\
E &= m \left(\frac{D-2}{2} \right), \quad S = \pi r_{\rm H}^{D-2}, \\
T &= \frac{r_{\rm H} \left(1 + g^2 r_{\rm H}^2\right)}{2\pi} \sum_{i=1}^{N} \frac{1}{r_{\rm H}^2} - \frac{1 - g^2 r_{\rm H}^2}{4\pi r_{\rm H}} \\
&= \frac{1}{4\pi r_{\rm H}} \left(\left(1 + g^2 r_{\rm H}^2\right)(D-2) - \left(1 - g^2 r_{\rm H}^2\right) \right).
\end{aligned} \tag{5.20}$$

From the Smarr law, one obtains

$$\begin{aligned}
&(D-3)\, E = (D-2)\, TS - \Theta_{\rm H} C, \\
&\frac{m}{2} (D-2)(D-3) = \frac{(D-2)\, r_{\rm H}^{D-3}}{4} \\
&\times \left(\left(1 + g^2 r_{\rm H}^2\right)(D-2) - \left(1 - g^2 r_{\rm H}^2\right) \right) - \Theta_{\rm H} C.
\end{aligned} \tag{5.21}$$

By using the polynomial equation defining the event horizon, $m = \frac{r_{\rm H}^{D-3}}{2}\left(1+g^2 r_{\rm H}^2\right)$, one gets

$$\begin{aligned}\Theta_{\rm H} C &= -\frac{1}{4} r_{\rm H}^{D-3}\left(1+g^2 r_{\rm H}^2\right)(D-2)(D-3) \\ &\quad + \frac{(D-2)\, r_{\rm H}^{D-3}}{4}\left[\left(1+g^2 r_{\rm H}^2\right)(D-2) - \left(1-g^2 r_{\rm H}^2\right)\right], \\ &= -\frac{r_{\rm H}^{D-1}\Lambda}{(D-1)}. \end{aligned} \tag{5.22}$$

From the definition of the cosmological charge $C = -\frac{\sqrt{|\Lambda|}}{\Omega_{D-2}}$, one can see that the cosmological potential reads as

$$\Theta_{\rm H} = -\frac{\sqrt{|\Lambda|}\Omega_{D-2} r_{\rm H}^{D-1}}{D-1}. \tag{5.23}$$

Using the definition of the effective thermodynamic volume, $\Theta_{\rm H} = -\sqrt{|\Lambda|}V_{\rm eff}$, one gets an effective volume for the D-dimensional Schwarzschild-AdS black holes

$$V_{\rm eff} = \frac{\Omega_{D-2} r_{\rm H}^{D-1}}{D-1}, \tag{5.24}$$

which does not make sense in the usual black hole thermodynamics without a cosmological constant. But, one can argue that $V_{\rm eff}$ survives in the vanishing cosmological constant limit, as the volume of the Schwarzschild black hole.

5.1.4 Reverse isoperimetric inequality

For the static black hole, since the area of the event horizon is $A = \Omega_{D-2} r_{\rm H}^{D-2}$, one can show that the reverse isoperimetric inequality is saturated

$$\left(\frac{(D-1)\, V_{\rm eff}}{\Omega_{D-2}}\right)^{\frac{1}{D-1}} \geq \left(\frac{A}{\Omega_{D-2}}\right)^{\frac{1}{D-2}}, \tag{5.25}$$

as was expected for Schwarzschild-AdS black holes [36]. Interestingly, for a given volume $V_{\rm eff}$, the bound is saturated for only the Schwarzschild-AdS black holes, and for any other solution, one obtains a reverse isoperimetric relation meaning that the Schwarzschild-AdS black hole has the maximum entropy among the same volume spaces. For example, the introduction of charge or rotation reduces the entropy-to-volume ratio [36]. In the rotating case for an even number of dimensions, one can

show that the effective volume reads

$$V_{\text{eff}} = \frac{m\Omega_{D-2}}{\Lambda\Xi}\left(-\sum_{i=1}^{N}\frac{1}{\Xi_i} + \frac{(D-2)}{2}\frac{(1-g^2r_{\text{H}}^2)}{1+g^2r_{\text{H}}^2}\right), \tag{5.26}$$

and the event horizon area reads as

$$A = \Omega_{D-2}\prod_{i=1}^{N}\frac{r_{\text{H}}^2+a_i^2}{\Xi_i}. \tag{5.27}$$

The effective volume, (5.26), and the event horizon area, (5.27), satisfy the inequality given in (5.25). Observe that one can take the $\Lambda \to 0$ limit of (5.26) to define the volume of asymptotically flat black holes in even dimensions as

$$V_{\text{eff}} = \frac{2m\Omega_{D-2}r_{\text{H}}^2}{D-1}, \tag{5.28}$$

where r_{H} is the largest root of $\prod_{i=1}^{N}(r_{\text{H}}^2+a_i^2) - 2mr_{\text{H}} = 0$ and the effective volume reduces to the Schwarzschild case (5.24) when all a_i vanish.

5.1.5 Kerr-Ads spacetimes with odd dimensions

For an odd number of spacetime dimensions with $D = 2N+1$, the thermodynamic quantities become

$$\begin{aligned}
&E = \frac{m}{\Xi}\left(\sum_{i=1}^{N}\frac{1}{\Xi_i} - \frac{1}{2}\right), \quad J_i = \frac{ma_i}{\Xi_i\Xi},\\
&S = \frac{\pi}{r_{\text{H}}}\prod_{i=1}^{N}\frac{r_{\text{H}}^2+a_i^2}{\Xi_i},\\
&T = \frac{r_{\text{H}}\left(1+g^2r_{\text{H}}^2\right)}{2\pi}\sum_{i=1}^{N}\frac{1}{r_{\text{H}}^2+a_i^2} - \frac{1}{2\pi r_{\text{H}}},\\
&\Omega_i = \frac{\left(1+g^2r_{\text{H}}^2\right)a_i}{r_{\text{H}}^2+a_i^2}, \;\; C = \pm\frac{\sqrt{|\Lambda|}}{\Omega_{D-2}},\\
&\left(1+g^2r_{\text{H}}^2\right)\prod_{i=1}^{N}\left(r_{\text{H}}^2+a_i^2\right) - 2mr_{\text{H}}^2 = 0,
\end{aligned} \tag{5.29}$$

where the first law and the Smarr relation reads the same as (5.18) and (5.19), and the Schwarzschild limit yields the same result as in the even-dimensional case. The effective volume for this odd-dimensional case differs from that of the even-dimensional, case which can be found to be

$$V_{\text{eff}} = \frac{m\Omega_{D-2}}{\Lambda\Xi}\left(-\sum_{i=1}^{N}\frac{1}{\Xi_i} - \frac{D-3}{2} + \frac{D-2}{1+g^2r_{\text{H}}^2}\right). \tag{5.30}$$

For asymptotically flat rotating black holes, one obtains the same limit (5.28).

5.2 Thermodynamics of Einstein-Gauss-Bonnet Gravity

Let us consider the action

$$I = \int d^D x \sqrt{-g} \left(\frac{1}{4\Omega_{D-2}} \left(R + \lambda \mathcal{L}_{GB} \right) \right), \tag{5.31}$$

with the Gauss-Bonnet (GB) scalar given as $\mathcal{L}_{\text{GB}} := R^{\mu\nu\rho\sigma} R_{\mu\nu\rho\sigma} - 4R^{\mu\nu} R_{\mu\nu} + R^2$, and λ is a coupling constant of M^2 dimension. This theory has the same particle content as general relativity and arises as an effective model in string theory. In $D = 4$, the GB part is topological and does not contribute to the field equations, but it does play a role in the thermodynamics of the black holes. Unfortunately, no rotating solution is known, but the spherically symmetric nonrotating solution was given in [91], and the line element reads as $ds^2 = g_{tt} dt^2 + g_{rr} dr^2 + r^2 d\Omega_{D-2}$ with

$$-g_{tt} = g_{rr}^{-1} = 1 + \frac{r^2}{2\lambda(D-3)(D-4)} \left(1 - \sqrt{1 + \frac{8m\lambda(D-3)(D-4)}{r^{D-1}}} \right), \tag{5.32}$$

which is asymptotically flat. One should note that the $D \to 4$ limit exists at the level of the action, but does not exist at the level of the solution [92, 93] since the GB term is a topological invariant in that dimension. Therefore for $D = 4$, the Schwarzschild metric is the unique spherically symmetric solution of which some thermodynamical coordinates receive corrections from the topological term as can be seen below. The location of the event horizon is the largest root of the polynomial

$$2m = r_{\text{H}}^{D-3} + (D-3)(D-4)\lambda r_{\text{H}}^{D-5}. \tag{5.33}$$

The temperature and the entropy are given as

$$\begin{aligned} T &= \frac{(D-3) r_{\text{H}}^2 + \lambda (D-3)(D-4)(D-5)}{4\pi r_{\text{H}}^3 + 8\pi r_{\text{H}} \lambda (D-3)(D-4)}, \\ S &= \pi r_{\text{H}}^{D-2} \left(1 + \frac{2\lambda (D-2)(D-3)}{r_{\text{H}}^2} \right), \end{aligned} \tag{5.34}$$

respectively. Observe that, for $D = 4$, the entropy of the Schwarzschild black hole receives a correction from the topological GB term. The energy is given by [31]

$$E = \frac{(D-2)}{2} m. \tag{5.35}$$

These thermodynamic quantities satisfy the following Smarr relation and the first law:

$$(D-3)E = (D-2)TS + 2(D-3)(D-4)\lambda\Phi \tag{5.36}$$

and

$$\delta E = T\delta S + (D-3)(D-4)\Phi\delta\lambda, \tag{5.37}$$

where the potential corresponding to the Gauss-Bonnet coupling constant is

$$\Phi = \frac{(D-2)r_{\rm H}^{D-5}}{4(D-4)}\left(\frac{-r_{\rm H}^2(D-2)+2\lambda(D-3)(D-4)}{r_{\rm H}^2+2\lambda(D-3)(D-4)}\right), \tag{5.38}$$

which is derived explicitly in Appendix-D: Derivation of the Charge Term for Einstein-Gauss-Bonnet Garvity in Generic D Dimensions and Appendix-E: Explicit Calculation of the Smarr Relation with Our Thermodynamical Quantities by using the method developed in [94]. For $D = 4$, this potential is divergent, but the correct limit in the Smarr formula (5.36) yields a finite contribution that reads

$$E = 2TS - \frac{2\lambda}{r_{\rm H}}, \tag{5.39}$$

which was first derived in [95] and was called the topological work.

CHAPTER 6

INSTABILITY AND INFORMATION PRODUCTION AROUND KERR BLACK HOLES: EFFECTS ON ENTROPY AND THE SHADOW

6.1 The Setup

6.1.1 Lyapunov Exponents and Instability

We start with the problem of instability for the particular case of geodesic motion around the Kerr black hole described by the metric in the (t, r, θ, ϕ) coordinates with $\hbar = c = G = 1$ units

$$\begin{aligned} ds^2 &= -\left(1 - \frac{2Mr}{\Sigma}\right) dt^2 - \frac{4Mar\sin^2\theta}{\Sigma} dt d\phi + \frac{\Sigma}{\Delta} dr^2 + \Sigma d\theta^2 \\ &\quad + \left(r^2 + a^2 + \frac{2Ma^2 r \sin^2\theta}{\Sigma}\right) \sin^2\theta d\phi^2, \end{aligned} \tag{6.1}$$

where a is the rotation parameter, and the metric functions read as

$$\Delta := r^2 - 2Mr + a^2, \qquad \Sigma := r^2 + a^2\cos^2\theta. \tag{6.2}$$

Using the two Killing symmetries $\xi_{(t)} = \partial_t$ and $\xi_{(\phi)} = \partial_\phi$ of the metric, we can reduce the phase space of the dynamics to the essential coordinates. Hence, the state vector of a particle or light can be defined as $\chi^\mu := (r, \theta, p_r, p_\theta)$ of which Hamilton's equations govern the time evolution:

$$\dot{\chi}^\mu = \Omega^{\mu\nu} \frac{\partial \mathcal{H}}{\partial \chi^\nu}, \tag{6.3}$$

where $\mathcal{H}$ represents the Hamiltonian and $\Omega^{\mu\nu}$ represents the symplectic matrix of the form

$$\Omega^{\mu\nu} = \begin{pmatrix} 0_2 & \mathbb{I}_2 \\ -\mathbb{I}_2 & 0_2 \end{pmatrix}, \tag{6.4}$$

where $\mathbb{I}_2$ and 0_2 represent the identity and zero matrices of rank 2, respectively. To quantify instability, let us assume that there are two trajectories in the phase space, denoted as $\chi^{\mu(0)}(t)$ and $\chi^{\mu}(t)$, infinitesimally close at the initial time $t = 0$; and at a later time t, their separation can be defined as $\delta\chi^{\mu}(t) := \chi^{\mu}(t) - \chi^{\mu(0)}(t)$. The time-evolution of this separation follows from the linearization of Hamilton's equations (6.3)

$$\delta\dot{\chi}^{\mu}(t) = J^{\mu}{}_{\nu}(t)\delta\chi^{\nu}(t), \qquad \text{where} \qquad J^{\mu}{}_{\nu}(t) := \Omega^{\mu\rho}\partial_{\nu}\partial_{\rho}\mathcal{H}. \tag{6.5}$$

Here $J^{\mu}{}_{\nu}(t)$ is the evolution-Jacobian for the system. Direct integration yields

$$\delta\chi^{\mu}(t) = e^{\int_0^t J^{\mu}{}_{\nu}(t')dt'}\delta\chi^{\nu}(0) =: L^{\mu}{}_{\nu}(t)\delta\chi^{\nu}(0), \tag{6.6}$$

where in the second equality, "Lyapunov matrix" is defined

$$L^{\mu}{}_{\nu}(t) := e^{\int_0^t J^{\mu}{}_{\nu}(t')dt'}. \tag{6.7}$$

The Lyapunov exponent is generically a complex number defined as a particular limit of this matrix

$$\lambda := \lim_{t\to\infty} \frac{1}{t} \log \frac{L^{\mu}{}_{\mu}(t)}{L^{\nu}{}_{\nu}(0)}. \tag{6.8}$$

A positive λ means that there is an instability in the system. Equivalently, the Lyapunov spectrum of the system can be analyzed by considering the eigenvalues of the evolution-Jacobian matrix $J^{\mu}{}_{\nu}(t)$, and the largest eigenvalue corresponds to the Lyapunov exponent. We shall use this approach in what follows. Next, we calculate the evolution matrix for the geodesics around the Kerr black hole.

6.1.2 Hamiltonian of geodesic motion

The Lagrangian of the massless and massive point particles can be taken to be

$$\mathcal{L} = \frac{1}{2} g_{\mu\nu} \frac{dx^{\mu}}{ds} \frac{dx^{\nu}}{ds}, \tag{6.9}$$

where s is an affine parameter. The corresponding Hamiltonian is

$$\mathcal{H} = p_{\mu}\frac{dx^{\mu}}{ds} - \mathcal{L} = \frac{1}{2} g^{\mu\nu} p_{\mu} p_{\nu} = -m^2, \tag{6.10}$$

where m is the mass of the particle with $m \geq 0$. Explicitly, one has

$$\mathcal{H} = \frac{1}{2}\left(V + K\right) = -m^2, \tag{6.11}$$

with the kinetic and potential parts given as

$$K := \frac{p_r^2}{g_{rr}} + \frac{p_\theta^2}{g_{\theta\theta}}, \qquad V := \frac{L_z^2 g_{tt} + E^2 g_{\phi\phi} + 2EL_z g_{t\phi}}{g_{tt}g_{\phi\phi} - g_{t\phi}^2}, \tag{6.12}$$

where $E = -p_t$ and $L_z = p_\phi$ are the conserved energy and angular momentum of the particle obtained from $\xi_{(t)}$ and $\xi_{(\phi)}$, respectively. With this Hamiltonian, one can calculate the corresponding evolution-Jacobian as

$$J^\mu{}_\nu = \frac{1}{2}\begin{pmatrix} \partial_r\left(\frac{2p_r}{g_{rr}}\right) & \partial_\theta\left(\frac{2p_r}{g_{rr}}\right) & \frac{2}{g_{rr}} & 0 \\ \partial_r\left(\frac{2p_\theta}{g_{\theta\theta}}\right) & \partial_\theta\left(\frac{2p_\theta}{g_{\theta\theta}}\right) & 0 & \frac{2}{g_{\theta\theta}} \\ -\partial_r\partial_r\left(K+V\right) & -\partial_\theta\partial_r\left(K+V\right) & -\partial_r\left(\frac{2p_r}{g_{rr}}\right) & -\partial_r\left(\frac{2p_\theta}{g_{\theta\theta}}\right) \\ -\partial_r\partial_\theta\left(K+V\right) & -\partial_\theta\partial_\theta\left(K+V\right) & -\partial_\theta\left(\frac{2p_r}{g_{rr}}\right) & -\partial_\theta\left(\frac{2p_\theta}{g_{\theta\theta}}\right) \end{pmatrix}. \tag{6.13}$$

The explicit form of this matrix is highly cumbersome to depict here. Consider the case for circular orbits, for which $p_r = 0$:

$$J^\mu{}_\nu = \frac{1}{2}\begin{pmatrix} 0 & 0 & \frac{2}{g_{rr}} & 0 \\ \partial_r\left(\frac{2p_\theta}{g_{\theta\theta}}\right) & \partial_\theta\left(\frac{2p_\theta}{g_{\theta\theta}}\right) & 0 & \frac{2}{g_{\theta\theta}} \\ -\partial_r\partial_r\left(K+V\right) & -\partial_\theta\partial_r\left(K+V\right) & 0 & -\partial_r\left(\frac{2p_\theta}{g_{\theta\theta}}\right) \\ -\partial_r\partial_\theta\left(K+V\right) & -\partial_\theta\partial_\theta\left(K+V\right) & 0 & -\partial_\theta\left(\frac{2p_\theta}{g_{\theta\theta}}\right) \end{pmatrix}. \tag{6.14}$$

If we further constrain this motion to the equatorial plane, $\theta = \frac{\pi}{2}$ and $p_\theta = 0$, we can redefine the state vector as $\chi^\mu = (r, p_r)$ and the evolution-Jacobian becomes a 2×2 matrix

$$J^\mu{}_\nu = \frac{1}{2}\begin{pmatrix} 0 & \frac{2}{g_{rr}} \\ -\partial_r\partial_r V & 0 \end{pmatrix}, \tag{6.15}$$

which was studied in [45]. As noted above, the maximum eigenvalue of the evolution-Jacobian matrix is the Lyapunov exponent. Next, we study massive orbits.

6.2 Massive Orbits

Let us investigate massive particle orbits on the equatorial plane [50]. To do that, we need to focus on the radial part of the geodesic equation, which reads as

$$\frac{dr}{ds} = \pm r^{-\frac{3}{2}}\sqrt{P}, \tag{6.16}$$

where

$$P := E^2\left(r^3 + a^2 r + 2a^2 M\right) - 4aMEL_z - (r - 2M)\, L_z^2 - rm^2\Delta. \tag{6.17}$$

For the special case of the circular orbits, one can write the energy and angular momentum as a function of the independent parameter $r = r_{\text{circ}}$

$$\begin{aligned} E_{\text{circ},\pm} &= m\frac{r^2 - 2Mr \pm a\sqrt{Mr}}{r\sqrt{r^2 - 3Mr \pm 2a\sqrt{Mr}}}, \\ L_{z,\text{circ},\pm} &= m\frac{\pm\sqrt{Mr}\left(r^2 \mp 2a\sqrt{Mr} + a^2\right)}{r\sqrt{r^2 - 3Mr \pm 2a\sqrt{Mr}}}, \end{aligned} \tag{6.18}$$

where $+$ sign corresponds to the prograde orbits, while $-$ sign corresponds to retrograde orbits. We study the stable and unstable orbits in the next two subsections as illustrative examples.

6.2.1 Stable Orbit Case

For the special case of the innermost *stable* circular orbits (ISCO), one can find the $r = r_{\text{ISCO}}$ as the solution of the polynomial

$$r^2 - 3a^2 - 6Mr \pm 8a\sqrt{Mr} = 0. \tag{6.19}$$

For the case with prograde innermost stable circular orbits with $M = 1$, $m = 1$, and $a = 0.5$, one finds

$$r_{\text{ISCO},+} = 4.233, \quad E_{\text{circ},+} = 0.917882, \quad L_{z,\text{circ},+} = 2.90287. \tag{6.20}$$

The corresponding Lyapunov exponents (6.8) turn out to be

$$\lambda_{\text{pro},\pm} = 0, \tag{6.21}$$

as expected because these orbits are stable. (In what follows, we shall define entropy using the Lyapunov exponents; hence, stable orbits with vanishing exponents, such as the one studied above, will be assigned a zero entropy.)

6.2.2 Unstable Orbit Case

Among the equatorial circular orbits, for the special case of the binding orbits for which $E = m$, one can find the radius as

$$r_{\text{bind},\pm} = 2M \mp a + 2\sqrt{M\,(M \mp a)}, \tag{6.22}$$

which should be used to determine the particle's energy and angular momentum. One can calculate the potential and kinetic terms by using (6.12) as

$$V = \left.\frac{r\,(L_z^2 - a^2E^2) - 2M(L_z - aE)^2 - E^2r^3}{r\,(a^2 + r(r-2M))}\right|_{r=r_{\text{bind}}}, \qquad K = 0. \tag{6.23}$$

The Lyapunov spectrum can be found as the eigenvalues of the evolution-Jacobian (6.15), which are

$$\begin{aligned}\lambda_\pm = \quad & \pm\frac{1}{r^{5/2}\,(a^2 + r(r-2M))} \\ & \times \left[2a^4M(L_z - aE)^2 + r^3\left(a^2L_z^2 - 4M^2(L_z - aE)(9L_z - 7aE)\right)\right. \\ & \quad +6Mr^2\left(a^2 + 4M^2\right)(L_z - aE)^2 - 12a^2M^2r(L_z - aE)^2 \\ & \quad \left.+6Mr^4(aE - L_z)(aE - 3L_z) + 2E^2Mr^6 - 3L_z^2r^5\right]^{1/2}, \end{aligned} \tag{6.24}$$

where $r = r_{\text{bind}}$. Even though we have an analytical formula, it is more illuminating to proceed numerically. However, one can analytically study various limits. For example, in the slowly rotating limit of the black hole, one has

$$\lambda_\pm = \lambda_\pm^{\textbf{Sch}}\left(1 + a\frac{(L_z - 4EM)(80EM + 9L_z)}{4\,(3L_z^2M - 64E^2M^3)}\right) + \mathcal{O}\left(\left(\frac{a}{M}\right)^2\right), \tag{6.25}$$

where the Schwarzschild black hole limit is given as

$$\lambda_\pm^{\textbf{Sch}} = \pm\frac{\left(32E^2M^2 - \frac{3L_z^2}{2}\right)^{1/2}}{16M^2}. \tag{6.26}$$

For this purpose, consider the prograde binding orbit:

$$r_{\text{bind},+} = 2M - a + 2\sqrt{M\,(M-a)}, \tag{6.27}$$

and assume the black hole parameters as $M = 1$ and $a = 0.5$. These values yield

$$\begin{aligned} r_{\text{bind},+} \quad &= 2.91421, \quad r_{\text{horizon}} = 1.86603, \\ E_{\text{circ},+} \quad &= m = 1, \quad L_{z,\text{circ},+} = 3.41421. \end{aligned} \tag{6.28}$$

As a result, from (6.24), the Lyapunov exponent can be computed to be

$$\lambda_{\text{pro},+} = 0.284271. \tag{6.29}$$

So, we can say that with a slight perturbation, a massive particle following the prograde binding orbit performs an exponentially unstable motion. One can see the relation between the Lyapunov exponent and the rotation parameter for the prograde binding orbit in the Fig. (6.1).

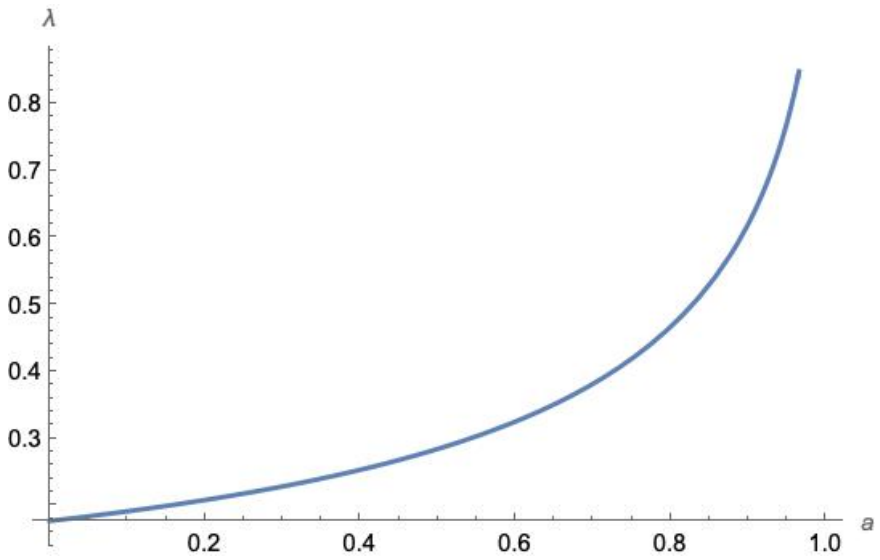

Figure 6.1: The Lyapunov exponent for the prograde binding orbit where the black hole parameter is $M = 1$ with $E_{\text{circ},+} = m = 1$ is plotted as a function of the rotation parameter.

Similarly, for the retrograde binding orbit, we have

$$r_{\text{bind},-} = 2M + a + 2\sqrt{M\,(M+a)}, \tag{6.30}$$

for the same black hole parameters $M = 1$ and $a = 0.5$, one finds

$$\begin{aligned} r_{\text{bind},-} &= 4.94949, \quad r_{\text{horizon}} = 1.86603, \\ E_{\text{circ},-} &= m = 1, \quad L_{z,\text{circ},-} = -4.44949. \end{aligned} \tag{6.31}$$

As a result, the positive Lyapunov exponent is found to be

$$\lambda_{\text{retro},+} = 0.128432, \tag{6.32}$$

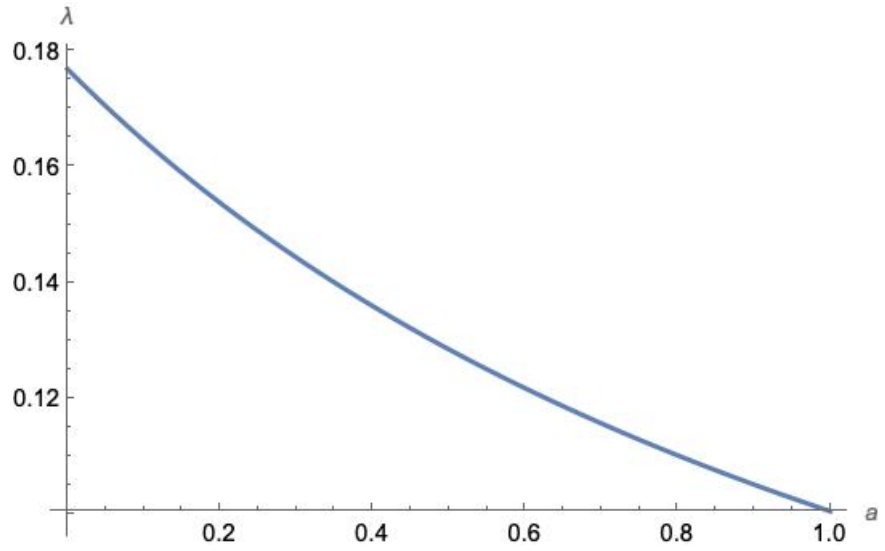

Figure 6.2: The Lyapunov exponent for the retrograde binding orbit where the black hole parameter is $M = 1$ with $E_{\text{circ},+} = m = 1$ is plotted as a function of the rotation parameter.

which shows that, for the retrograde binding orbit, perturbations lead to an exponentially unstable motion. One can see the relation between the Lyapunov exponent and the rotation parameter for the retrograde binding orbit in Fig. (6.2).

We stress that these results are for the equatorial-plane limits of the binding orbits. We can extend these results to the non-equatorial binding orbits for $2.91421 < r < 4.94949$. To do this, one can consider the radial part of the geodesic equation without the equatorial plane assumption. In this case, it reads as

$$\Sigma \frac{dr}{ds} = \pm\sqrt{\mathcal{R}(r)}, \tag{6.33}$$

where

$$\begin{aligned} \mathcal{R}(r) := \quad & \left(E\left(r^2+a^2\right) - aL_z\right)^2 - \left(r^2 - 2Mr + a^2\right) \\ & \times \left(m^2r^2 + \mathcal{Q} + \left(Ea - L_z\right)^2\right), \end{aligned} \tag{6.34}$$

and $\mathcal{Q}$ is the Carter's constant related to a symmetric rank two Killing tensor. Explicitly, it reads

$$\mathcal{Q} := p_\theta^2 + \cos^2\theta \left(\frac{L_z^2}{\sin^2\theta} + a^2\left(m^2 - E^2\right)\right). \tag{6.35}$$

Defining the dimensionless quantities,

$$\alpha := \frac{a}{M}, \quad x := \frac{r}{M}, \quad \ell := \frac{L_z}{Mm}, \quad \tilde{Q} := \frac{\mathcal{Q}}{M^2m^2}, \quad \tilde{E} := \frac{E}{m}, \tag{6.36}$$

one can rewrite (6.34) as

$$\mathcal{R}(x) := \left(\tilde{E}\left(x^2+\alpha^2\right)-\alpha\ell\right)^2-\left(x^2-2x+\alpha^2\right) \times\left(x^2+\tilde{Q}+\left(\tilde{E}\alpha-\ell\right)^2\right). \tag{6.37}$$

Conditions for spherical orbits,

$$\mathcal{R}(x)=0, \quad \frac{d\mathcal{R}(x)}{dx}=0, \tag{6.38}$$

can be solved for dimensionless angular momentum

$$\ell=-\frac{1}{\alpha^2(x-1)}\left[\alpha^3\tilde{E}+\alpha^2\sqrt{\alpha^2x\left(\left(\tilde{E}^2-1\right)x+1\right)} +x(x-2)\sqrt{\alpha^2x\left(\left(\tilde{E}^2-1\right)x+1\right)}-\alpha\tilde{E}x^2\right], \tag{6.39}$$

and the dimensionless Carter's constant as

$$\tilde{Q}=\frac{x^2}{\alpha^3(x-1)^2}\left[\alpha^3\left(\left(2\tilde{E}^2-1\right)x+1\right)+2\alpha^3\tilde{E}\sqrt{x\left(\left(\tilde{E}^2-1\right)x+1\right)} +\alpha x\left(x\left(-\left(\tilde{E}^2((x-4)x+5)\right)+(x-5)x+8\right)-4\right) +2\alpha\tilde{E}(x-2)x\sqrt{x\left(\left(\tilde{E}^2-1\right)x+1\right)}\right]. \tag{6.40}$$

For the special case of binding orbits, $E=m$ or $\tilde{E}=1$,

$$\ell=\frac{\alpha^2-2x^{3/2}+x^2}{\alpha-\alpha\sqrt{x}}, \tag{6.41}$$

and

$$\tilde{Q}=\frac{x^2\left(\alpha^2-\left(\sqrt{x}-2\right)^2x\right)}{\alpha^2\left(\sqrt{x}-1\right)^2}. \tag{6.42}$$

To illustrate these relations, we plot the angular momentum and the Carter's constant as a function of radius for the case where $M=1$, $m=1$, and $\alpha=a=0.5$ in figures (6.3) and (6.4), respectively.

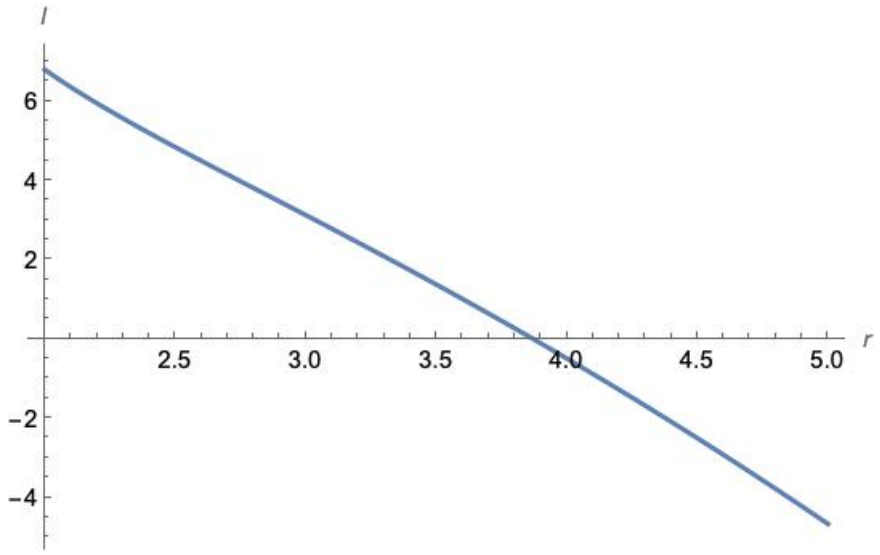

Figure 6.3: The angular momentum is plotted as a function of the radius for the case where $M = 1$, $m = E = 1$, and $\alpha = a = 0.5$.

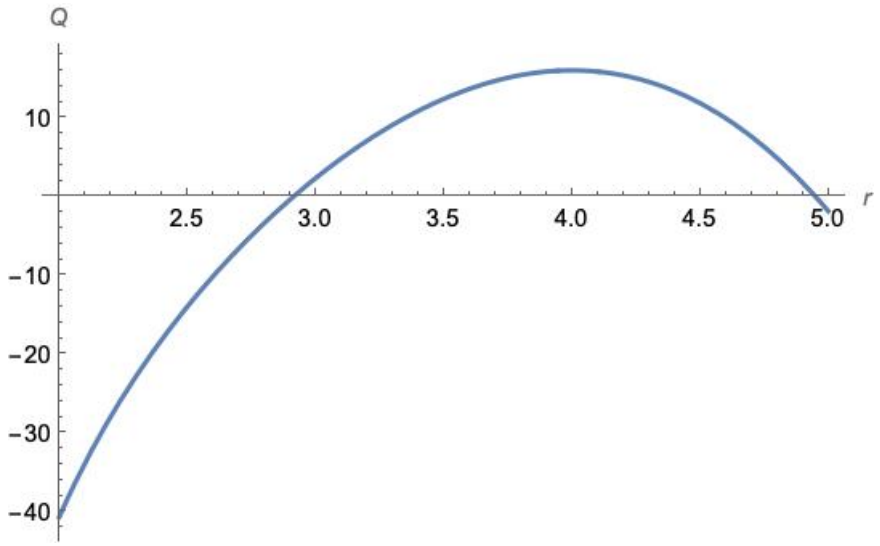

Figure 6.4: The Carter's constant is plotted as a function of the radius for the case where $M = 1$, $m = E = 1$, and $\alpha = a = 0.5$.

Since there is a non-zero Carter's constant, the motion is not bounded to the equatorial plane, which means $p_\theta \neq 0$ and hence we must use (6.14) instead of (6.15) to calculate the Lyapunov exponents. As a result, instead of (6.24), we have to find the largest eigenvalue of the matrix (6.14) and use it as the Lyapunov exponent. The analytical formula is more complicated than (6.24), hence, we shall proceed numerically. As an example, let us concentrate on the previous case where $M = 1$ and $E = m = 1$, so $x = r = 3$ and $\alpha = a = 0.5$. For this case, we have

$$\ell = 3.12083, \quad \tilde{Q} = 2.32497. \tag{6.43}$$

By assuming that the particle is on the equatorial plane when it is perturbed, the Lyapunov exponent can be computed to be

$$\lambda_{\text{non-eq},+} = 0.310321, \tag{6.44}$$

which is larger than the Lyapunov exponents of both prograde and retrograde binding orbits. For non-equatorial spherical binding orbits, i.e., for particles which are not on the equatorial plane when perturbed, one can see the angular dependence of the Lyapunov exponent in Fig.(6.5). As the figure shows, the instability first increases slightly for low orbital inclinations (around $\pi/2$, i.e., the equatorial plane), then decreases sharply for higher inclinations.

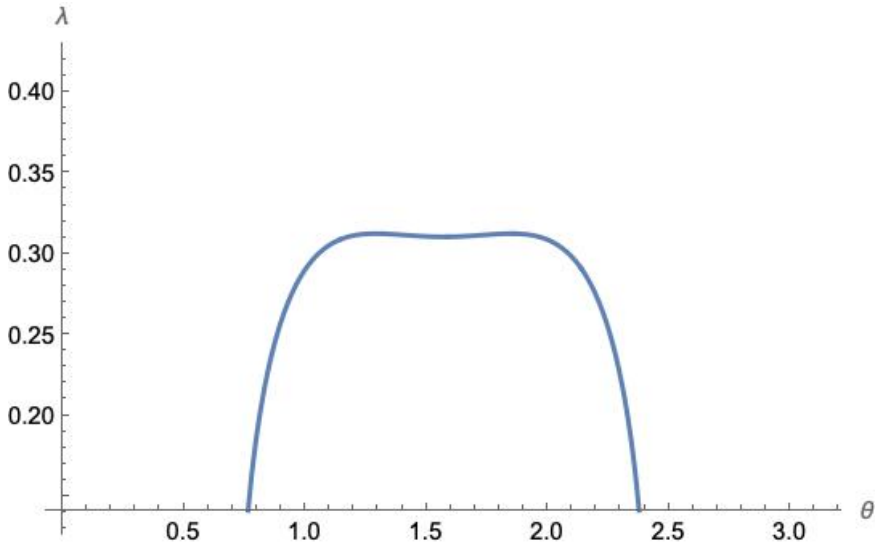

Figure 6.5: The angular dependence of the Lyapunov exponent for the case where $M = 1$, $E = m = 1$, $x = r = 3$ and $\alpha = a = 0.5$ is plotted.

Figures (6.6) and (6.7) show the radial dependence of the Lyapunov exponents for the binding orbits on the equatorial plane when they are perturbed, for different values of the rotation parameter.

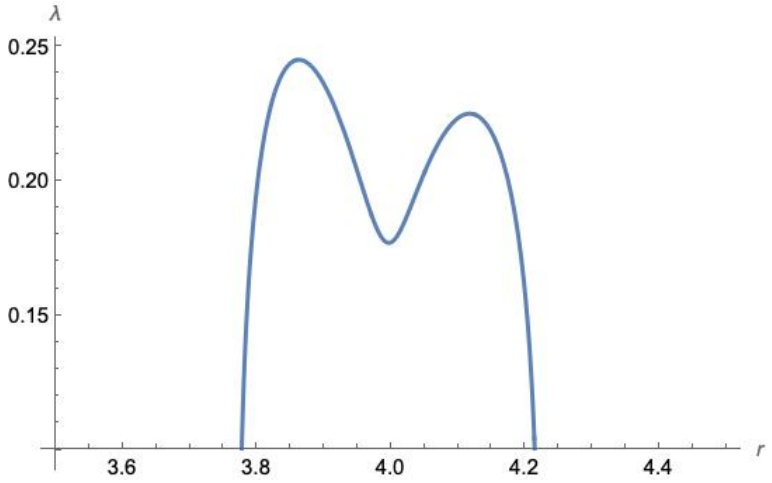

Figure 6.6: The radial dependence of the Lyapunov exponent for the case where $M = 1$, $E = m = 1$, $\theta = \pi/2$, and $\alpha = a = 0.1$ is plotted.

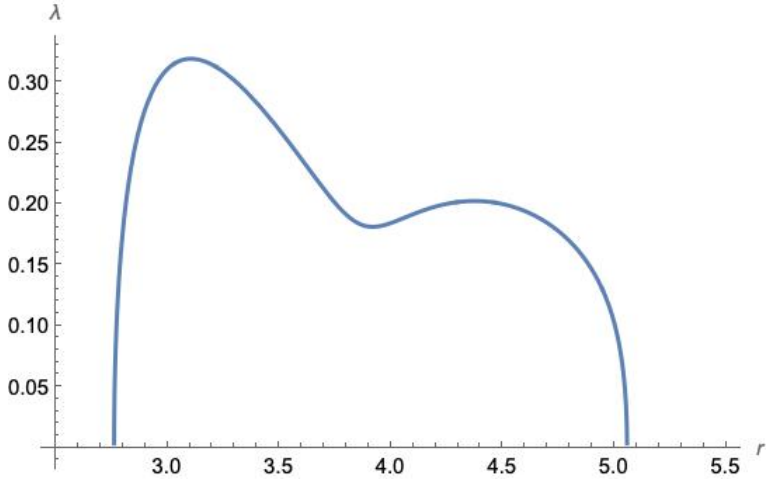

Figure 6.7: The radial dependence of the Lyapunov exponent for the case where $M = 1$, $E = m = 1$, $\theta = \pi/2$, and $\alpha = a = 0.5$ is plotted.

Figure (6.8) shows the relation between the Lyapunov exponent and the energy of the particle for the case where $M = 1$, $m = 1$, $x = r = 3$, and $\alpha = a = 0.5$, and the particle is on the equatorial plane when it is perturbed. It is crucial to note that for higher energy values, the Lyapunov exponent is positive, indicating instability.

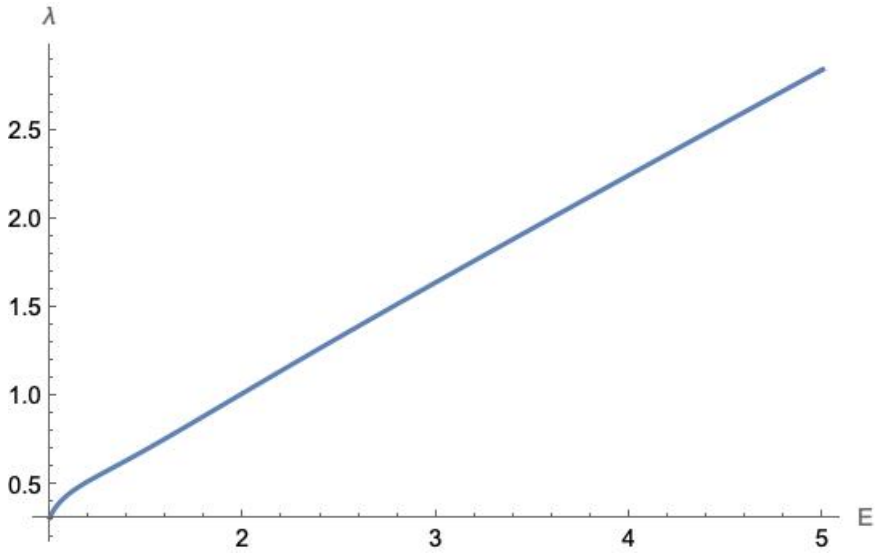

Figure 6.8: The plot shows the relation between the Lyapunov exponent and energy for the case where $M = 1$, $m = 1$, $x = r = 3$, and $\alpha = a = 0.5$, and the particle is on the equatorial plane when it is perturbed.

6.2.2.1 Normalization of the Lyapunov Exponents

The Lyapunov exponent found via the evolution-Jacobian is not invariant under changes in the (time) parameterization. Hence, we need to find a relevant timescale to make it invariant. To achieve this, let us first study the angular part of the geodesic equation. The angular dependence is in radians.

$$\Sigma \frac{d\theta}{ds} = \pm\sqrt{\Theta(\theta)}, \tag{6.45}$$

where

$$\Theta(\theta) := \mathcal{Q} - \cos^2\theta \left(a^2 \left(m^2 - E^2 \right) + \frac{L_z^2}{\sin^2\theta} \right), \tag{6.46}$$

of which the non-dimensional form is

$$\tilde{\Theta}(\theta) := \tilde{Q} - \cos^2\theta \left(\alpha^2 \left(1 - \tilde{E}^2 \right) + \frac{\ell^2}{\sin^2\theta} \right). \tag{6.47}$$

We first determine the angular turning points by solving $\tilde{\Theta}(\theta) = 0$. For simplicity, we define $u = \cos^2\theta$ and rewrite it as

$$\tilde{\Theta}(u) = \tilde{Q} - u\left(\alpha^2\left(1-\tilde{E}^2\right) + \frac{\ell^2}{1-u}\right) = 0, \tag{6.48}$$

of which the solutions are

$$u_\pm = \Delta_\theta \pm \sqrt{\Delta_\theta^2 - \frac{\tilde{Q}}{\alpha^2\left(1-\tilde{E}^2\right)}}, \qquad \Delta_\theta = \frac{1}{2}\left(1 + \frac{\tilde{Q}+\ell^2}{\alpha^2\left(1-\tilde{E}^2\right)}\right). \tag{6.49}$$

Let us define the function [1]

$$G_\theta := \pm\int_{\theta_i}^{\theta_f} \frac{d\theta}{\sqrt{\Theta}}, \tag{6.50}$$

along the trajectory where θ_i and θ_f are the initial and final points. For one complete orbit, we can write

$$G_\theta^1 = 2\int_{\theta_-}^{\theta_+} \frac{d\theta}{\sqrt{\Theta}}, \tag{6.51}$$

where θ_- and θ_+ are the angular turning points defined as $\theta_\pm := \arccos\left(\mp\sqrt{u_+}\right)$. As a result, the number of oscillations around the equatorial plane, along the trajectory, can be found as

$$n = \frac{G_\theta}{G_\theta^1}. \tag{6.52}$$

In 6.1.1, we defined the Lyapunov exponent as a measure of temporal instability. To make this exponent an invariant quantity, we can redefine it with respect to the *number* of oscillations as

$$\delta r(n) = e^{\lambda_P n}\delta r(0), \tag{6.53}$$

where $\delta r(0)$ is the perturbation around the initial orbit. This new Lyapunov exponent, or the principal Lyapunov exponent, λ_P, is related to the old one as

$$\lambda_P = \lambda_+\tau, \tag{6.54}$$

where λ_+ is defined in (6.8) as the positive one and $\tau = G_\theta^1$. For the special case of the binding orbits, $E = m$ or $\tilde{E} = 1$,

$$\tilde{\Theta}(u) = \tilde{Q} - \frac{u\ell^2}{1-u} = 0. \tag{6.55}$$

Therefore,

$$u = \frac{\tilde{Q}}{\tilde{Q}+\ell^2}. \tag{6.56}$$

[1] This integral can be expressed in terms of elliptic functions; we do not need the explicit forms here. For details, see [46].

For the normalization of our exemplary case with $M = 1$, $E = m = 1$, $a = \alpha = 0.5$, $r = x = 3$, we can find

$$G^1_\theta = 2\int_{\theta_-}^{\theta_+} \frac{d\theta}{\sqrt{\tilde{\Theta}(\theta)}} = 0.355709. \tag{6.57}$$

In conclusion, the principal Lyapunov exponent becomes

$$\lambda_P = \lambda_+ \tau = \lambda_+ G^1_\theta = 0.114918. \tag{6.58}$$

6.2.3 Kolmogorov-Sinai entropy of the unstable orbits and the Bekenstein bound

The Kolmogorov-Sinai (KS) entropy is a useful concept in quantifying the randomness of a deterministic dynamical system. Its full definition would constitute a long discussion for which we refer to Chapter 9 of the book [38]. We only need the Pesin's theorem here, which states that under certain conditions, the KS entropy, h_{KS}, is equal to the sum of the positive principal Lyapunov exponents:

$$h_{\text{KS}} = \sum_i \lambda^i_+. \tag{6.59}$$

For the non-equatorial binding orbit with $M = 1$, $E = m = 1$, $r = x = 3$ and $a = \alpha = 0.5$, we found that $\lambda_{\text{non-eq},P} = 0.114918$. The corresponding Kolmogorov-Sinai entropy becomes

$$h_{\text{KS}} = 0.114918. \tag{6.60}$$

The question is this: can we interpret this rather mathematical entropy from a physical point of view? If so, does this entropy satisfy the Bekenstein bound? To do this, we need to "resolve" the point particle in this unstable orbit, i.e., assign it a volume. For this purpose, we shall use the method of [3] in which one assigns an entropy to a bounded spherical volume [2] with a process very similar to the one suggested by Gibbons and Hawking [17]. Making proper adjustments in the action to introduce the volume constraint, one obtains the following saddle point approximation for the action,

$$I_{\text{saddle}} = -\frac{1}{16\pi G}\int d^D x\sqrt{g}R = -\Omega_{D-2}\frac{R_V^{D-2}}{4G} = -\frac{A_V}{4G}. \tag{6.61}$$

[2] Note that the robustness of this nice method was tested as it also works for some higher derivative gravity theories [24].

Using this, the spherical volume has the associated entropy

$$S = \frac{A_V}{4G}. \tag{6.62}$$

The volume regularization and the entropy associated with a finite volume in spacetime require a complete discussion on its own, which is beyond the scope of this work. Here, we apply the technique found in [3] to Einstein's gravity. At this point, let us identify the Kolmogorov-Sinai entropy ($h_{\rm KS} = 0.114918$) as the entropy of the bounded spherical volume. Then, its area, volume, and radius are

$$A_V = 0.459672, \qquad V = 0.0293053, \qquad R_V = 0.191258. \tag{6.63}$$

The Bekenstein bound is defined as

$$S \leq \frac{2\pi ER}{\hbar}, \tag{6.64}$$

where we take $\hbar = 1$, $G = 1$, $R = R_V$ and $E = m = 1$ for the binding orbit. This shows that

$$S = 0.114918 \leq 2\pi ER = 1.20171. \tag{6.65}$$

The Bekenstein bound is satisfied. One can conclude that interpreting the Kolmogorov-Sinai entropy as a physical entropy is viable, and this example lends support to Bekenstein's conjecture on the maximum entropy of material systems. Note that the discussion on Bekenstein's conjecture is still not finalized; see [40] for a review of the problem. We have finished our discussion of unstable massive orbits and the associated entropy. Next, we shall discuss the unstable light orbits, especially the connection between the Lyapunov exponents and the subring structure on the black hole shadow.

6.3 Massless Orbits

The radial and angular parts of the geodesic equations [11],[96] for a massless particle following an orbit that is not constrained to move on the equatorial plane are

$$\begin{aligned} \Sigma\frac{dr}{d\tilde{s}} &= \sqrt{\mathcal{R}}, \\ \Sigma\frac{d\theta}{d\tilde{s}} &= \sqrt{\Theta}, \end{aligned} \tag{6.66}$$

where

$$\mathcal{R} = \left(r^2 + a^2 - a\ell\right)^2 - \left(r^2 - 2Mr + a^2\right)\left(\tilde{Q} + (a-\ell)^2\right),$$
$$\Theta = \tilde{Q} + \cos^2\theta\left(a^2 - \frac{\ell^2}{\sin^2\theta}\right), \tag{6.67}$$

and $\tilde{s} := Es$, $\ell := \frac{L_z}{E}$ and $\tilde{Q} := \frac{\mathcal{Q}}{E^2}$. By using the spherical orbit conditions,

$$\mathcal{R} = 0, \quad \frac{d\mathcal{R}}{dr} = 0, \tag{6.68}$$

one can write

$$\ell = -\frac{r^3 - 3Mr^2 + a^2(r+M)}{a(r-M)},$$
$$\tilde{Q} = \frac{r^3}{a^2(r-M)^2}\left(4a^2M - r(r-3M)^2\right). \tag{6.69}$$

On the equatorial plane, two specific analytical expressions can be found, namely prograde and retrograde photon orbits, which are

$$r_{\text{photon},\pm} = 2M\left(1 + \cos\left(\frac{2}{3}\arccos\left(\mp\frac{a}{M}\right)\right)\right). \tag{6.70}$$

Between the prograde and retrograde orbits, one can find orbits restricted between $\theta_- \leq \theta \leq \theta_+$ whose values can be found with the help of the angular part of the geodesic equation [97]. By defining $u := \cos^2\theta$, one can solve

$$\Theta = \tilde{Q} + u\left(a^2 - \frac{\ell^2}{1-u}\right) = 0 \tag{6.71}$$

to find the angular turning points, $\theta_\pm = \arccos\left(\mp\sqrt{u_+}\right)$, where

$$u_\pm = \Delta_\theta \pm \sqrt{\Delta_\theta^2 + \frac{\tilde{Q}}{a^2}}, \quad \Delta_\theta = \frac{1}{2}\left(1 - \frac{\tilde{Q} + \ell^2}{a^2}\right). \tag{6.72}$$

As an example, consider a black hole with $a = 0.5$ and $M = 1$. For this case, we have

$$r_+ = 2.3473, \quad r_- = 3.53209, \tag{6.73}$$

as limiting cases of the equatorial plane. Therefore, there is a non-equatorial orbit with $r = 3$. For this orbit, we have

$$\tilde{Q} = 27, \quad \ell = -1, \tag{6.74}$$

so that is a retrograde orbit. For this orbit, the angular turning points become

$$\theta_- = 10.8462^\circ, \quad \theta_+ = 169.154^\circ. \tag{6.75}$$

Next, we compute the Lyapunov exponents for these non-equatorial light orbits and show their relation to the subring structure.

6.3.1 Lyapunov Exponents and Shadow

For this case, we do not restrict the motion to the equatorial plane. Henceforth, the evolution Jacobian becomes

$$J^{\mu}_{\nu} = \frac{1}{2}\begin{pmatrix} 0 & 0 & \frac{2}{g_{rr}} & 0 \\ \partial_r\left(\frac{2p_\theta}{g_{\theta\theta}}\right) & \partial_\theta\left(\frac{2p_\theta}{g_{\theta\theta}}\right) & 0 & \frac{2}{g_{\theta\theta}} \\ -\partial_r\partial_r\left(K+V\right) & -\partial_\theta\partial_r\left(K+V\right) & 0 & -\partial_r\left(\frac{2p_\theta}{g_{\theta\theta}}\right) \\ -\partial_r\partial_\theta\left(K+V\right) & -\partial_\theta\partial_\theta\left(K+V\right) & 0 & -\partial_\theta\left(\frac{2p_\theta}{g_{\theta\theta}}\right) \end{pmatrix}. \tag{6.76}$$

The kinetic and potential terms are

$$K = \frac{p_\theta^2}{g_{\theta\theta}}, \tag{6.77}$$

and

$$V \;=\; E^2\frac{\ell^2 g_{tt}(r,\theta) + g_{\phi\phi}(r,\theta) + 2\ell g_{t\phi}(r,\theta)}{g_{tt}(r,\theta)g_{\phi\phi}(r,\theta) - g_{t\phi}^2(r,\theta)}. \tag{6.78}$$

Since we are considering constant-radius spherical photon orbits, we took $p_r = 0$. The Lyapunov exponents are the eigenvalues of this matrix. The expressions are too cumbersome, so we did not write them here explicitly. For the specific case of $M = 1$, $a = 0.5$, and the orbit with radius $r = 3$, let us assume that a slight perturbation occurs on the particle at the moment that the particle is at $\theta = \frac{\pi}{3}$. The corresponding angular momentum can be found as

$$p_\theta = \sqrt{\tilde{Q} + \cos^2\theta\left(a^2 - \frac{\ell^2}{\sin^2\theta}\right)}. \tag{6.79}$$

The corresponding Lyapunov exponents become

$$\begin{aligned} &\lambda_1 = 0 - 0.260123i, \quad &&\lambda_2 = 0 + 0.260123i, \\ &\lambda_3 = -0.597417, &&\lambda_4 = 0.597417. \end{aligned} \tag{6.80}$$

For normalization, we can use

$$G^1_\theta := 2\int_{\theta_-}^{\theta_+}\frac{d\theta}{\sqrt{\tilde{\Theta}(\theta)}} = 1.16949. \tag{6.81}$$

In conclusion, the principal Lyapunov exponent becomes

$$\lambda_P = \lambda_+\tau_M = \lambda_+ G^1_\theta = 0.698674. \tag{6.82}$$

	The largest Lyapunov exponent (λ_4)	The principal Lyapunov exponent (λ_P)
$\theta = \pi/2$	0.580475	0.678861
$\theta = \pi/3$	0.597417	0.698674

Table 6.1: For the case of $M = 1$, $a = 0.5$ and $r = 3$, the largest Lyapunov exponents and the corresponding principal Lyapunov exponents for the particles at $\theta = \pi/2$ and $\theta = \pi/3$ can be seen. As can be noticed, they are slightly different.

If, on the other hand, this particle is perturbed while it is on the equatorial plane, $\theta = \frac{\pi}{2}$, we have

$$\begin{aligned} &\lambda_1 = 0 - 0.148783i, \quad \lambda_2 = 0 + 0.148783i, \\ &\lambda_3 = -0.580475, \qquad \lambda_4 = 0.580475. \end{aligned} \tag{6.83}$$

For normalization, we can use

$$G^1_\theta = 2\int_{\theta_-}^{\theta_+} \frac{d\theta}{\sqrt{\tilde{\Theta}(\theta)}} = 1.16949. \tag{6.84}$$

In conclusion, the principal Lyapunov exponent becomes

$$\lambda_P = \lambda_+ \tau_M = \lambda_+ G^1_\theta = 0.678861. \tag{6.85}$$

The most important consequence of these results, which can be seen in table 6.1, is that, even though most particles from the accretion disc are assumed to originate from the equatorial plane, considering deviations from this plane is necessary for a more accurate result when relaxing this assumption. This is best seen by focusing on the black hole shadow. In our previous work, we investigated the black hole shadows in detail [98]. Nevertheless, in that paper, we assumed that photons emitted from an orbiting black hole make an infinite number of turns around it. In other words, we did not consider the subring structure of the shadow image. Let us consider a photon hitting a point at radius $\rho = \rho_c + \delta\rho$ on the image plane where the shadow edge is at ρ_c. The radial deviation on the image plane, $\delta\rho$, is linearly related to the radial deviation around the black hole caused by perturbation, $\delta r(0)$ in 6.53. As a result, for

such a photon to orbit $\frac{n}{2}$ times before hitting the image, it must satisfy

$$\frac{\delta\rho_n}{\rho_c} \approx e^{-\lambda_P n} \tag{6.86}$$

around the shadow edge [4]. This is an approximate relation used in [4] as equation (11). One can understand this relation as follows: Subrings corresponding to fewer oscillations are visible and easier to interpret. Yet as the number of oscillations increases, they come closer together and approach the shadow limit, making them harder to resolve. Nonetheless, we are interested in a smaller number of subrings for observational and interferometric details, where small deviations in the Lyapunov exponent are important. Hence, the visible and consequential difference between the Lyapunov exponents considered on the equatorial (6.85) and on the non-equatorial orbits (6.82) should be considered, which was one of the main aspects of the current paper.

CHAPTER 7

CONCLUSIONS

7.1 Light Rings Around Five Dimensional Stationary Black Holes and Naked Singularities

Recent developments [1, 9] suggest that the environment of a black hole (an ultracompact object with a horizon) has rather unique observable properties which are best studied by light rings. These are null, unstable circular orbits and are closely related to the ringdown and shadow of black holes and the stability of the black hole itself. Ultracompact objects without horizons that could mimic black holes also have light rings at least one of which is stable (proven under certain conditions on the matter forming the ultracompact object [9]). The stability of the light ring yields a nonlinear instability of the ultracompact object whose fate has been studied for bosonic stars [99].

In [1], topological arguments were established to prove that assuming the existence of a Killing horizon in four-dimensional spacetime, there exists a light ring for each rotation sense for a vacuum axially symmetric, topologically sphere, circular, stationary, asymptotically flat metric. In the current work, we extended these topological arguments to five-dimensional generic stationary black holes without referring to the field equations and showed that there exists a light ring for each rotation sense of the five-dimensional stationary geometry with a Killing horizon. We assumed asymptotic flatness such that far away from the black hole region, the stationary solution reduces to the Myers-Perry spinning solution. We also studied the static case. When applying the topological techniques to five-dimensional black holes, one encounters the difficulty that generically there are two distinct conserved angular momenta for the light

which eventually complicates the effective potential: namely, the impact parameters of light enter the effective potential. But these parameters do not spoil the topological arguments in proving the existence of light rings for generic stationary metrics without referring to the underlying field equations. Yet, these parameters do change the location of the light rings in the r, θ coordinates. Our computations and the examples show that the techniques developed in [1] are robust.

Finally, we have also studied the naked singularity case for which the black hole has no horizon and showed that one of the light rings disappears and one is left with a single light ring. We have also discussed the four-dimensional naked singularity and showed that the prograde light ring of the Kerr black hole disappears while the retrograde orbit is intact. This has opened up an interesting discussion regarding a plausible test of the cosmic censorship which was discussed in Chapter 3.

7.2 Instability of a Kerr-type Naked Singularity due to Light and Matter Accretion and Its Shadow

The Kerr metric is a solution to the vacuum Einstein equations [10] that is assumed to represent the gravitational field of all astrophysical black holes with only two hairs, its mass m and angular momentum J. [The Kerr-Newman black hole has the electric charge as the third hair but astrophysical black holes are expected to be neutral.] Such a uniqueness is so remarkable that it also leads to a rather unique environment which can be observable due to the unstable nature of the photon orbits, among which the constant radii orbits are particularly relevant. In this work, we have studied the Kerr-type naked singularity to understand its shadow and its accretion. We found that a shadow image taken from the polar plane cannot distinguish a naked Kerr-type singularity with a spin parameter up to a maximum value ($\alpha = \sqrt{6\sqrt{3}-9}$) from a Kerr black hole; while for naked singularities with spins higher than the maximum value, the shadow becomes quite distinct from that of the Kerr black hole.

We have also studied the timelike orbits that are traced by massive particles around a naked singularity and showed that the rapidly spinning singularity immediately slows down due to the falling matter. Therefore, if a naked singularity is surrounded by a

thin accretion disk around its equator, then it slows down and an event horizon is expected to form. In this process, the retrograde orbits play a dominant role as their capture cross-sections are larger than the prograde orbits. In this present work, we have studied the bare essentials of the shadow and the accretion of Kerr-type naked singularities: this work could be extended in various directions such as studying various other naked singularities in more general gravity theories or studying more realistic accretion disks around such singularities. Without referring to an underlying theory such as General relativity, one can also study the naked singularity version of some phenomenological metrics, such as the Johannsen-Psaltis [100] metric that modifies the Kerr black hole with some additional parameters.

7.3 Partition Function of a Volume of Space in a Higher Curvature Theory

Following Jacobson and Visser [3], who generalized the notion of the gravitational entropy of horizons to the constrained finite spatial volume of n-ball topologies in (cosmological) Einstein gravity, we computed the quantum gravity partition function at the saddle point approximation in an infinite-order gravity theory of the Born-Infeld form in $2 + 1$ dimensions. The theory has 2 propagating degrees of freedom at the perturbative level and is locally nontrivial, unlike three-dimensional Einstein gravity. Our computations support the conclusions of [3]: The dimension of the Hilbert space of all states of a given disk with a boundary is equal to the exponential of the Bekenstein-Hawking, Gibbons-Hawking, or Wald entropy of it.

7.4 Refined Thermodynamics of Black Holes with Proper Conserved Charges

Understanding the macroscopic and microscopic thermodynamics of the gravitational field, especially in the case of strong gravitational fields of black holes will probably get us close to the quantum regime of gravity. Several decades of works along this direction have shown that the stationary gravitational fields that solve Einstein's theory with a cosmological constant obey the laws of thermodynamics in close analogy with matter fields, so close that one can talk about black hole chemistry, just like the chemistry of fluids with the usual volume, pressure, and other thermodynamic coor-

dinates. But there is a major difference between the thermodynamics of matter and the gravitational field: in the former, we have a consistent microscopic theory, and we can leave the regime of thermodynamics that captures the gross features of a many-body system behind and work in the microscopic theory when high energy processes are involved, while in the latter we only have proposed effective theories, instead of a consistent microscopic theory, in which the Einstein-Hilbert action is augmented with higher powers of curvature. With the addition of these higher powers, one needs to define effective thermodynamics. These higher powers bring in new scales to the theory and modify the beautiful scaling laws that lead to the Gibbs-Duhem-Smarr formula, a relation that ties the thermodynamics coordinates that describe the gross features of the gravitational field. This relation must be consistent with the first law of thermodynamics. This requirement forces one to carefully define the conserved charges and thermodynamical coordinates of the gravitational field. Recently [26] a generic procedure was outlined on how consistent thermodynamics can be defined in the presence of many dimensionful coupling constants by introducing auxiliary fields. In the current work, we have used those ideas plus the conserved charge construction in a generic gravity theory based on the background, or asymptotic Killing symmetries instead of the Komar charges, which is difficult to write for a generic theory. The versatility of this description is that it applies to any gravity theory that has a maximally symmetric vacuum solution. We applied the techniques to the rotating solutions of the D-dimensional cosmological Einstein theory and the spherically symmetric solutions of the Einstein-Gauss-Bonnet theory. The refined first law and the refined Smarr relations are satisfied. As a by-product of these refined laws, one gets an effective volume of black holes in generic D dimensions for both asymptotically anti–de Sitter and flat black holes. Also, the volume and the surface area of the black holes satisfy the reverse isoperimetric inequality, which becomes an equality for the Schwarzschild black hole.

7.5 Instability and Information Production Around Kerr Black Holes: Effects on Entropy and the Shadow

We considered some exponentially unstable motion undergone by massless and massive particles in the vicinity of a Kerr black hole. This leads us to two significant consequences. First, we showed that for massive particle orbits, the exponentially unstable motion of the massive particles that end inside the black hole can be interpreted in terms of black hole thermodynamics via the relation between the Lyapunov exponents and the Kolmogorov-Sinai entropy. Even though the KS entropy is an a priori mathematical construct, here we suggested a physical interpretation that obeys the expected bounds of the theory, such as the Bekenstein bound [39]. This interpretation required us to introduce a physical volume for the particle on the unstable massive orbit. For this purpose, we used the method of [3]. The fact that the Kolmogorov-Sinai entropy can be interpreted as a physical entropy that obeys the entropy bound conjecture is a promising result that may help build a bridge between information theory and black hole thermodynamics. Second, we investigated the instability of light and extended the method used [4] to cover non-equatorial-plane contributions to the black hole image. This addition provides nontrivial contributions to the subring structure of the shadow image, enabling a precise determination of the black hole mass and angular momentum. In general, as a viable approximation, photons emanating from the accretion disc on the equatorial plane are considered when constructing the shadow image. This does not cause any problems for the higher-order subrings or the shadow itself, for which it is assumed ($n \to \infty$). Nevertheless, deviations caused by non-equatorial photons may be relevant for lower-order subrings, especially for $n = 1$, $n = 2$, and $n = 3$, and one should consider them to obtain more accurate results for observable parameters. An outstanding problem we have not solved is to assign a Kolmogorov-Sinai type entropy for the null orbits: at this stage, we have not found a convincing volume regularization for these null orbits a la [3]. The method discussed can also be applied to different theories of gravity and to observational tools such as gravitational waves and near-horizon studies. [101],[102],[103],[104],[105].

REFERENCES

[1] P. V. P. Cunha and C. A. R. Herdeiro, Stationary Black Holes and Light Rings, Phys. Rev. Lett. **124**, 181101 (2020).

[2] D. Charbulák, Z. Stuchlík, Spherical photon orbits in the field of Kerr naked singularities, Eur. Phys. J. C **78**, 879 (2018).

[3] T. Jacobson and R. M. Visser, Partition Function for a Volume of Space, Phys. Rev. Lett. **130**, 221501 (2023).

[4] M. D. Johnson, A. Lupsasca, A. Strominger, G. N. Wong, S. Hadar, D. Kapec, R. Narayan, A. Chael, C. F. Gammie and P. Galison, *et al.* Universal interferometric signatures of a black hole's photon ring, Sci. Adv. **6**, no.12, eaaz1310 (2020).

[5] B. P. Abbott *et al.* (LIGO Scientific and Virgo Collaborations), Observation of Gravitational Waves from a Binary Black Hole Merger, Phys. Rev. Lett. **116**, 061102 (2016).

[6] R. Abbott *et al.* (LIGO Scientific and Virgo Collaborations), GW190521: A Binary Black Hole Merger with a Total Mass of $150\ M_{\odot}$, Phys. Rev. Lett. **125**, 101102 (2020).

[7] R. Abbott *et al.* (LIGO Scientific, KAGRA and VIRGO Collaborations), Observation of gravitational waves from two neutron star–black hole coalescences, Astrophys. J. Lett. **915**, L5 (2021).

[8] K. Akiyama *et al.* (Event Horizon Telescope Collaborations), First M87 event horizon telescope results. I. The shadow of the supermassive black hole, Astrophys. J. **875**, L1 (2019).

[9] P. V. P. Cunha, E. Berti, and C. A. R. Herdeiro, Light-Ring Stability for Ultracompact Objects, Phys. Rev. Lett. **119**, 251102 (2017).

[10] R. P. Kerr, Gravitational Field of a Spinning Mass as an Example of Algebraically Special Metrics, Phys. Rev. Lett. **11**, 237 (1963).

[11] E. Teo, Spherical photon orbits around a kerr black hole, Gen. Relativ. Gravit., **35**, 1909, (2003).

[12] A. Tavlayan and B. Tekin, Exact formulas for spherical photon orbits around kerr black holes, Phys. Rev. D **102**, 104036 (2020).

[13] R. Penrose, Gravitational collapse and space-time singularities, Phys. Rev. Lett. **14**, 57-59 (1965).

[14] R. Penrose, Gravitational collapse: The role of general relativity, Riv. Nuovo Cimento **1**, 252 (1969).

[15] J. D. Bekenstein, Black holes and entropy, Phys. Rev. D **7**, 2333 (1973).

[16] S. W. Hawking, Particle creation by black holes, Commun. Math. Phys. **43**, 199 (1975); **46**, 206(E) (1976).

[17] G. W. Gibbons and S. W. Hawking, Action integrals and partition functions in quantum gravity, Phys. Rev. D **15**, 2752 (1977).

[18] V. Balasubramanian, P. Horava, and D. Minic, Deconstructing de Sitter, J. High Energy Phys. 05 (2001) 043.

[19] W. Fischler, Taking de Sitter seriously, Talk given at *Proceedings of the Role of Scaling Laws in Physics and Biology (celebrating the 60th birthday of Geoffrey West), Santa Fe, 2000* (unpublished).

[20] T. Banks, Cosmological breaking of supersymmetry? Int. J. Mod. Phys. A **16**, 910 (2001).

[21] E. K. Morvan, J. P. van der Schaar, and R. M. Visser, On the Euclidean action of de Sitter black holes and constrained instantons, SciPost Phys. **14**, 022 (2023).

[22] I. Affleck, On constrained instantons, Nucl. Phys. **B191**, 429 (1981).

[23] J. Cotler and K. Jensen, Gravitational constrained instantons, Phys. Rev. D **104**, 081501 (2021).

[24] A. Tavlayan and B. Tekin, Partition function of a volume of space in a higher curvature theory, Phys. Rev. D **108**, L041902 (2023).

[25] L. Smarr, Mass formula for Kerr black holes, Phys. Rev. Lett. **30**, 71 (1973); 30, 521(E) (1973).

[26] K. Hajian and B. Tekin, Coupling constants as conserved charges in black hole thermodynamics, Phys. Rev. Lett. **132**, 191401 (2024).

[27] D. Kastor, S. Ray, and J. Traschen, Smarr formula and an extended first law for Lovelock gravity, Classical Quantum Gravity **27**, 235014 (2010)

[28] A. Komar, Covariant conservation laws in general relativity, Phys. Rev. **113**, 034 (1959).

[29] L. F. Abbott and S. Deser, Stability of gravity with a cosmological constant, Nucl. Phys. B**195**, 76 (1982).

[30] S. Deser and B. Tekin, Gravitational energy in quadratic-curvature gravities, Phys. Rev. Lett. **89**, 101101 (2002).

[31] S. Deser and B. Tekin, Energy in generic higher curvature gravity theories, Phys. Rev. D **67**, 084009 (2003).

[32] S. W. Hawking, C. J. Hunter, and M. Taylor, Rotation and the AdS / CFT correspondence, Phys. Rev. D **59**, 064005 (1999).

[33] G. W. Gibbons, H. Lu, D. N. Page, and C. N. Pope, Rotating black holes in higher dimensions with a cosmological constant, Phys. Rev. Lett. **93**, 171102 (2004).

[34] G. W. Gibbons, H. Lu, D. N. Page, and C. N. Pope, The general Kerr-de Sitter metrics in all dimensions, J. Geom. Phys. **53**, 49 (2005).

[35] R. C. Myers and M. J. Perry, Black holes in higher dimensional space-times, Ann. Phys. (N.Y.) **172**, 304 (1986).

[36] M. Cvetič, G. W. Gibbons, D. Kubizňák, and C. N. Pope, Black hole enthalpy and an entropy inequality for the thermodynamic volume, Phys. Rev. D **84**, 024037 (2011).

[37] K. Akiyama *et al.* [Event Horizon Telescope], First Sagittarius A* Event Horizon Telescope Results. I. The Shadow of the Supermassive Black Hole in the Center of the Milky Way, Astrophys. J. Lett. **930**, no.2, L12 (2022).

[38] J. R. Dorfman, An Introduction to Chaos in Nonequilibrium Statistical Mechanics. Cambridge: Cambridge University Press (Cambridge Lecture Notes in Physics) (1999).

[39] J. D. Bekenstein, A Universal Upper Bound on the Entropy to Energy Ratio for Bounded Systems, Phys. Rev. D **23**, 287 (1981).

[40] R. M. Wald, Jacob Bekenstein and the Development of Black Hole Thermodynamics, [arXiv:1805.02302 [physics.hist-ph]].

[41] L. Bombelli and E. Calzetta, Chaos around a black hole, Class. Quant. Grav. **9**, 2573-2599 (1992).

[42] J. J. Levin, Chaos may make black holes bright, Phys. Rev. D **60**, 064015 (1999).

[43] N. J. Cornish and J. J. Levin, Lyapunov timescales and black hole binaries, Class. Quant. Grav. **20**, 1649-1660 (2003).

[44] S. Dalui, B. R. Majhi and P. Mishra, Presence of horizon makes particle motion chaotic, Phys. Lett. B **788**, 486-493 (2019).

[45] A. Deich, N. Yunes and C. Gammie, Lyapunov exponents to test general relativity, Phys. Rev. D **110**, no.4, 044033 (2024).

[46] S. E. Gralla and A. Lupsasca, Lensing by Kerr Black Holes, Phys. Rev. D **101**, no.4, 044031 (2020).

[47] A. J. M. Medved, D. Martin, and M. Visser, Dirty black holes: Symmetries at stationary nonstatic horizons, Phys. Rev. D **70**, 024009 (2004).

[48] D. C. Wilkins, Bound geodesics in the Kerr metric, Phys. Rev. D **5**, 814 (1972).

[49] B. Carter, Global structure of the Kerr family of gravitational fields, Phys. Rev. **174**, 1559 (1968).

[50] V. P. Frolov and A. Zelnikov, Introduction to black hole physics, OUP Oxford (2011).

[51] V. Patel, D. Tahelyani, A. B. Joshi *et al.*, Light trajectory and shadow shape in the rotating naked singularity, Eur. Phys. J. C **82**, 798 (2022).

[52] J. M. Bardeen, In: Gravitational radiation and gravitational collapse; Proceedings of the Symposium, Warsaw, Poland, September 5-8, 1973. (A75-19176 06-90) Dordrecht, D. Reidel Publishing Co., 1974, p. 132-144 (1974).

[53] A. Tavlayan and B. Tekin, Radii of spherical timelike orbits around Kerr black holes, Phys. Rev. D **104**, 124059 (2021).

[54] J. M. Bardeen, Kerr Metric Black Holes, Nature **226**, 64-65 (1970).

[55] K. S. Thorne, Disk accretion onto a black hole. 2. Evolution of the hole, Astrophys. J. **191**, 507-520 (1974).

[56] F. de Felice, Classical instability of a naked singularity, Nature **273**, 429-431 (1978).

[57] Z. Stuchlik, Evolution of Kerr naked singularities, Bulletin of the Astronomical Institutes of Czechoslovakia **32**, 68-72 (1981).

[58] Z. Stuchlik and J. Schee, Appearance of Keplerian discs orbiting Kerr superspinars, Class. Quantum Grav. **27**, 21 (2010).

[59] Z. Stuchlik, S. Hledik and K. Truparova, Evolution of Kerr superspinars due to accretion counterrotating thin discs, Class. Quantum Grav. **28**, 155017 (2011).

[60] G. Torok and Z. Stuchlik, Radial and vertical epicyclic frequencies of Keplerian motion in the field of Kerr naked singularities - Comparison with the black hole case and possible instability of naked-singularity accretion discs, Astronomy and Astrophysics **437**, 775-788 (2005).

[61] Z. Stuchlik and J. Schee, Observational phenomena related to primordial Kerr superspinars, Class. Quantum Grav. **29**, 6 (2012).

[62] K. Hioki and K. i. Maeda, Measurement of the Kerr Spin Parameter by Observation of a Compact Object's Shadow, Phys. Rev. D **80**, 024042 (2009).

[63] Y. Hou, M. Guo and B. Chen, Revisiting the shadow of braneworld black holes, Phys. Rev. D **104**, 024001 (2021).

[64] R. Kumar and S. G. Ghosh, Photon ring structure of rotating regular black holes and no-horizon spacetimes, Class. Quantum Grav. **38**, 085010 (2021).

[65] I. Gullu, T. C. Sisman, and B. Tekin, Born-Infeld extension of new massive gravity, Classical Quantum Gravity **27**, 162001 (2010).

[66] E. A. Bergshoeff, O. Hohm, and P. K. Townsend, Massive Gravity in Three Dimensions, Phys. Rev. Lett. **102**, 201301 (2009).

[67] B. Tekin, A tribute to S. Deser: Conserved quantities in generic gravity theories, arXiv:2307.12758.

[68] I. Gullu, T. C. Sisman, and B. Tekin, c-functions in the Born-Infeld extended new massive gravity, Phys. Rev. D **82**, 024032 (2010).

[69] S. Nam, J. D. Park, and S. H. Yi, AdS black hole solutions in the extended new massive gravity, J. High Energy Phys. 07 (2010) 058.

[70] M. Gurses, T. C. Sisman, and B. Tekin, Some exact solutions of all $f(R_{/mu/nu})$ theories in three dimensions, Phys. Rev. D **86**, 024001 (2012).

[71] A. Sinha, On the new massive gravity and AdS/CFT, J. High Energy Phys. 06 (2010) 061.

[72] M. F. Paulos, New massive gravity extended with an arbitrary number of curvature corrections, Phys. Rev. D **82**, 084042 (2010).

[73] T. Ç. Şişman, Born-Infeld gravity theories in D-dimensions, Ph.D thesis, Middle East Technical University, 2012.

[74] D. P. Jatkar and A. Sinha, New Massive Gravity and AdS_4 Counterterms, Phys. Rev. Lett. **106**, 171601 (2011).

[75] E. Bergshoeff and M. Ozkan, 3D Born-Infeld gravity and supersymmetry, J. High Energy Phys. 08 (2014) 149.

[76] R. M. Wald, Black hole entropy is the Noether charge, Phys. Rev. D **48**, R3427 (1993).

[77] D. G. Ozen, S. Kurekci, and B. Tekin, Entropy in Born-Infeld gravity, Phys. Rev. D **96**, 124038 (2017).

[78] R. Brustein, D. Gorbonos, and M. Hadad, Wald's entropy is equal to a quarter of the horizon area in units of the effective gravitational coupling, Phys. Rev. D **79**, 044025 (2009).

[79] K. Hajian, H. Özşahin, and B. Tekin, First law of black hole thermodynamics and Smarr formula with a cosmological constant, Phys. Rev. D **104**, 044024 (2021).

[80] M. Henneaux and C. Teitelboim, The cosmological constant as a canonical variable, Phys. Lett. **143B**, 415 (1984).

[81] D. Chernyavsky and K. Hajian, Cosmological constant is a conserved charge, Classical Quantum Gravity **35**, 125012 (2018).

[82] E. Altas and B. Tekin, Conserved charges in AdS: A new formula, Phys. Rev. D **99**, 044026 (2019).

[83] E. Altas and B. Tekin, New approach to conserved charges of generic gravity in AdS spacetimes, Phys. Rev. D **99**, 044016 (2019).

[84] S. Deser, I. Kanik, and B. Tekin, Conserved charges of higher D Kerr-AdS spacetimes, Classical Quantum Gravity **22**, 3383 (2005).

[85] J. D. Brown and C. Teitelboim, Dynamical neutralization of the cosmological constant, Phys. Lett. B **195**, 177 (1987).

[86] M. M. Caldarelli, G. Cognola, and D. Klemm, Thermodynamics of Kerr-Newman-AdS black holes and conformal field theories, Classical Quantum Gravity **17**, 399 (2000).

[87] D. Kastor, S. Ray, and J. Traschen, Enthalpy and the mechanics of AdS black holes, Classical Quantum Gravity **26**, 195011 (2009).

[88] D. Kubiznak and R. B. Mann, P-V criticality of charged AdS black holes, J. High Energy Phys. **07** (2012) 033.

[89] D. Kubiznak, R. B. Mann, and M. Teo, Black hole chemistry: Thermodynamics with Lambda, Classical Quantum Gravity **34**, no.6, 063001 (2017).

[90] B. P. Dolan, *Where Is the PdV in the First Law of Black Hole Thermodynamics?* (2012), https://doi.org/10.5772/52455.

[91] D. G. Boulwere and S. Deser, String-generated gravity models, Phys. Rev. Lett. **55**, 2656 (1985).

[92] M. Gürses, T. Ç. Şişman, and B. Tekin, Is there a novel Einstein–Gauss–Bonnet theory in four dimensions?, Eur. Phys. J. C **80**, 647 (2020).

[93] M. Gürses, T. Ç. Şişman, and B. Tekin, Comment on Einstein-Gauss-Bonnet gravity in 4-dimensional space-time, Phys. Rev. Lett. **125**, 149001 (2020).

[94] S. Haroon, R. A. Hennigar, R. B. Mann, and F. Simovic, Thermodynamics of Gauss-Bonnet-de Sitter black holes, Phys. Rev. D **101**, 084051 (2020).

[95] S. Liberati and C. Pacilio, Smarr formula for Lovelock black holes: a Lagrangian approach, Phys. Rev. D **93**, 084044 (2016).

[96] S. E. Gralla and A. Lupsasca, Null geodesics of the Kerr exterior, Phys. Rev. D **101**, no.4, 044032 (2020).

[97] E. Himwich, M. D. Johnson, A. Lupsasca and A. Strominger, Universal polarimetric signatures of the black hole photon ring, Phys. Rev. D **101**, no.8, 084020 (2020).

[98] A. Tavlayan and B. Tekin, Instability of a Kerr-type naked singularity due to light and matter accretion and its shadow, Class. Quant. Grav. **41**, no.6, 065004 (2024).

[99] P. V. P. Cunha, C. Herdeiro, E. Radu, and N. Sanchis-Gual, The fate of the light-ring instability, arXiv:2207.13713.

[100] T. Johannsen and D. Psaltis, A Metric for Rapidly Spinning Black Holes Suitable for Strong-Field Tests of the No-Hair Theorem, Phys. Rev. D **83**, 124015 (2011).

[101] A. Deich, A. Cárdenas-Avendaño and N. Yunes, Chaos in quadratic gravity, Phys. Rev. D **106**, no.2, 024040 (2022).

[102] N. J. Cornish, Chaos and gravitational waves, Phys. Rev. D **64**, 084011 (2001).

[103] N. Kan and B. Gwak, Bound on the Lyapunov exponent in Kerr-Newman black holes via a charged particle, Phys. Rev. D **105**, no.2, 026006 (2022).

[104] X. Lyu, J. Tao and P. Wang, Probing the thermodynamics of charged Gauss Bonnet AdS black holes with the Lyapunov exponent, Eur. Phys. J. C **84**, no.9, 974 (2024).

[105] K. Hashimoto and N. Tanahashi, Universality in Chaos of Particle Motion near Black Hole Horizon, Phys. Rev. D **95**, no.2, 024007 (2017).

APPENDICES

A Calculation of the Ricci Scalar

In the first axis limit, $\theta \to 0$, we assumed that $g_{t\phi_1}$ and $g_{\phi_1\phi_2}$ approach zero faster than or as fast as $g_{\phi_1\phi_1}$. Here we provide a proof of this assumption. First, we introduce $\rho := \sqrt{g_{\phi_1\phi_1}}$ and z is a coordinate that is orthogonal to ρ. The metric can be rewritten as

$$\begin{aligned} ds^2 &= g_{tt}(\rho,z)\,dt^2 + 2g_{t\phi_1}(\rho,z)\,dtd\phi_1 \\ &\quad +2g_{t\phi_2}(\rho,z)\,dtd\phi_2 + 2g_{\phi_1\phi_2}(\rho,z)\,d\phi_1 d\phi_2 \\ &\quad +\rho^2 d\phi_1^2 + g_{\phi_2\phi_2}(\rho,z)\,d\phi_2^2 \\ &\quad +g_{\rho\rho}(\rho,z)\,d\rho^2 + g_{zz}(\rho,z)\,dz^2. \end{aligned} \tag{A.1}$$

Around the axis, $\rho \to 0$, the metric components can be expanded as

$$\begin{aligned} g_{tt} &\approx -1 + O(\rho), \;\; g_{t\phi_2} \approx 1 + O(\rho), \\ g_{\rho\rho} &\approx 1 + O(\rho), \;\; g_{zz} \approx 1 + O(\rho), \\ g_{\phi_2\phi_2} &\approx 1 + O(\rho), \\ g_{t\phi_1} &\approx g^{(1)}_{t\phi_1}(z)\,\rho + g^{(2)}_{t\phi_1}(z)\,\rho^2 + O\left(\rho^2\right), \\ g_{\phi_1\phi_2} &\approx g^{(1)}_{\phi_1\phi_2}(z)\,\rho + g^{(2)}_{\phi_1\phi_2}(z)\,\rho^2 + O\left(\rho^2\right). \end{aligned} \tag{A.2}$$

The scalar curvature in the first order of expansion can be computed to be

$$R \approx \frac{g^{(1)}_{t\phi_1}(z)^2 - 2g^{(1)}_{t\phi_1}(z)\,g^{(1)}_{\phi_1\phi_2}(z) - g^{(1)}_{\phi_1\phi_2}(z)^2}{2\rho^2\left(g^{(1)}_{t\phi_1}(z)^2 - 2g^{(1)}_{t\phi_1}(z)\,g^{(1)}_{\phi_1\phi_2}(z) - g^{(1)}_{\phi_1\phi_2}(z)^2 + 2\right)}.$$

For R to be finite as $\rho \to 0$, one must have $g^{(1)}_{t\phi_1}(z) = 0$ and $g^{(1)}_{\phi_1\phi_2}(z) = 0$. This completes our proof. The same procedure can be followed for the second axis limit, $\theta \to \frac{\pi}{2}$, and we reach the conclusion that $g_{t\phi_2}$ and $g_{\phi_1\phi_2}$ approach to zero faster than or as fast as $g_{\phi_2\phi_2}$.

B An Estimation of Mass from the Retrograde ISCO

Using [1] (3.67) and the solutions of the quartic equation, one can show that if the initial rotation parameter α_0 of the singularity (with initial mass m_0) satisfies $\alpha_0 > 1$, then this parameter is reduced to 1 after the total mass of the particles falling from a retrograde ISCO has reached the value

$$\bar{m} = \frac{m_0}{3\sqrt{2}}\left(\sqrt{\beta_+ + 2 - \beta_-} + \sqrt{\beta_- + 4 - \beta_+ + \frac{4\alpha_0\sqrt{2}}{\sqrt{\beta_+ + 2 - \beta_-}}}\right),$$

where

$$\beta_\pm := (\alpha_0 \pm 1)^{2/3}(\alpha_0 \mp 1)^{1/3} = \sqrt[3]{(\alpha_0^2 - 1)(\alpha_0 \pm 1)}.$$

In particular, up to order 2 ,

$$\frac{\bar{m}}{m_0} - 1 \underset{\alpha_0 \to 1^+}{=} \frac{5}{32}(\alpha_0 - 1) - \frac{81}{2048}(\alpha_0 - 1)^2 + o\left((\alpha_0 - 1)^2\right)$$

thus yielding the equivalent

$$\frac{\delta m}{m_0} \underset{\alpha_0 \to 1}{\sim} \frac{5(\alpha_0 - 1)}{32} = 0.15625(\alpha_0 - 1).$$

This is a somewhat good approximation as it may be observed that the relative error

$$\max_{1<\alpha_0<2}\left|\frac{\delta m - 5m_0(\alpha_0 - 1)/32}{\delta m}\right| < 11.5\%.$$

C Thermodynamic Quantities for Kerr-Ads Spacetimes

For an action of the form

$$I = \frac{1}{16\pi}\int d^D x\sqrt{-g}\left[R - 2\Lambda\right], \tag{C.1}$$

with a metric in generalized Boyer-Lindquist coordinates

$$\begin{aligned} ds^2 &= -W\left(1 + g^2r^2\right)dt^2 + \frac{2m}{U}\left(Wdt - \sum_{i=1}^{N}\frac{a_i\mu_i^2}{\Xi_i}d\phi_i\right)^2 \\ &+ \sum_{i=1}^{N}\frac{r^2 + a_i^2}{\Xi_i}\left(\mu_i^2 d\phi_i^2 + d\mu_i^2\right) + \frac{U}{V - 2m}dr^2 \\ &- \frac{g^2}{W\left(1 + g^2r^2\right)}\left(\sum_{i=1}^{N}\frac{r^2 + a_i^2}{\Xi_i}\mu_i d\mu_i + \epsilon r^2\nu d\nu\right)^2 + \epsilon r^2 d\nu^2, \end{aligned} \tag{C.2}$$

[1] This appendix was provided by an anonymous reviewer to whom we thank.

where

$$W := \sum_{i=1}^{N} \frac{\mu_i^2}{\Xi} + \epsilon\nu^2, \quad V := r^{\epsilon-2}\left(1+g^2r^2\right)\prod_{i=1}^{N}\left(r^2+a_i^2\right),$$
$$U := \frac{V}{1+g^2r^2}\left(1-\sum_{i=1}^{N}\frac{a_i^2\mu_i^2}{r^2+a_i^2}\right), \tag{C.3}$$

with the additional constraint

$$\sum_{i=1}^{N}\mu_i^2 + \epsilon\nu^2 = 1, \tag{C.4}$$

the thermodynamic quantities are derived in [36]. Here, $D = 2N+2$ and $\epsilon = 1$ for an even number of dimensions, and $D = 2N+1$ and $\epsilon = 0$ for an odd number of dimensions. However, in this current work, an action of the form

$$I = \frac{1}{4\Omega_{D-2}}\int d^Dx\sqrt{-g}\left(R-2\Lambda\right), \tag{C.5}$$

is being used, and as a result, some of these thermodynamic quantities should be rescaled due to the differences between the normalization constants. In the first part of this section, an even number of dimensions with $D = 2N+2$ is considered. The temperature, the angular velocities, and the equation defining the event horizon are directly related to the metric, which are independent of normalization constants. Hence, they remain the same. Nevertheless, the entropy is directly related to the form of the action and should be rescaled; one gets

$$S = \pi\prod_{i=1}^{N}\frac{r_{\rm H}^2+a_i^2}{\Xi_i}, \quad T = \frac{r_{\rm H}\left(1+g^2r_{\rm H}^2\right)}{2\pi}\sum_{i=1}^{N}\frac{1}{r_{\rm H}^2+a_i^2} - \frac{1-g^2r_{\rm H}^2}{4\pi r_{\rm H}},$$
$$\Omega_i = \frac{\left(1+g^2r_{\rm H}^2\right)a_i}{r_{\rm H}^2+a_i^2}, \quad 2m = \frac{1}{r_{\rm H}}\left(1+g^2r_{\rm H}^2\right)\prod_{i=1}^{N}\left(r_{\rm H}^2+a_i^2\right).$$

The energy and angular momenta are derived in [84], which read as

$$E = \frac{m}{\Xi}\sum_{i=1}^{N}\frac{1}{\Xi_i}, \quad J_i = \frac{ma_i}{\Xi_i\Xi}. \tag{C.6}$$

The cosmological charge and cosmological potential are derived in [79] and, after rescaling the cosmological charge term due to the difference between the normalization constants of two actions, read as

$$C = \pm\frac{\sqrt{|\Lambda|}}{\Omega_{D-2}} \quad \text{and} \quad \Theta_{\rm H} = \pm\sqrt{|\Lambda|}V_{\rm eff}. \tag{C.7}$$

After inserting these quantities into the Smarr relation, one gets

$$
\begin{aligned}
&(D-3)\,E=(D-2)\left(TS+\sum_{i=1}^{N}\Omega_i J_i\right)-\Theta_{\mathrm{H}}C,\\
&(D-3)\left(\frac{m}{\Xi}\sum_{i=1}^{N}\frac{1}{\Xi_i}\right)=(D-2)\left(\left(\frac{r_{\mathrm{H}}\left(1+g^2r_{\mathrm{H}}^2\right)}{2\pi}\sum_{i=1}^{N}\frac{1}{r_{\mathrm{H}}^2+a_i^2}-\frac{1-g^2r_{\mathrm{H}}^2}{4\pi r_{\mathrm{H}}}\right)\right.\\
&\left.\times\left(\pi\prod_{i=1}^{N}\frac{r_{\mathrm{H}}^2+a_i^2}{\Xi_i}\right)+\left(\sum_{i=1}^{N}\left(\frac{\left(1+g^2r_{\mathrm{H}}^2\right)a_i}{r_{\mathrm{H}}^2+a_i^2}\right)\left(\frac{ma_i}{\Xi_i\Xi}\right)\right)\right)\\
&-\left(\frac{\sqrt{|\Lambda|}}{\Omega_{D-2}}\right)\left(\sqrt{|\Lambda|}V_{\text{eff}}\right),\\
&(D-3)\left(\frac{m}{\Xi}\sum_{i=1}^{N}\frac{1}{\Xi_i}\right)-(D-2)\left(\frac{m}{\Xi}\sum_{i=1}^{N}\left(\frac{\left(1+g^2r_{\mathrm{H}}^2\right)a_i^2}{\left(r_{\mathrm{H}}^2+a_i^2\right)\Xi_i}\right)\right)=(D-2)\\
&\times\left(\left(\frac{r_{\mathrm{H}}\left(1+g^2r_{\mathrm{H}}^2\right)}{2\pi}\sum_{i=1}^{N}\frac{1}{r_{\mathrm{H}}^2+a_i^2}-\frac{1-g^2r_{\mathrm{H}}^2}{4\pi r_{\mathrm{H}}}\right)\left(\pi\prod_{i=1}^{N}\frac{r_{\mathrm{H}}^2+a_i^2}{\Xi_i}\right)\right)\\
&-\left(\frac{\sqrt{|\Lambda|}}{\Omega_{D-2}}\right)\left(\sqrt{|\Lambda|}V_{\text{eff}}\right),\\
&(D-3)\left(\frac{m}{\Xi}\sum_{i=1}^{N}\frac{1}{\Xi_i}\right)-(D-2)\left(\frac{m\left(1+g^2r_{\mathrm{H}}^2\right)}{\Xi}\sum_{i=1}^{N}\left(\frac{a_i^2}{\left(r_{\mathrm{H}}^2+a_i^2\right)\Xi_i}\right)\right)\\
&=(D-2)\left(\frac{1}{\Xi}\left(\frac{r_{\mathrm{H}}\left(1+g^2r_{\mathrm{H}}^2\right)}{2}\sum_{i=1}^{N}\frac{1}{r_{\mathrm{H}}^2+a_i^2}-\frac{1-g^2r_{\mathrm{H}}^2}{4r_{\mathrm{H}}}\right)\left(\prod_{i=1}^{N}r_{\mathrm{H}}^2+a_i^2\right)\right)\\
&-\left(\frac{\sqrt{|\Lambda|}}{\Omega_{D-2}}\right)\left(\sqrt{|\Lambda|}V_{\text{eff}}\right),\\
&(D-3)\left(m\sum_{i=1}^{N}\frac{1}{\Xi_i}\right)-(D-2)\left(m\left(1+g^2r_{\mathrm{H}}^2\right)\sum_{i=1}^{N}\left(\frac{a_i^2}{\left(r_{\mathrm{H}}^2+a_i^2\right)\Xi_i}\right)\right)\\
&=(D-2)\left(\left(\frac{r_{\mathrm{H}}\left(1+g^2r_{\mathrm{H}}^2\right)}{2}\sum_{i=1}^{N}\frac{1}{r_{\mathrm{H}}^2+a_i^2}-\frac{1-g^2r_{\mathrm{H}}^2}{4r_{\mathrm{H}}}\right)\left(\prod_{i=1}^{N}r_{\mathrm{H}}^2+a_i^2\right)\right)\\
&-\Xi\left(\frac{\sqrt{|\Lambda|}}{\Omega_{D-2}}\right)\left(\sqrt{|\Lambda|}V_{\text{eff}}\right),\\
&(D-3)\left(m\sum_{i=1}^{N}\frac{1}{\Xi_i}\right)-(D-2)\left(m\left(1+g^2r_{\mathrm{H}}^2\right)\sum_{i=1}^{N}\left(\frac{a_i^2}{\left(r_{\mathrm{H}}^2+a_i^2\right)\Xi_i}\right)\right)\\
&=(D-2)\left(\left(\frac{r_{\mathrm{H}}\left(1+g^2r_{\mathrm{H}}^2\right)}{2}\sum_{i=1}^{N}\frac{1}{r_{\mathrm{H}}^2+a_i^2}-\frac{1-g^2r_{\mathrm{H}}^2}{4r_{\mathrm{H}}}\right)\left(\frac{2mr_{\mathrm{H}}}{1+g^2r_{\mathrm{H}}^2}\right)\right)\\
&-\Xi\left(\frac{\sqrt{|\Lambda|}}{\Omega_{D-2}}\right)\left(\sqrt{|\Lambda|}V_{\text{eff}}\right),
\end{aligned}
$$

$$
\begin{aligned}
&(D-3)\left(\sum_{i=1}^{N}\frac{1}{\Xi_i}\right)-(D-2)\left(\left(1+g^2r_{\rm H}^2\right)\sum_{i=1}^{N}\left(\frac{a_i^2}{\left(r_{\rm H}^2+a_i^2\right)\Xi_i}\right)\right)\\
&=(D-2)\left(r_{\rm H}^2\sum_{i=1}^{N}\frac{1}{r_{\rm H}^2+a_i^2}-\frac{1-g^2r_{\rm H}^2}{2\left(1+g^2r_{\rm H}^2\right)}\right)-\frac{\Xi}{m}\left(\frac{\sqrt{|\Lambda|}}{\Omega_{D-2}}\right)\left(\sqrt{|\Lambda|}V_{\rm eff}\right),\\
&-(D-2)\left(r_{\rm H}^2\sum_{i=1}^{N}\frac{1}{r_{\rm H}^2+a_i^2}+\left(1+g^2r_{\rm H}^2\right)\sum_{i=1}^{N}\left(\frac{a_i^2}{\left(r_{\rm H}^2+a_i^2\right)\Xi_i}\right)\right)\\
&+(D-3)\left(\sum_{i=1}^{N}\frac{1}{\Xi_i}\right)=(D-2)\left(-\frac{1-g^2r_{\rm H}^2}{2\left(1+g^2r_{\rm H}^2\right)}\right)\\
&-\frac{\Xi}{m}\left(\frac{\sqrt{|\Lambda|}}{\Omega_{D-2}}\right)\left(\sqrt{|\Lambda|}V_{\rm eff}\right),\\
&(D-3)\left(\sum_{i=1}^{N}\frac{1}{\Xi_i}\right)-(D-2)\left(\sum_{i=1}^{N}\frac{1}{\Xi_i}\right)=(D-2)\\
&\times\left(-\frac{1-g^2r_{\rm H}^2}{2\left(1+g^2r_{\rm H}^2\right)}\right)-\frac{\Xi}{m}\left(\frac{\sqrt{|\Lambda|}}{\Omega_{D-2}}\right)\left(\sqrt{|\Lambda|}V_{\rm eff}\right),\\
&\left(\sum_{i=1}^{N}\frac{1}{\Xi_i}\right)=(D-2)\left(\frac{1-g^2r_{\rm H}^2}{2\left(1+g^2r_{\rm H}^2\right)}\right)+\frac{\Xi}{m}\left(\frac{\sqrt{|\Lambda|}}{\Omega_{D-2}}\right)\left(\sqrt{|\Lambda|}V_{\rm eff}\right),\\
&\frac{m}{\Xi}\left(\left(\sum_{i=1}^{N}\frac{1}{\Xi_i}\right)-(D-2)\left(\frac{1-g^2r_{\rm H}^2}{2\left(1+g^2r_{\rm H}^2\right)}\right)\right)=\left(\frac{-\Lambda}{\Omega_{D-2}}\right)V_{\rm eff},\\
&V_{\rm eff}=\frac{m\Omega_{D-2}}{\Lambda\Xi}\left(-\sum_{i=1}^{N}\frac{1}{\Xi_i}+\left(\frac{D-2}{2}\right)\left(\frac{1-g^2r_{\rm H}^2}{1+g^2r_{\rm H}^2}\right)\right).
\end{aligned}
\tag{C.8}
$$

One can derive the thermodynamic quantities for odd dimensions by using the same approach and get

$$
\begin{aligned}
&(D-3)\,E=(D-2)\left(TS+\sum_{i=1}^{N}\Omega_iJ_i\right)-\Theta_{\rm H}C,\\
&(D-3)\left(\frac{m}{\Xi}\right)\left(\sum_{i=1}^{N}\frac{1}{\Xi_i}-\frac{1}{2}\right)\\
&=(D-2)\left(\left(\frac{r_{\rm H}\left(1+g^2r_{\rm H}^2\right)}{2\pi}\sum_{i=1}^{N}\frac{1}{r_{\rm H}^2+a_i^2}-\frac{1}{2\pi r_{\rm H}}\right)\left(\frac{\pi}{r_{\rm H}}\prod_{i=1}^{N}\frac{r_{\rm H}^2+a_i^2}{\Xi_i}\right)\right.\\
&\left.+\left(\sum_{i=1}^{N}\left(\frac{\left(1+g^2r_{\rm H}^2\right)a_i}{r_{\rm H}^2+a_i^2}\right)\left(\frac{ma_i}{\Xi_i\Xi}\right)\right)\right)-\left(\frac{\sqrt{|\Lambda|}}{\Omega_{D-2}}\right)\left(\sqrt{|\Lambda|}V_{\rm eff}\right),
\end{aligned}
$$

$$(D-3)\left(\frac{m}{\Xi}\sum_{i=1}^{N}\frac{1}{\Xi_i}\right)-(D-3)\left(\frac{m}{2\Xi}\right)-(D-2)\left(\frac{m}{\Xi}\sum_{i=1}^{N}\left(\frac{(1+g^2r_{\rm H}^2)\,a_i^2}{(r_{\rm H}^2+a_i^2)\,\Xi_i}\right)\right)$$
$$=(D-2)\left(\left(\frac{r_{\rm H}\,(1+g^2r_{\rm H}^2)}{2\pi}\sum_{i=1}^{N}\frac{1}{r_{\rm H}^2+a_i^2}-\frac{1}{2\pi r_{\rm H}}\right)\left(\frac{\pi}{r_{\rm H}}\prod_{i=1}^{N}\frac{r_{\rm H}^2+a_i^2}{\Xi_i}\right)\right)$$
$$-\left(\frac{\sqrt{|\Lambda|}}{\Omega_{D-2}}\right)\left(\sqrt{|\Lambda|}V_{\rm eff}\right),$$
$$(D-3)\left(\frac{m}{\Xi}\sum_{i=1}^{N}\frac{1}{\Xi_i}\right)-(D-3)\left(\frac{m}{2\Xi}\right)$$
$$-(D-2)\left(\frac{m\,(1+g^2r_{\rm H}^2)}{\Xi}\sum_{i=1}^{N}\left(\frac{a_i^2}{(r_{\rm H}^2+a_i^2)\,\Xi_i}\right)\right)=(D-2)$$
$$\times\left(\frac{1}{\Xi}\left(\frac{(1+g^2r_{\rm H}^2)}{2}\sum_{i=1}^{N}\frac{1}{r_{\rm H}^2+a_i^2}-\frac{1}{2r_{\rm H}^2}\right)\left(\prod_{i=1}^{N}r_{\rm H}^2+a_i^2\right)\right)$$
$$-\left(\frac{\sqrt{|\Lambda|}}{\Omega_{D-2}}\right)\left(\sqrt{|\Lambda|}V_{\rm eff}\right),$$
$$(D-3)\left(m\sum_{i=1}^{N}\frac{1}{\Xi_i}\right)-(D-3)\left(\frac{m}{2}\right)$$
$$-(D-2)\left(m\left(1+g^2r_{\rm H}^2\right)\sum_{i=1}^{N}\left(\frac{a_i^2}{(r_{\rm H}^2+a_i^2)\,\Xi_i}\right)\right)=(D-2)$$
$$\times\left(\left(\frac{(1+g^2r_{\rm H}^2)}{2}\sum_{i=1}^{N}\frac{1}{r_{\rm H}^2+a_i^2}-\frac{1}{2r_{\rm H}^2}\right)\left(\prod_{i=1}^{N}r_{\rm H}^2+a_i^2\right)\right)$$
$$-\Xi\left(\frac{\sqrt{|\Lambda|}}{\Omega_{D-2}}\right)\left(\sqrt{|\Lambda|}V_{\rm eff}\right),$$
$$(D-3)\left(m\sum_{i=1}^{N}\frac{1}{\Xi_i}\right)-(D-3)\left(\frac{m}{2}\right)$$
$$-(D-2)\left(m\left(1+g^2r_{\rm H}^2\right)\sum_{i=1}^{N}\left(\frac{a_i^2}{(r_{\rm H}^2+a_i^2)\,\Xi_i}\right)\right)=(D-2)$$
$$\times\left(\left(\frac{(1+g^2r_{\rm H}^2)}{2}\sum_{i=1}^{N}\frac{1}{r_{\rm H}^2+a_i^2}-\frac{1}{2r_{\rm H}^2}\right)\left(\frac{2mr_{\rm H}^2}{1+g^2r_{\rm H}^2}\right)\right)$$
$$-\Xi\left(\frac{\sqrt{|\Lambda|}}{\Omega_{D-2}}\right)\left(\sqrt{|\Lambda|}V_{\rm eff}\right),$$

$$
\begin{aligned}
&(D-3)\left(\sum_{i=1}^{N}\frac{1}{\Xi_i}\right)-\left(\frac{D-3}{2}\right)-(D-2)\left(\left(1+g^2r_{\rm H}^2\right)\sum_{i=1}^{N}\left(\frac{a_i^2}{\left(r_{\rm H}^2+a_i^2\right)\Xi_i}\right)\right)\\
&=(D-2)\left(r_{\rm H}^2\sum_{i=1}^{N}\frac{1}{r_{\rm H}^2+a_i^2}-\frac{1}{1+g^2r_{\rm H}^2}\right)-\frac{\Xi}{m}\left(\frac{\sqrt{|\Lambda|}}{\Omega_{D-2}}\right)\left(\sqrt{|\Lambda|}V_{\rm eff}\right),\\
&(D-3)\left(\sum_{i=1}^{N}\frac{1}{\Xi_i}\right)-\left(\frac{D-3}{2}\right)\\
&-(D-2)\left(r_{\rm H}^2\sum_{i=1}^{N}\frac{1}{r_{\rm H}^2+a_i^2}+\left(1+g^2r_{\rm H}^2\right)\sum_{i=1}^{N}\left(\frac{a_i^2}{\left(r_{\rm H}^2+a_i^2\right)\Xi_i}\right)\right)=(D-2)\\
&\times\left(-\frac{1}{1+g^2r_{\rm H}^2}\right)-\frac{\Xi}{m}\left(\frac{\sqrt{|\Lambda|}}{\Omega_{D-2}}\right)\left(\sqrt{|\Lambda|}V_{\rm eff}\right),\\
&(D-3)\left(\sum_{i=1}^{N}\frac{1}{\Xi_i}\right)-\left(\frac{D-3}{2}\right)-(D-2)\left(\sum_{i=1}^{N}\frac{1}{\Xi_i}\right)=(D-2)\\
&\times\left(-\frac{1}{1+g^2r_{\rm H}^2}\right)-\frac{\Xi}{m}\left(\frac{\sqrt{|\Lambda|}}{\Omega_{D-2}}\right)\left(\sqrt{|\Lambda|}V_{\rm eff}\right),\\
&\left(\sum_{i=1}^{N}\frac{1}{\Xi_i}\right)+\left(\frac{D-3}{2}\right)=(D-2)\left(\frac{1}{1+g^2r_{\rm H}^2}\right)+\frac{\Xi}{m}\left(\frac{\sqrt{|\Lambda|}}{\Omega_{D-2}}\right)\left(\sqrt{|\Lambda|}V_{\rm eff}\right),\\
&\frac{m}{\Xi}\left(\left(\sum_{i=1}^{N}\frac{1}{\Xi_i}\right)+\left(\frac{D-3}{2}\right)-(D-2)\left(\frac{1}{1+g^2r_{\rm H}^2}\right)\right)=\left(\frac{-\Lambda}{\Omega_{D-2}}\right)V_{\rm eff},\\
&V_{\rm eff}=\frac{m\Omega_{D-2}}{\Lambda\Xi}\left(-\sum_{i=1}^{N}\frac{1}{\Xi_i}-\left(\frac{D-3}{2}\right)+(D-2)\left(\frac{1}{1+g^2r_{\rm H}^2}\right)\right).
\end{aligned}
\tag{C.9}
$$

D Derivation of the Charge Term for Einstein-Gauss-Bonnet Gravity in Generic D Dimensions

For an action of the form

$$
I=\int d^Dx\sqrt{-g}\frac{1}{16\pi G}\left(R-2\Lambda+\frac{\lambda_{\rm GB}\mathcal{L}}{(D-3)(D-4)}\right),
\tag{D.1}
$$

with a metric of the form

$$
ds^2=-f(r)dt^2+\frac{dr^2}{f(r)}+r^2d\Omega^2,
\tag{D.2}
$$

where

$$
f(r)=1+\frac{r^2}{2\lambda_{\rm GB}}-\frac{r^{2-D/2}\sqrt{r^D+4\lambda_{\rm GB}\left(r\omega_{D-3}+r^D/L^2\right)}}{2\lambda_{\rm GB}},
\tag{D.3}
$$

$$\Lambda = \frac{(D-1)(D-2)}{2L^2}, \tag{D.4}$$

and

$$\omega_{D-3} = \frac{16\pi G m}{(D-2)\Omega_{D-2}}, \tag{D.5}$$

the thermodynamic quantities are calculated in [94]. Another important function defined in [94] is the pure dS vacuum of the theory that reads as

$$f_0(r) = 1 + r^2 \left(\frac{1 - \sqrt{1 + \frac{4\lambda_{\rm GB}}{L^2}}}{2\lambda_{\rm GB}} \right). \tag{D.6}$$

In the asymptotically flat limit, $\Lambda \to 0$, the case that is being investigated in our current work, these terms become

$$f(r) = 1 + \frac{r^2}{2\lambda_{\rm GB}} - \frac{\sqrt{r^4 + 4\lambda_{\rm GB}\omega_{D-3} r^{5-D}}}{2\lambda_{\rm GB}} \tag{D.7}$$

and

$$f_0(r) = 1. \tag{D.8}$$

D.1 Energy

The energy term is given in [94] as

$$\begin{aligned} E = & \frac{(D-2)\Omega_{D-2} r_c^{D-5}}{24\pi G} \Big[\sqrt{f(r_c)} \left(-3r_c^2 + 2\lambda_{\rm GB} \left(f(r_c) - 3 \right) \right) \\ & - \sqrt{f_0(r_c)} \left(-3r_c^2 + 2\lambda_{\rm GB} \left(f_0(r_c) - 3 \right) \right) \Big], \end{aligned} \tag{D.9}$$

where r_c gives the location of the cavity. In the asymptotically flat limit, $\Lambda \to 0$ and $r_c \to \infty$, one gets

$$E = m. \tag{D.10}$$

D.2 Entropy

The entropy term is given in [94] as

$$S = \frac{\Omega_{D-2} r_{\rm H}^{D-2}}{4G} + \frac{(D-2)\lambda_{\rm GB}\Omega_{D-2} r_{\rm H}^{D-4}}{2G(D-4)}, \tag{D.11}$$

where

$$\lambda_{\rm GB} + r_{\rm H}^2 = r_{\rm H}^{5-D}\omega_{D-3}. \tag{D.12}$$

D.3 Temperature

The horizon temperature is

$$T = \frac{1}{4\pi}\left(\frac{(D-3)r_{\rm H}^2 + (D-5)\lambda_{\rm GB}}{r_{\rm H}^3 + 2\lambda_{\rm GB} r_{\rm H}}\right). \tag{D.13}$$

D.4 Charge

In the asymptotically flat limit, the Smarr relation is given in [94] as

$$(D-3)E = (D-2)TS + 2\Phi_{\rm GB}\lambda_{\rm GB}. \tag{D.14}$$

Therefore, the charge term can be found as

$$\Phi_{\rm GB} = \frac{(D-3)E - (D-2)TS}{2\lambda_{\rm GB}}. \tag{D.15}$$

It is known that

$$E = m = \frac{(D-2)\Omega_{D-2}\omega_{D-3}}{16\pi G} = \frac{(D-2)\Omega_{D-2}\left(r_{\rm H}^{D-5}\lambda_{\rm GB} + r_{\rm H}^{D-3}\right)}{16\pi G}. \tag{D.16}$$

When the corresponding terms are inserted, one gets

$$
\begin{aligned}
\Phi_{\rm GB} &= \frac{1}{2\lambda_{\rm GB}}\left[(D-3)\left(\frac{(D-2)\Omega_{D-2}\left(r_{\rm H}^{D-5}\lambda_{\rm GB}+r_{\rm H}^{D-3}\right)}{16\pi G}\right)\right. \\
&\quad -(D-2)\left(\frac{1}{4\pi}\left(\frac{(D-3)r_{\rm H}^2+(D-5)\lambda_{\rm GB}}{r_{\rm H}^3+2\lambda_{\rm GB}r_{\rm H}}\right)\right) \\
&\quad \left.\times\left(\frac{\Omega_{D-2}r_{\rm H}^{D-2}}{4G}+\frac{(D-2)\lambda_{\rm GB}\Omega_{D-2}r_{\rm H}^{D-4}}{2G(D-4)}\right)\right] \\
&= \frac{(D-2)\Omega_{D-2}r_{\rm H}^{D-5}}{32\pi G\lambda_{\rm GB}}\left[\left((D-3)\left(\lambda_{\rm GB}+r_{\rm H}^2\right)\right)\right. \\
&\quad \left.-\left(\frac{(D-3)r_{\rm H}^2+(D-5)\lambda_{\rm GB}}{r_{\rm H}^2+2\lambda_{\rm GB}}\right)\left(r_{\rm H}^2+\frac{2(D-2)\lambda_{\rm GB}}{(D-4)}\right)\right] \\
&= \frac{(D-2)\Omega_{D-2}r_{\rm H}^{D-5}}{32\pi G\lambda_{\rm GB}}\left[\left((D-3)\left(\lambda_{\rm GB}+r_{H}^2\right)\right)\right. \\
&\quad \left.-\left(\frac{(D-3)r_{\rm H}^2+(D-5)\lambda_{\rm GB}}{r_{\rm H}^2+2\lambda_{\rm GB}}\right)\left(\frac{r_{\rm H}^2(D-4)+2(D-2)\lambda_{\rm GB}}{(D-4)}\right)\right] \\
&= \frac{(D-2)\Omega_{D-2}r_{\rm H}^{D-5}}{32\pi G\lambda_{\rm GB}(D-4)\left(r_{\rm H}^2+2\lambda_{\rm GB}\right)}\left[\left((D-3)(D-4)\left(r_{\rm H}^2+\lambda_{\rm GB}\right)\right.\right. \\
&\quad \left.\times\left(r_{\rm H}^2+2\lambda_{\rm GB}\right)\right)-\left((D-3)r_{\rm H}^2+(D-5)\lambda_{\rm GB}\right) \\
&\quad \left.\times\left((D-4)r_{\rm H}^2+2(D-2)\lambda_{\rm GB}\right)\right] \\
&= \frac{(D-2)\Omega_{D-2}r_{\rm H}^{D-5}}{32\pi G\lambda_{\rm GB}(D-4)\left(r_{\rm H}^2+2\lambda_{\rm GB}\right)}\left[r_{\rm H}^4\left((D-3)(D-4)\right.\right. \\
&\quad -(D-3)(D-4))+\lambda_{\rm GB}r_{\rm H}^2\left(3(D-3)(D-4)-2(D-2)(D-3)\right. \\
&\quad \left.\left.\left.-(D-4)(D-5)\right)+\lambda_{\rm GB}^2\left(2(D-3)(D-4)-2(D-2)(D-5)\right)\right] \\
&= \frac{(D-2)\Omega_{D-2}r_{\rm H}^{D-5}}{32\pi G\lambda_{\rm GB}(D-4)\left(r_{\rm H}^2+2\lambda_{\rm GB}\right)}\left[\lambda_{\rm GB}r_{\rm H}^2\left(3D^2-21D+36-2D^2+10D\right.\right. \\
&\quad \left.\left.-12-D^2+9D-20\right)+2\lambda_{\rm GB}^2\left((D-3)(D-4)-(D-2)(D-5)\right)\right] \\
&= \frac{(D-2)\Omega_{D-2}r_{\rm H}^{D-5}}{32\pi G(D-4)\left(r_{\rm H}^2+2\lambda_{\rm GB}\right)} \\
&\quad \times\left[r_{\rm H}^2\left(-2D+4\right)+2\lambda_{\rm GB}\left(D^2-7D+12-D^2+7D-10\right)\right] \\
&= \frac{(D-2)\Omega_{D-2}r_{\rm H}^{D-5}}{32\pi G(D-4)\left(r_{\rm H}^2+2\lambda_{\rm GB}\right)}\left[-2r_{\rm H}^2\left(D-2\right)+4\lambda_{\rm GB}\right] \\
&= \frac{(D-2)\Omega_{D-2}r_{\rm H}^{D-5}}{16\pi G(D-4)\left(r_{\rm H}^2+2\lambda_{\rm GB}\right)}\left[-r_{\rm H}^2\left(D-2\right)+2\lambda_{\rm GB}\right]. \qquad \text{(D.17)}
\end{aligned}
$$

Because of differences between the normalization constants of two actions, the charge term associated with the action used in our work should be

$$\Phi=\frac{16\pi G}{4\Omega_{D-2}}\Phi_{\rm GB}, \qquad \text{(D.18)}$$

and the coupling constant should be

$$\lambda_{\rm GB} = (D-3)(D-4)\lambda. \tag{D.19}$$

As a result, the corresponding charge term, the Smarr relation, and the first law become

$$\begin{aligned}\Phi &= \frac{(D-2)r_{\rm H}^{D-5}}{4(D-4)\left(r_{\rm H}^2+2\lambda(D-3)(D-4)\right)}\left[-r_{\rm H}^2\,(D-2)+2\lambda(D-3)(D-4)\right] \\ &= \frac{(D-2)r_{\rm H}^{D-5}}{4(D-4)}\left(\frac{-r_{\rm H}^2(D-2)+2\lambda(D-3)(D-4)}{r_{\rm H}^2+2\lambda(D-3)(D-4)}\right),\end{aligned} \tag{D.20}$$

$$(D-3)E = (D-2)TS + 2(D-3)(D-4)\Phi\lambda, \tag{D.21}$$

and

$$\delta E = T\delta S + (D-3)(D-4)\Phi\delta\lambda, \tag{D.22}$$

respectively.

E Explicit Calculation of the Smarr Relation with Our Thermodynamical Quantities

In our current work, the Smarr relation becomes

$$(D-3)E = (D-2)TS + 2(D-3)(D-4)\lambda\tilde{\Phi}, \tag{E.1}$$

with the corresponding thermodynamic quantities

$$E = \frac{D-2}{2}m, \tag{E.2}$$

$$T = \frac{(D-3)r_{\rm H}^2+(D-3)(D-4)(D-5)\lambda}{4\pi r_{\rm H}^3+8\pi r_{\rm H}\lambda(D-3)(D-4)}, \tag{E.3}$$

$$\tilde{S} = \pi r_{\rm H}^{D-2} + 2(D-2)(D-3)\pi\lambda r_{\rm H}^{D-4}, \tag{E.4}$$

and

$$2M = r_{\rm H}^{D-3} + (D-3)(D-4)\lambda r_{\rm H}^{D-5}. \tag{E.5}$$

When these terms are inserted into the Smarr relation, it becomes

$$
\begin{aligned}
&(D-3)\frac{(D-2)m}{2} = (D-2)\left(\frac{(D-3)r_{\rm H}^2+(D-3)(D-4)(D-5)\lambda}{4\pi r_{\rm H}^3+8\pi r_{\rm H}\lambda(D-3)(D-4)}\right)\\
&\times\left(\pi r_{\rm H}^{D-2}+2(D-2)(D-3)\pi\lambda r_{\rm H}^{D-4}\right)+2(D-3)(D-4)\lambda\\
&\times\left(\frac{(D-2)r_{\rm H}^{D-5}}{4(D-4)}\left(\frac{-r_{\rm H}^2(D-2)+2\lambda(D-3)(D-4)}{r_{\rm H}^2+2\lambda(D-3)(D-4)}\right)\right),\\
&\frac{M}{2} = \left(\frac{r_{\rm H}^2+(D-4)(D-5)\lambda}{4r_{\rm H}^2+8\lambda(D-3)(D-4)}\right)\left(r_{\rm H}^{D-3}+2(D-2)(D-3)\lambda r_{\rm H}^{D-5}\right)\\
&+2\lambda\left(\frac{r_{\rm H}^{D-5}}{4}\left(\frac{-r_{\rm H}^2(D-2)+2\lambda(D-3)(D-4)}{r_{\rm H}^2+2\lambda(D-3)(D-4)}\right)\right),\\
&\frac{\left(r_{\rm H}^{D-3}+(D-3)(D-4)\lambda r_{\rm H}^{D-5}\right)}{4} = \left(\frac{r_{\rm H}^2+(D-4)(D-5)\lambda}{4r_{\rm H}^2+8\lambda(D-3)(D-4)}\right)\\
&\times\left(r_{\rm H}^{D-3}+2(D-2)(D-3)\lambda r_{\rm H}^{D-5}\right)\\
&+2\lambda\left(\frac{r_{\rm H}^{D-5}}{4}\left(\frac{-r_{\rm H}^2(D-2)+2\lambda(D-3)(D-4)}{r_{\rm H}^2+2\lambda(D-3)(D-4)}\right)\right),\\
&\frac{(r_{\rm H}^2+(D-3)(D-4)\lambda)}{4} = \left(\frac{r_{\rm H}^2+(D-4)(D-5)\lambda}{4r_{\rm H}^2+8\lambda(D-3)(D-4)}\right)\\
&\times\left(r_{\rm H}^2+2(D-2)(D-3)\lambda\right)\\
&+2\lambda\left(\frac{1}{4}\left(\frac{-r_{\rm H}^2(D-2)+2\lambda(D-3)(D-4)}{r_{\rm H}^2+2\lambda(D-3)(D-4)}\right)\right),\\
&r_{\rm H}^2+(D-3)(D-4)\lambda = \left(\frac{r_{\rm H}^2+(D-4)(D-5)\lambda}{r_{\rm H}^2+2\lambda(D-3)(D-4)}\right)\\
&\times\left(r_{\rm H}^2+2(D-2)(D-3)\lambda\right)\\
&+2\lambda\left(\frac{-r_{\rm H}^2(D-2)+2\lambda(D-3)(D-4)}{r_{\rm H}^2+2\lambda(D-3)(D-4)}\right),\\
&\left(r_{\rm H}^2+(D-3)(D-4)\lambda\right)\left(r_{\rm H}^2+2\lambda(D-3)(D-4)\right)\\
&=\left(r_{\rm H}^2+(D-4)(D-5)\lambda\right)\left(r_{\rm H}^2+2(D-2)(D-3)\lambda\right)\\
&+2\lambda\left(-r_{\rm H}^2(D-2)+2(D-3)(D-4)\lambda\right),\\
&r_{\rm H}^4+r_{\rm H}^2\lambda\left(2(D-3)(D-4)+(D-3)(D-4)\right)+2\lambda^2\left((D-3)^2(D-4)^2\right)\\
&=r_{\rm H}^4+r_{\rm H}^2\lambda\left(2(D-2)(D-3)+(D-4)(D-5)-2(D-2)\right)\\
&+\lambda^2\left(2(D-2)(D-3)(D-4)(D-5)+4(D-3)(D-4)\right),\\
&r_{\rm H}^4+3r_{\rm H}^2\lambda\left(D^2-7D+12\right)+2\lambda^2\left((D-3)^2(D-4)^2\right)\\
&=r_{\rm H}^4+r_{\rm H}^2\lambda\left(2D^2-10D+12+D^2-9D+20-2D+4\right)\\
&+\lambda^2\left(2(D-2)(D-3)(D-4)(D-5)+4(D-3)(D-4)\right),\\
&r_{\rm H}^2\lambda\left(3D^2-21D+36\right)-3r_{\rm H}^2\lambda\left(D^2-7D+12\right)\\
&+\lambda^2(D-3)(D-4)\left(2(D-2)(D-5)+4\right)-2\lambda^2\left((D-3)^2(D-4)^2\right)=0,
\end{aligned}
$$

$$
\begin{aligned}
&3r_{\mathrm{H}}^2\lambda\left(D^2-7D+12-D^2+7D-12\right)\\
&+2\lambda^2(D-3)(D-4)\left(D^2-7D+10+2-(D-3)(D-4)\right)=0,\\
&2\lambda^2(D-3)(D-4)\left((D-3)(D-4)-(D-3)(D-4)\right)=0. \qquad \text{(E.6)}
\end{aligned}
$$

Hence, as a result, the Smarr relation is satisfied for a generic D-dimensional Einstein-Gauss-Bonnet gravity.

CURRICULUM VITAE

EDUCATION

B.Sc.: Electrical and Electronics Engineering, METU (2011-2017).

M.Sc.: Physics, METU (2017-2021).

PROFESSIONAL EXPERIENCE

Research Assistant in the Department of Physics (2019-).

PUBLICATIONS

1) A. Tavlayan and B. Tekin, "Event horizon detecting invariants," Phys. Rev. D **101**, no.8, 084034 (2020).

2) A. Tavlayan and B. Tekin, "Exact Formulas for Spherical Photon Orbits Around Kerr Black Holes," Phys. Rev. D **102**, no.10, 104036 (2020).

3) A. Tavlayan and B. Tekin, "Radii of spherical timelike orbits around Kerr black holes," Phys. Rev. D **104**, no.12, 124059 (2021).

4) A. Tavlayan and B. Tekin, "Light rings around five dimensional stationary black holes and naked singularities," Phys. Rev. D **107**, no.2, 024016 (2023).

5) A. Tavlayan and B. Tekin, "Instability of a Kerr-type naked singularity due to light and matter accretion and its shadow," Class. Quant. Grav. **41**, no.6, 065004 (2024).

6) A. Tavlayan and B. Tekin, "Partition function of a volume of space in a higher curvature theory," Phys. Rev. D **108**, no.4, L041902 (2023).

7) A. Tavlayan and B. Tekin, “Refined thermodynamics of black holes with proper conserved charges,” Phys. Rev. D **110**, no.8, 084049 (2024).

8) A. Tavlayan and B. Tekin, “Instability and information production around Kerr black holes: effects on entropy and the shadow,” Eur. Phys. J. C **85**, no.11, 1259 (2025).

AWARDS

1) METU Graduate Awards for the thesis in 2022.

2) METU Academic Performance Award in 2025.

SCHOLARSHIPS

1) TÜBİTAK 2210-A Scholarship Program.

2) TÜBİTAK 2211-A Scholarship Program.